The Pennsylvania State University

The Graduate School

Department of Materials Science
Ceramic Science and Engineering Program

SPECTROSCOPIC ELLIPSOMETRIC AND ELECTRICAL STUDY OF PROCESSING EFFECTS IN FERROELECTRIC THIN FILMS

A Thesis in
Ceramic Science

by
Brady J. Gibbons

Submitted in Partial Fulfillment
of the Requirements
for the Degree of

Master of Science

May 1995

I grant the Pennsylvania State University the nonexclusive right to use this work for the University's own purposes and to make single copies of the work available to the public on a not-for-profit basis if copies are not otherwise available.

Brady J. Gibbons

We approve the thesis of Brady J. Gibbons.

Date of Signature

_____   12-15-94

Susan Trolier-McKinstry
Assistant Professor of Ceramic Science
   and Engineering
Thesis Adviser

_____   Dec 19, 1994

Robert E. Newnham
Alcoa Professor of Solid State Science

_____   12|12|1994

Saluru B. Krupanidhi
Associate Professor of Engineering
   Science and Mechanics

_____   Jan 3, 1995

David J. Green
Professor of Ceramic Science
   and Engineering
In Charge of Ceramic Science Option

ABSTRACT

Thin film ferroelectrics are promising candidates for use in such devices as microsensors and microactuators, optoelectronic devices, surface acoustic wave substrates and computer memories. Integration of ferroelectrics into these applications requires optimizing both the properties of the material and the device microstructure. Relatively little quantitative work has been done in the latter area. Thus, this thesis investigates the microstructure - processing - property relationships of thin film lead zirconate titanate (PZT). Specifically, the effects of processing on the microstructural, optical and electrical properties were studied.

PZT films of varying thicknesses were prepared via the sol-gel method. The films were then annealed using two methods: conventional annealing and rapid thermal processing (RTP). Scanning electron micrographs showed dense microstructures for the conventionally processed samples. The grain size increased from 0.05 - 0.08 μm for samples fired at 650° C for 60 minutes to 0.68 μm and 1.05 μm for samples fired at 700° C for 30 and 45 minutes, respectively. The grain growth was influenced more by the temperature of processing than the time. The RTP'd samples showed decreasing pyrochlore content with hold time. At 700° C for 30 seconds, x-ray diffraction data showed only the perovskite phase was present. The water to PZT molar ratio used for controlled hydrolysis was found to have a strong effect on the final microstructures. An optimal ratio of 1.5:1 was determined.

Spectroscopic ellipsometry (SE) was used to non-destructively depth profile the thin films. Samples fired at 650° C for 60 minutes or 700° C for 30 or 45 minutes had comparable levels of surface roughness, with thicknesses of 300 Å to 500 Å. For the 700° C for 60 minute films, the roughness increased to 500 Å - 600 Å. It was concluded that the total surface roughness was not correlated to the film thickness. Based on this data, schematic grain morphologies for the samples annealed at 700° C could be interpreted.

Here, again, the temperature was a more important variable than the time in determining the total surface roughness. The RTP'd films exhibited a surface roughness of 175 Å to 250Å.

Dispersion behavior data was also obtained from the SE measurements. The conventionally annealed films displayed anomalously high apparent refractive indices which is attributed to changes in the substrate during annealing. To account for this, roughening of the Pt substrate was incorporated into the SE models. Films annealed at longer times and higher temperatures generally had better fits using this approach. This also reduced the refractive index of the PZT to more typical values. RTP'd films showed little deviation from the reference optical data for PZT. This was expected due to the smaller thermal budget of the process.

The relative dielectric constant of conventionally annealed films was measured and showed values up to 890. This value decreased as the annealing time was increased. The drop off of the dielectric constant at longer times was attributed to pyrochlore formation and/or lead loss. The RTP'd samples showed dielectric constants centered around 820. Hysteresis loops were obtained before and after fatiguing. These showed an increase of the coercive field, E_c, from 8.3 MV/m to 10.1 MV/m and a decrease of remanent polarization, P_r, from 21.8 $\mu C/cm^2$ to 10.7 $\mu C/cm^2$ for the conventionally annealed samples. The RTP'd samples dropped in P_r from 23.2 $\mu C/cm^2$ to 20.3 $\mu C/cm^2$ and increased in E_c from 7.8 MV/m to 11.0 MV/m. The fatigue behavior was measured from 10^8 to 10^9 cycles.

In situ SE measurements of fatigue were hindered by the lack of samples with a large enough area that was pinhole free so as to avoid electrical shorting. Some data was obtained and small changes in Δ and Ψ were observed. Additional work to clarify the cause of these changes is necessary.

TABLE of CONTENTS

LIST of TABLES

LIST of FIGURES

X

x

ACKNOWLEDGMENTS

I wish to express my sincere gratitude to my thesis advisor, Dr. Susan Trolier-McKinstry. Her guidance and support were indispensable to me in completing this research. I would also like to thank my committee members, Dr. Newnham and Dr. Krupanidhi for their encouragement and help throughout this process.

I would like to also recognize the people at IMRL who assisted me in learning the intricacies of working at this lab as well as helped me to work through the difficult and frustrating times during the past two years. Richard Meyer, Jr., Pavadee Aungkavattana, David Cann, Maureen Mulvihill and Heather Hawkins are those I would especially like to thank. I can only repay what they have done for me by doing the same for them when it is called for.

Finally, I want to acknowledge my family for the undying love and support they have given me for the past 24 years. Dad, mom and sis, this is as much for you as it is for me. Thanks for everything.

Chapter 1

INTRODUCTION

1.1   Background of Ferroelectrics

A ferroelectric material is defined as one in which there is a spontaneous alignment of electric dipoles by their mutual interaction (Kingery, 1960). The ferroelectric character is established when it can be shown that the spontaneous polarization can be reoriented between at least two equilibrium orientations by an appropriately applied electric field (Cross and Hardtl, 1980). Valasek (1921) was the first to use the word ferroelectric in describing these types of materials. He was exploiting the similarities between the nonlinear dielectric properties of Rochelle salt and the ferromagnetic behavior of iron. Of the 32 crystal point groups, 20 are piezoelectric and of those, 10 are pyroelectric and potentially ferroelectric. More than 38 separate families of ferroelectrics have been identified which can be tailored for uses in several different applications and environments (Cross and Hardtl, 1980).

There are numerous areas where ferroelectric materials have been applied in novel ways. Bulk ferroelectrics have been used in piezoelectric and dielectric applications such as sensors and actuators for military and biomedical uses, rotating and linear motor devices, micropositioning equipment, vibration and noise control devices, as well as several other areas. Ferroelectrics in thin film form have received much greater research interest during the last two decades. Since the development of silicon transistor technology, thin films of many materials have been explored in order to enhance the performance of these devices and develop new ones. Ferroelectric films have been researched for use as microsensors and microactuators, optoelectronic devices, surface acoustic wave substrates, and as a replacement for computer memory devices. The principle advantages of ferroelectric thin films for the latter application are their nonvolatility, their larger charge density storage

2

ability and their faster response speeds. Thus, ferroelectric memories could potentially store much more information in environments which would degrade the properties of current device technology (Swartz and Wood, 1992). Wu (1974) was the first to develop a metal - ferroelectric - semiconductor transistor for use as a memory device. More recently, research groups at Ramtron Corp., Krysalis Corp., and others have fabricated ferroelectric dynamic random access memories (DRAM), junction field effect transistors (JFET), and other working transistor devices (Araujo et al., 1990; Lampe et al., 1992; Scott et al., 1991).

The majority of the ferroelectrics being investigated today are of the perovskite crystal structure family. Compounds of this family have the form ABO_3. This structure is shown in figure 1.1, where the A ions sit at the corners of the cubic unit cell, the B ion is at the center and the Oxygen sit at the face centers.
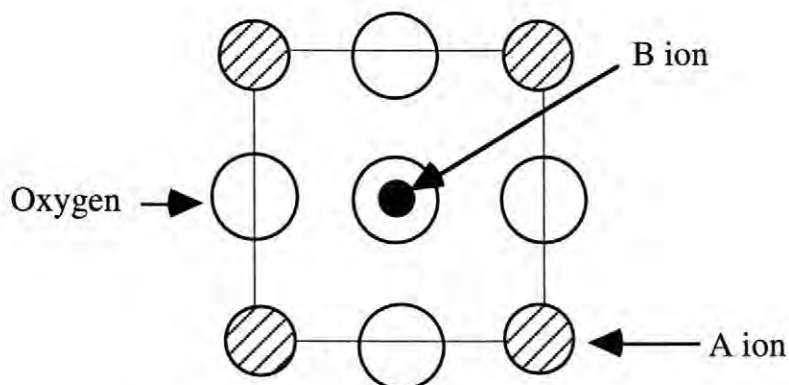
Figure 1.1 : The prototype perovskite crystal structure.

Among the most investigated of this type of ferroelectrics are $BaTiO_3$, $PbTiO_3$, and $KNbO_3$. In addition, solid solutions based on the perovskite lattice, such as $Pb(Zr,Ti)O_3$, $(Pb,La)(Zr,Ti)O_3$, and $Pb(Mg_{1/3}Nb_{2/3})O_3$-$PbTiO_3$ have found wide application.

1.2   Properties of Ferroelectrics

The following terms are used extensively in describing the properties of ferroelectrics:

Spontaneous Polarization, P_s: *the value of the polarization within a single ferroelectric domain with no applied field. (C/m^2)*

Remanent Polarization, P_r: *the value of the polarization that remains after removal of an electric field. (C/m^2)*

Coercive Field, E_c: *the electric field required to return the polarization from P_r to zero. (V/m)*

These values are displayed schematically in figure 1.2. In ferroelectric materials there is a transition point, called the Curie point, at which the material changes from a paraelectric state to a ferroelectric state. Upon transforming to the ferroelectric state, the material undergoes a change in the basic unit cell structure (from the cubic perovskite structure to a distorted state) due to a displacement of the centers of positive and negative charge in the cell. This is the origin of the spontaneous electric dipole and hence the spontaneous polarization. The values of P_r and P_s are dependent upon the temperature. Above T_c, they are zero and below T_c they increase with decreasing temperature. Citing $BaTiO_3$ as an example, the unit cell goes from a cubic state to a tetragonal state at 130° C. In the tetragonal form the titanium ion at the center of the cell undergoes a slight shift in any one of the <100> family of directions, thus causing the spontaneous dipole in the unit cell. As the material cools through T_c, the dipoles do not all align in the same variant. Therefore, a twinned microstructure develops. In these twinned regions, called domains, a net polarization exists because the dipoles are aligned within a domain. However, macroscopically the polarizations in each domain arrange themselves such that there is no net polarization measurable in the ceramic. As a field is applied to a material in this state, the domains aligned with the field will grow at the expense of the others. When the field is removed, many of the domains stay in the new orientation, leading to a ceramic with a net remanent polarization value.

The degree of the alignment of the electric dipoles in a ferroelectric polycrystal is quantified by the saturation polarization (P_s). It is defined as the charge per unit area on the

4

surface perpendicular to the polar axis of the crystal. This is analogous to the saturation magnetization that can be measured in ferromagnetic materials. All of the dielectric properties of ferroelectrics can be related to magnetic quantities measured in ferromagnets. This can be seen in figure 1.2 where a ferroelectric's polarization versus applied electric field is compared to a ferromagnet's magnetization versus applied magnetic field.
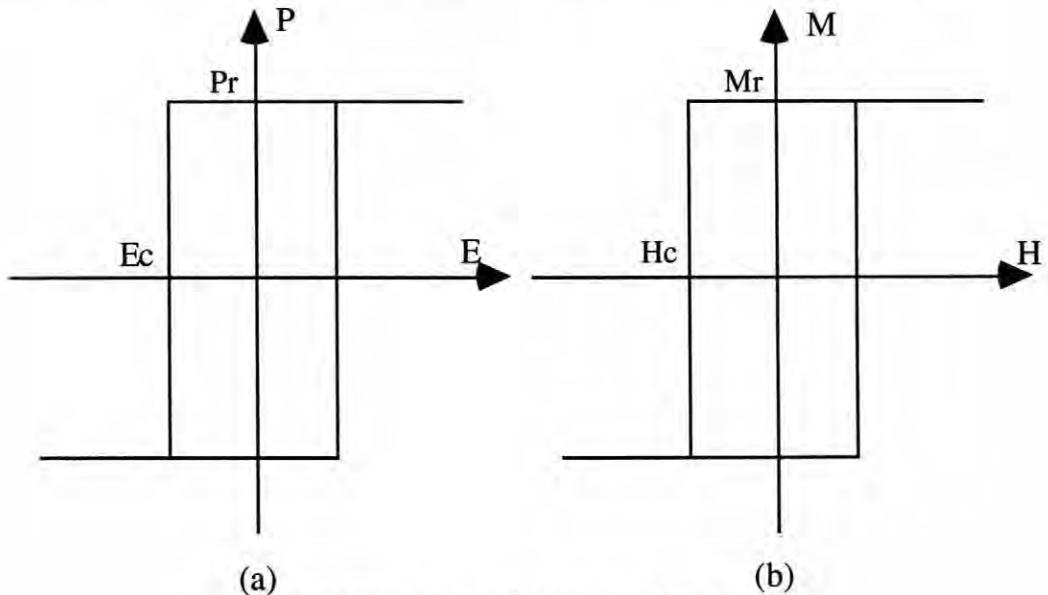
Figure 1.2 : (a) P vs. E for an idealized ferroelectric.
(b) M vs. H for an idealized ferromagnet. Where P =
polarization, E = Electric field, M = magnetization
and H = Magnetic field.

The quantities P_r and M_r are the remanent values of polarization and magnetization, respectively. As mentioned above, after applying a high enough field to the material, the spontaneous dipoles in the domains will align in the same direction and upon removal of the field, there will be a measurable value of polarization left in the sample due to the change in orientation of some of the dipoles. In order to return the sample to a state of zero net polarization, a field equal to the coercive field (E_c or H_c) must be applied. The area inside of the hysteresis loop is proportional to an energy loss. In ferroelectrics, that energy loss is partially attributed to the movement of domain walls through the crystal as an

alternating field is applied. As the wall moves through the grain, the center ion in each unit cell is reoriented into a direction more closely aligned with the applied field.

One of the most widely investigated ferroelectrics is the material $Pb(Zr_{1-x}Ti_x)O_3$, (PZT) due to its superior piezoelectric and ferroelectric properties. The phase diagram of PZT is shown in figure 1.3. The key to its exceptional properties is the morphotropic phase boundary (MPB) located at $x = 0.48$. On the titanium-rich side, there is a tetragonal ferroelectric phase with six possible orientations of P_S. On the zirconium-rich side of the MPB, there is a rhombohedral ferroelectric phase with eight possible orientations of P_S. Therefore, compositions in the region of the MPB have a total of 14 possible orientations for the polar vector. This permits much easier alignment of the dipoles and thus a higher remanent polarization. Also, due to the many different orientations the B site ion may adopt, the dielectric constant near the MPB is very high because the B ion is easily reoriented by an electric field.

The properties of PZT make it attractive for use in thin film form as a nonvolatile memory material. However, there are several requirements associated with applying this technology. First, the deposition method of the PZT must be chosen such that the maximum time and temperature it takes to deposit the film is compatible with existing semiconductor technology. Also, the hysteretic characteristics of the material are important. High values of the remanent polarization in order to distinguish memory states as well as relatively low coercive fields to ensure operation at standard semiconductor voltages (<5 V) are necessary. PZT deposited in a pure, homogeneous manner does have these characteristics but the procedure for obtaining the desired composition and crystallinity must be optimized for each method of deposition (Xu and Mackenzie, 1992). Another important consideration is the choice of electrode materials used in the device. Any reactions or interdiffusion at the film/electrode interface will be detrimental to the operation of the device. Last is the lifetime of the memory element, that is, the number of polarization reversal cycles the film can undergo without a significant decrease
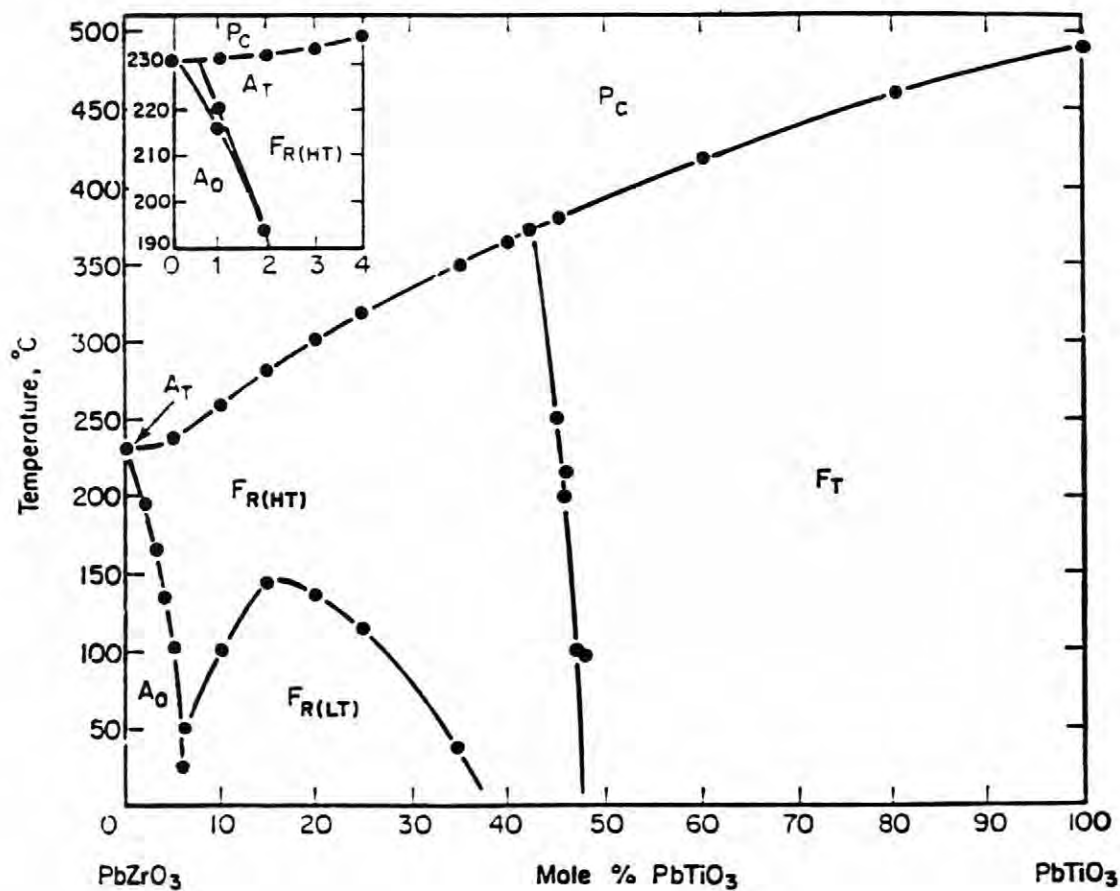
Figure 1.3 : PbTiO3-PbZrO3 phase diagram (from Jaffe, Cook and Jaffe, 1971).

in the value of remanent polarization. In order to be competitive with current memory materials, the device should be able to withstand 10^{15} switching cycles (Swartz and Wood, 1992).

It is the last issue that has been the focus of much research in recent years (Yoo and Desu, 1992; Pan et al, 1993; Mansour and Vest, 1992). Many of these studies have focused on observing the degradation of electrical properties during fatigue. In addition, various microstructural and electrical evaluations on the films have been conducted to try to determine the mechanism(s) of fatigue. None of these studies have utilized an optical technique to observe fatigue in ferroelectric thin films. One of the purposes of this thesis is to use spectroscopic ellipsometry as a tool to characterize these films before, during and after the fatigue process. This technique was chosen because it is a nondestructive and noninvasive way to examine this effect *in situ*. In doing so, it may be possible to further specify the relationships between the microstructure and processing of the films and the fatigue characteristics.

1.3   Background to Spectroscopic Ellipsometry

Spectroscopic ellipsometry (SE) is an optical technique whereby light of a known polarization state and wavelength is reflected off of a sample and the exiting light is analyzed for the relative changes in amplitude and phase. This process is repeated for several different wavelengths. The changes that are measured at each wavelength allow for the determination of the complex reflection coefficients of the sample and thus some of the physical parameters of the sample such as the complex dielectric function, ε^*, or the film thickness (Collins, 1990).

Today, SE is being used to investigate many types of materials in various ways. Besides the above information, spectroscopic ellipsometry can provide several kinds of *in situ* data. McKinstry (1992) studied the crystallization behavior in PZT thin films by observing data at several temperatures. As improvements in the detection technology

arose, spectra collection times have dropped to as low as 40 ms using an Optical Multichannel Analyzer (OMA). With this, real time measurements of evolving surfaces, interface regions, and defect regions are possible. Eventually, it should be possible to obtain a full spectra in a time less than it takes to create a monolayer in the film (Collins, 1990). This would allow even more detailed investigations on film growth or other surface modifications.

In this work, spectroscopic ellipsometry is used to characterize the microstructure of PZT thin film samples as a function of the processing conditions. In addition, spectroscopic ellipsometry is used to examine the microstructural influence on electrical fatigue *in situ*. That is, to obtain ellipsometric data before, during and after fatiguing a PZT thin film. Of the several proposed mechanisms of fatigue in ferroelectric thin films, ellipsometry could be used to detect microcracking, electrode delamination and space charge effects, if they are large enough. Thakoor and Maserjian (1994) have shown that a photoresponse probe with light at a wavelength near the band gap of PZT can give some insight on the space charge distribution in a PZT thin film memory capacitor. The two other mechanisms may be detected by including either a layer of air in the geometrical model of the sample between the electrode and film or by observing changes in the dispersion characteristics of the film.

1.4   Thesis Objective

The major objective of this thesis was to study the microstructure-processing-property relationships in PZT thin films. In particular, the effect of various processing parameters on the electrical properties, including fatigue, was studied. In doing so, the method of film deposition had to be chosen such that high quality, defect-free films could be produced. As mentioned, there are several processes from which to choose. Chemical vapor deposition (CVD), sol-gel, sputtering, etc. all provide films which exhibit the desired

properties. The sol-gel process was chosen due to the advantages of high compositional control and low cost, among others.

Samples were prepared using two routes. Conventional furnace annealing and rapid thermal processing (RTP) were chosen so as to provide a wide variety of microstructural differences. Spectroscopic ellipsometry was utilized to characterize the microstructures of the films to give insight into how the different processing parameters affect the films and their resultant electrical properties. To study the fatigue behavior, SE was also used before, during and after the fatiguing of the samples. To do this, a system for fatiguing the films *in situ* had to be developed. This consisted of designing a signal generation system that would provide the necessary wave forms and voltage output to drive the large amount of charge required to switch the ferroelectric. It was hoped that this data would be useful in identifying the mechanism(s) responsible for fatigue in ferroelectric films, as well as the influence of the processing and the microstructure on the properties of the films. A better understanding of these factors will be very helpful in the development of higher quality and more reliable devices for use in innovative applications.

Chapter 2

LITERATURE REVIEW

2.1   Review of Deposition Methods

As semiconductor technology expanded throughout the 1970's and 1980's research into the fabrication of thin films grew accordingly. Ferroelectric thin films were found to exhibit electrical properties (dielectric constant, polarization, etc.) which, when utilized appropriately, would drastically improve the performance of existing silicon based devices. However, in order to exploit these materials, the technology demanded that thin film ferroelectrics were to be fabricated with high purity, compositional and microstructural control, and reproducibility; all while retaining their superior electronic properties. In addition, the crystallization and densification of these films had to occur at a low enough temperature to permit integration of these films into practical devices. Appropriate techniques to satisfy these needs have been developed and are just now being optimized for ferroelectric materials.

There are several deposition techniques utilized to make ferroelectric thin films. Some of the more common ways and their advantages and disadvantages are summarized in table 2.1.

Table 2.1 : Summary of deposition methods (from Swartz and Wood, 1992).

Attribute	Sputtering	Laser Ablation	MOCVD	Sol-Gel
State of Development	+	o	—	o
Potential for Low Annealing Temperatures	+	+	+	+
Deposition of Complex Compositions	—	+	—	+
Sensitivity to Substrate Material	o	o	o	o
Potential for Rapid Growth Rates	o	+	+	—
Potential for High Film Quality	o	o	+	o
Potential for Film Epitaxy	+	+	+	o
Amount of Process Development Required	o	o	—	o
Difficulty/Cost of Scale-up	—	o	+	+
Cost of Production Equipment	—	—	o	+
Future Prospects	o	o	+	+

(+) ideal or very good deposition method
(o) acceptable deposition method
(—) unacceptable method or considerable further R&D required

For this study, sol-gel processing was used to prepare the PZT films. Since it is a wet chemical method, it has many advantages over other processes such as sputtering, CVD, MOCVD, and others. These advantages include low processing temperatures for the films, good composition control, good homogeneity, and the ability to prepare large area films at lower cost (Blum, 1992). Some disadvantages to this method include irreproducibility when variables are not carefully controlled and the inability to produce crack free films greater than 1 micron thick (Swartz and Wood, 1992). For this thesis, existing sol-gel technology was used to fabricate thin films of PZT. Fukushima et al (1975) were the first to exploit this method to fabricate $BaTiO_3$ thin films. The first reports of using this process for the PZT compositions were by Wu et al (1984) and Fukushima et al (1984).

In sol-gel processing, the precursors are commonly metal alkoxides, which are high valent cations bonded to an oxygen and an alkyl group. By hydrolyzing and gelling the precursors, a three dimensional network takes shape according to the reactions (Yi and Sayer 1991):

$$M(OR)_n + H_2O \rightarrow M(OR)_{n-1}(OH) + ROH \quad \text{(hydrolysis)}$$

$$M(OR)_n + M(OR)_{n-1}(OH) \rightarrow M_2O(OR)_{2n-2} + ROH \quad \text{(condensation)}$$

$$M(OR)_{n-1}(OH) + M(OR)_{n-1}(OH) \rightarrow M_2O(OR)_{2n-2} + H_2O \quad \text{(condensation)}$$
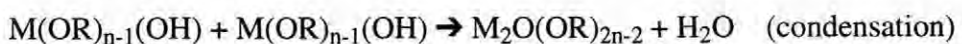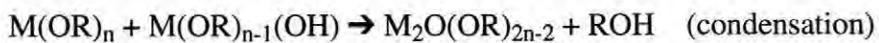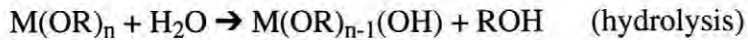
During the film preparation, if the hydrolysis reaction occurs too quickly (or if there is excess water in the system), premature gelation may occur and the homogeneity of the sol can be degraded. Also, the temperatures of the reactions and the amounts of additives must be very carefully controlled. The process yields a solution with the constituent ions mixed together on a molecular level. The local atomic arrangement of the sol is near to that of the crystalline phase (Xu and Mackenzie, 1992). The sol can be applied to the substrate by dipping, spinning or spraying. This allows for the tailoring of the process for specific requirements, i.e., depositing on a featured substrate rather than a flat one. Upon deposition, the films are annealed to crystallize and densify the material. This can be done

conventionally or by using a rapid thermal processing technique (RTP). The more common method is conventional annealing at temperatures of 650° C to 700° C for 15 - 60 minutes. However, it has been shown that lead loss from the films and/or pyrochlore formation is common using this method (Kwok and Desu, 1991; Tani and Payne, 1994). The RTP method utilizes high intensity tungsten-halogen lamps to heat the films at a rate of 100° C/s. Generally, the samples are annealed at 700° C for 10 - 60 seconds. Due to the small thermal budget, the lead loss is drastically reduced and the formation of the perovskite phase is enhanced (Chen, et al. 1992; Huang, et al. 1992).

Ferroelectric films of several compositions have been made using the sol-gel process. Chen (1992) worked on PZT and PLZT, others include Tuttle, et al. (1993) and Udayakumar, et al. (1993). Throughout the literature, properties of PZT films prepared conventionally and by the RTP method show remanent polarizations ranging from 25 $\mu C/cm^2$ to 35 $\mu C/cm^2$ and relative dielectric constants from 800 to 1300.

2.2   Thin Film Applications

Ferroelectric thin films offer properties such as a high dielectric constant, polarization switching, piezoelectricity, pyroelectricity and electro-optic effects. This has lead researchers to propose these materials for uses in many areas. These applications include microactuators, infrared sensors, thin film capacitors, surface acoustic wave substrates, electro-optic displays and shutters, optical waveguides, and memory devices. In many cases, the utilization of ferroelectric thin films in these types of applications has been limited by the ability to integrate the films with existing technology. However, as described previously, the deposition techniques for device quality films have been improved greatly over the past decade. Thus many of these applications are just beginning to reach the stage of development and commercialization.

One application towards which considerable research has been directed is the use of ferroelectric thin films as nonvolatile memories (FRAMs) or dynamic random access

memories (DRAMs). Recent developments in this area are reviewed in the following section.

2.2.1 Ferroelectric Memory Devices

The idea of utilizing a ferroelectric material for a binary memory device originated in the 1950's. In addition to the properties described above, researchers were attracted to ferroelectrics due to their lower power requirements, higher density, and higher speed than existing memory materials (Fatuzzo and Merz, 1967). However, at that time the bulk ferroelectrics used required high operating voltages, lacked a well defined coercive field, and had low fatigue limits (Araujo et al, 1990). An attempt to overcome these problems was made in 1966 when Zuleeg and Wieder constructed the first integrated ferroelectric memory. They used CdS on a single crystal of triglycine sulfate (TGS). In 1974, Wu developed a prototype memory using a polycrystalline $Bi_4Ti_3O_{12}$ thin film with an n-channel metal-ferroelectric-semiconductor architecture. The material was sputtered onto a silicon substrate and the remanent polarization of the ferroelectric was used to control the surface conductivity of the silicon. This design is close to one of the designs used today (Araujo et al, 1990).

2.2.2 Operation of a Ferroelectric Memory

A nonvolatile memory based on a ferroelectric is controlled through the polarization switching of microscopic regions in the thin film. The two polarization states correspond to binary values of "0" or "1," respectively. To construct a ferroelectric memory, an array of capacitors is integrated with the memory circuit. These capacitors can be as small as 4 μm^2 (Swartz and Wood, 1992). Commercialization of these devices is in the very early stages and the extent of development will depend on the memory density and level of performance that can be attained. The latest memories have a 256 Kb density with a 100 ns read/write time at 3 V (Sumi et al, 1994).
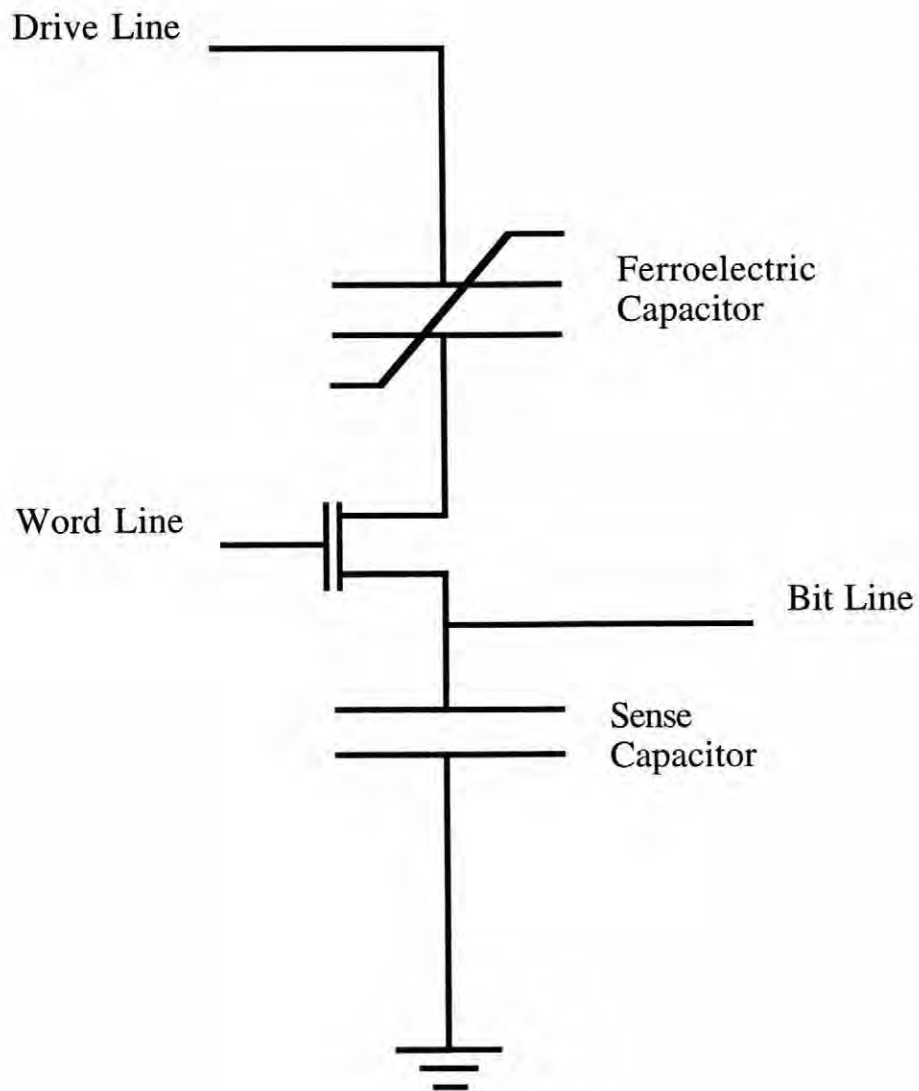
Figure 2.1 : Schematic of ferroelectric memory circuit (from Abt, 1990).

The schematic of a basic memory element is shown in figure 2.1 (Abt, 1990). It is based on a simple Sawyer-Tower circuit. To create individually addressable bits, a transistor is placed between the capacitors. Voltage is applied to the ferroelectric capacitor via the drive line, the word line controls the switching transistor, and the state of the capacitor is analyzed through an amplifier at the bit line. By selecting an appropriate word line and bit line and then measuring the signal, the sense of the bit can be identified (Abt, 1990). The conventions that have been established to define a "1" and a "0" are:

1) Negative voltage applied to the capacitor corresponds to a down state.
This is called a stored "1."

2) Positive voltage applied to the capacitor corresponds to an up state. This
is called a stored "0."

The memory element described above can be utilized in two modes of operation, a DRAM structure and a nonvolatile memory mode. In a DRAM device, data is stored as charge on the capacitor. The capacitor must be refreshed regularly to retain the data. Currently, low dielectric constant materials such as Si_3N_4 are used as the capacitors. However, by utilizing a material with a much higher dielectric constant, i.e. a ferroelectric, the size of the capacitor can be markedly reduced. Thus, the storage density of the DRAM can be increased. The major requirement on the materials for this type of memory is a resistance to time dependent dielectric breakdown (Swartz and Wood, 1992). It has been demonstrated that ferroelectric thin films can withstand 40 V square wave pulses lasting 30 µs, but when voltages as low as 5 V are applied for relatively long periods, shorting often occurs (Araujo et al, 1990). This limits the utility of ferroelectric films in DRAM operations. Recently, advances in fabrication technology have shown large improvements in this area (Kinney and Gealy, 1994).

The alternate type of operation of a ferroelectric memory device is the nonvolatile mode. This is the type based on the directional polarization of the ferroelectric as described

above. Here, the refresh operation of the memory cell is eliminated. That is, when the power to the cell is turned off, the polarization state remains intact. At present, the primary material being investigated for these devices is PZT.

In order to incorporate PZT into a non-volatile memory, there are several requirements on the microstructural and electrical properties of the films which have to be optimized (Kwok et al., 1990; Sanchez et al., 1991). As mentioned above, a high P_r and low E_c are desired. Microstructurally, the grain size of the PZT is desired to be less than 100 nm. This allows for more switchable regions in the memory element. Investigations into the switching kinetics of the films have demonstrated that switching times not greater than 50 ns for several different sizes of electroded areas at 5 V or less can be achieved (Lampe et al, 1992; Larsen et al, 1991). This is significant because standard silicon based circuits operate at these voltage levels. In addition to the film material, the optimization of electrode materials has also been studied. Interdiffusion or reaction mechanisms occurring at the electrode/film interface are extremely detrimental to the performance of the device as will be discussed later. Vijay and Desu (1993) and Eom et al (1993) have compared several materials in combination with PZT including platinum, ruthenium oxide, indium tin oxide and others.

The last issue that has recently been widely investigated is the fatigue and retention properties of the ferroelectric memory element. Since the DRAM mode of operation is not based on the polarization switching, this is not a critical issue. However, in the nonvolatile memory mode a large number of detectable polarization reversals must be ensured. This issue is addressed in the following section.

2.2.3 Fatigue in Ferroelectric Thin Films

The lifetime of a nonvolatile ferroelectric memory element (FRAM) is based on the number of polarization reversals the film can undergo without a significant decrease in the amount of switched charge. If the degradation is so severe that the difference between the

up and down states, "0" and "1," cannot be detected, the device has become useless. In the FRAM device described above, each time a bit of data is read or written, the polarization of that particular element is switched. For large scale applications, the fatigue life should be at least 10^{15} cycles (Swartz and Wood, 1992). Numerous studies have been completed to try and understand the mechanism(s) that cause fatigue. A brief description follows.

The mechanisms that have been investigated most extensively include; growth of oxygen deficient conducting dendrites (Duiker and Beale, 1988), microcracking (Saleneck, 1972), space charge effects (Takahashi, 1970; Carl and Hardtl, 1978; Lambeck and Jonker, 1986) and electrode effects (Taylor, 1967; Vijay and Desu, 1993). It should be noted that the some of these mechanisms occur more frequently in bulk ferroelectrics than thin films.

Peng and Bursill (1986) were the first to demonstrate the existence of what they assumed to be dark oxygen-deficient filaments at the electrode/ferroelectric thin film interface. Duiker and Beale (1988) modeled in some detail this failure mechanism. They report that impact ionization of the titanium ion causes a charge conversion. This then causes a liberation of oxygen ions. Thus, the oxygen vacancies left behind are semiconducting and the surrounding material visually appears dark. These dendrites continue to grow until an electrical short develops and failure occurs. To corroborate this, Scott et al (1991) measured the oxygen concentration across PZT films. They found that the concentration drops off near the electrode/film interface.

Microcracking and certain electrode effects occur during fatigue of bulk ferroelectrics (Jaffe et al 1971; Jiang et al, 1994). It was demonstrated that a contact deterioration between the electrode and film could occur if the sample surface was not prepared properly. This delamination caused a significant decrease in the remanent polarization after 10^6 cycles (Jiang et al., 1994). Because ferroelectrics are both piezoelectric and electrostrictive, during switching a large strains can be generated. When the aforementioned delamination occurs, not all areas of the ceramic will experience enough

field to switch their polarization. This causes stress concentrations between these regions and intergranular cracking can occur leading to failure. These mechanisms have also been studied in PZT thin films (Johnson et al, 1990).

An alternate fatigue mechanism that has been proposed is a space charge effect occurring at the grain boundaries, the domain walls, the electrode/film interfaces, or throughout the volume of the film. Kudzin et al. (1975) proposed that space charge accumulates at the domain walls, which in turn stabilizes the position of the wall. This decreases the amount of switched charge during each cycle, and thus the remanent polarization is diminished. More recently, fatigue has been related to a build up of space charge at the electrode/film interface (Swartz and Wood, 1992). This planar layer of space charge increases the interfacial resistance and decreases the interfacial capacitance, creating an inactive layer. Thus the amount of switched charge during cycling is decreased. Yoo and Desu (1992) have modeled this effect in some detail and have observed that by controlling the number of intrinsic defects through doping and proper heat treating, the fatigue life can be increased.

Other studies on fatigue have demonstrated that the choice of electrode materials is critical in determining the fatigue life (Vijay and Desu, 1993; Lee et al, 1993). Vijay and Desu (1993) compared PZT thin films with platinum, indium tin oxide (ITO) and ruthenium oxide electrodes. There were severe interfacial reactions with the ITO electrodes at temperatures above 500° C. However, the RuO_2 electrodes were stable to 600° C. When comparing the fatigue properties, PZT films with RuO_2 electrodes showed no degradation up to 2×10^{11} cycles while the films on platinum electrodes started to decay at 10^7 cycles. They attributed this to the increased stability of the electrode/film interface. In particular they stated that the reduced lattice mismatch and the more stable work function of the oxide results in reduced defect entrapment at the interface. Lee et al. (1993) recently compared $YBa_2Cu_3O_x$ (YBCO) to platinum for use as top electrodes on a PZT thin film deposited on a YBCO substrate. They demonstrated that the platinum-electroded films

underwent a large fatigue with a significant drop at 10^7 cycles. The YBCO-electroded samples, however, displayed a low remanent polarization with an improved fatigue resistance.

In this study, PZT thin films with platinum bottom and gold top electrodes were chosen. This was because one of the objectives of our study was not to increase the fatigue life of a ferroelectric memory element, but to understand the mechanism causing the fatigue.

Chapter 3

EXPERIMENTAL PROCEDURE

3.1 Sol-Gel Process and Film Fabrication

In this work, a modification of the process first reported by Budd, Dey, and Payne (1985) was utilized to prepare the sol-gel PZT films. Figure 3.1 shows a flow chart of the solution preparation and coating. The lead acetate trihydrate was dissolved in 2-Methoxyethanol and heated to 125°C under argon to distill off the water of hydration. After this first step, the solution was allowed to cool to room temperature before zirconium (IV) propoxide and titanium (IV) isopropoxide were added in a humidity controlled glove box. This was done to avoid contamination of the solution by water vapor or other impurities. The solution was then refluxed at 80°C for 4 hours to promote a thorough mixing of the components.

Before the solution was spun onto the substrate, molar ratios of 1.5:1, 3:1 or 4:1 (distilled - deionized water to PZT) was added to the solution. This was done by mixing solvent with the water in a 2:1 ratio and slowly adding it to the room temperature solution. When hydrolysis occurs, M-OH groups replace the alkoxy groups and a three dimensional network begins to form. This increases the viscosity of the sol. For depositing the solution, the viscosity was kept in a range where it adhered to the substrate homogeneously. It is also likely that the film will absorb water from the atmosphere during the spin coating and pyrolysis so this must be accounted for, as well. It has been shown that over-hydrolysis is detrimental to the electrical properties of the film (Lakeman and Payne 1992). In previous studies, a molar ratio of 2 moles of water per one mole of PZT was shown to result in the highest quality films.

In addition, 4 vol% formamide is added to the solution before spin coating. As very thin films go through the drying stages, cracks can occur. These appear due to the

```
┌─────────────────────────────────────┐
│ Clean glassware with distilled water,│
│     chromic acid, propanol and       │
│         2-methoxyethanol             │
└─────────────────────────────────────┘
              ↓
┌─────────────────────────────────────┐
│        Add 2-methoxyethanol          │
│            as solvent                │
└─────────────────────────────────────┘
              ↓
┌─────────────────────────────────────┐
│ Add lead acetate trihydrate and distill │
│       in an  Argon atmosphere        │
└─────────────────────────────────────┘
              ↓
┌─────────────────────────────────────┐
│   Add Titanium Isopropoxide and      │
│ Zirconium Propoxide to solution      │
│           and reflux                 │
└─────────────────────────────────────┘
              ↓
┌─────────────────────────────────────┐
│    Clean Pt coated Si substrates     │
│           ultrasonically             │
└─────────────────────────────────────┘
              ↓
┌─────────────────────────────────────┐
│           Spin coat                  │
│      3000 rpm for 20 seconds         │
└─────────────────────────────────────┘
              ↓
┌─────────────────────────────────────┐
│ Pyrolyze film at 350° C - 400° C     │
└─────────────────────────────────────┘
              ↓
┌─────────────────────────────────────┐
│           Anneal film                │
└─────────────────────────────────────┘
```

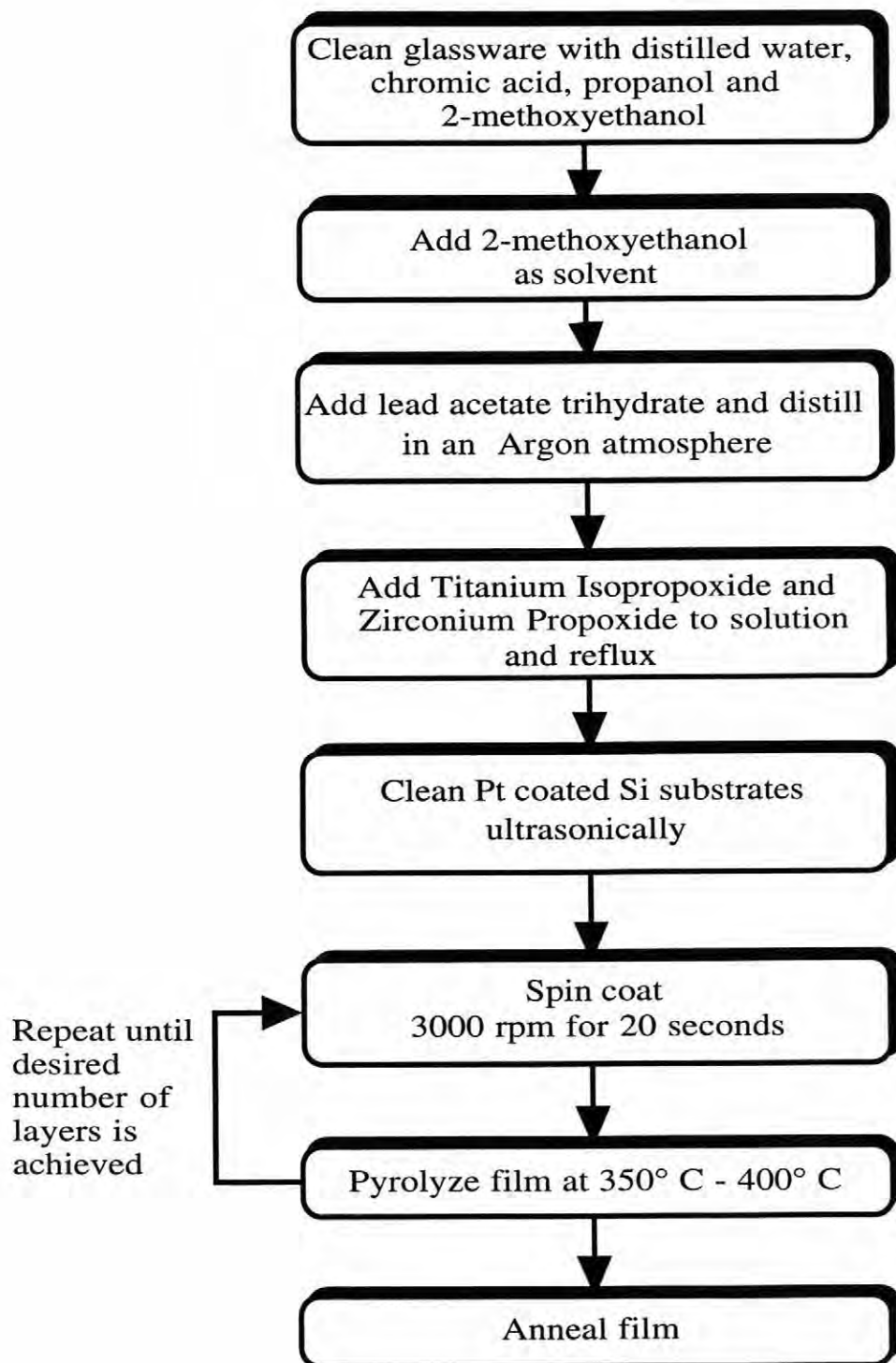Repeat until desired number of layers is achieved

Figure 3.1 : Flow chart of the sol-gel process.

fact that different sized pores in the film dry at different rates (Yi and Sayer, 1991). Capillary forces cause the bigger pores to dry much faster than smaller ones. Thus, when the larger pores dry, a stress concentration occurs at the bottom of the pore. When the stress reaches a critical value, a crack will develop. Adding formamide produces larger and more uniformly sized pores. This helps to dry the pores at a more constant rate, and thus reduce the possibility of cracking.

In this study, the substrates used were obtained from Nova Electronic Materials. They were 3 inch Si wafers with a one micron thermally grown SiO_2 layer and a 200 Å Ti interlayer to promote bonding of the top 1000 - 1500 Å layer of platinum. The substrates were cleaned ultrasonically in a 2-propanol solution just prior to deposition. The solution was spin coated on to the substrate as this permits good thickness homogeneity across the substrate. The substrate was held to the spin coater (Integrated Technologies #P6204) by a vacuum connection and the entire wafer was covered with solution. The wafer was then spun at 3000 rpm for 20 seconds. After each deposition the films were pyrolyzed to remove the organics. Due to their high area to volume ratio, it has been shown through differential thermal analysis that pyrolysis occurs at temperatures below 400°C for one minute (Lakeman and Payne, 1992). In this study, pyrolysis was carried out at 330°C. This was repeated until the desired number of layers was achieved, from five to nine. Once the last layer had been pyrolyzed, the films were conventionally annealed at temperatures and times ranging from 650°C - 700°C and 15 minutes - 60 minutes. Films were also rapid thermally annealed in an AG Associates Heatpulse 210T-02 at 700° C and 750° C for 10, 15, and 30 seconds.

3.2   Introduction to Spectroscopic Ellipsometry

Ellipsometry is a technique in which polarized light of a known wavelength is reflected off of a sample and the relative changes in phase and amplitude of the parallel (p) and perpendicular (s) components of the light are measured. Those changes are

characteristic of the depth profile of the dielectric function of the film. To analyze the light after reflection from the surface, a rotating analyzer is employed. By rotating the analyzer, the intensity of the light can be sampled at several analyzer angles during a full rotation and thus the state of polarization, or ellipticity of the light, can be determined. At a single wavelength, this does not yield enough information to obtain a complete characterization of most thin film samples. Therefore, we use a spectroscopic technique where the wavelength can be changed so that additional measurements can be acquired. This provides sufficient data that depth profiling can be performed (McMarr, 1985).

Each sample reflects light in a different manner according to its complex Fresnel p and s reflection coefficients (parallel and perpendicular to the plane of incidence, respectively). Therefore, a relationship must exist between the polarization state of the light after reflection and the reflection coefficients of the sample. An incident light wave that is monochromatic and polarized at some angle, P, with respect to a reference laboratory frame can be described by:

$$E(r,t) = (E_x X + E_y Y)e^{(ikZ - i\omega t)} \qquad (1)$$

Where X and Y are unit vectors orthogonal to the propagation direction, Z, of the light. E_x and E_y are the components of the incident light in the plane of incidence and perpendicular to the plane of incidence, respectively. The light that is reflected from the sample surface can then be characterized by a similar equation:

$$E(r,t) = (r_p E_x X + r_s E_y Y)e^{(ik'Z - i\omega t)} \quad (2)$$

Where r_p and r_s are the complex reflection coefficients parallel and perpendicular to the plane of incidence, respectively. Spectroscopic ellipsometry permits measurements of the complex reflection coefficients at many wavelengths.

A different way to examine this technique is to use Jones matrix representations. The entire ellipsometer configuration with a sample can be described by the following series of matrices:

$$\begin{bmatrix} E_1 \\ E_2 \end{bmatrix}_{t,e} = \begin{bmatrix} 1 & 0 \\ 0 & 0 \end{bmatrix} \begin{bmatrix} \cos A & \sin A \\ -\sin A & \cos A \end{bmatrix} \begin{bmatrix} r_p & 0 \\ 0 & r_s \end{bmatrix} \begin{bmatrix} \cos P & -\sin P \\ \sin P & \cos P \end{bmatrix} \begin{bmatrix} 1 \\ 0 \end{bmatrix} E_o \quad (3)$$

Here, P and A are the angles that the polarizer and analyzer make with respect to the reference x-y frame of the laboratory. E_o is the electric field of the incident light. The common term $\exp(ikZ - i\omega t)$ is left off for simplicity. This equation gives the electric field of the exiting light in the analyzer transmission - extinction reference frame. It is straightforward to see that the exiting electric field components (E_1 and E_2) depend only upon the sample's complex reflection coefficients. Thus, the coefficients can be determined since all other quantities are either known or measured. The ellipsometric parameter is the complex ratio of the two coefficients and by convention, the two ellipsometric angles are related by:

$$\rho = \frac{r_p}{r_s} = \tan \Psi e^{i\Delta} \quad (4)$$

This relation can be substituted into the representation above and the result is:

$$\begin{bmatrix} E_1 \\ E_2 \end{bmatrix}_{t,e} = \begin{bmatrix} 1 & 0 \\ 0 & 0 \end{bmatrix} \begin{bmatrix} \cos A & \sin A \\ -\sin A & \cos A \end{bmatrix} \begin{bmatrix} \rho & 0 \\ 0 & 1 \end{bmatrix} \begin{bmatrix} \cos P & -\sin P \\ \sin P & \cos P \end{bmatrix} \begin{bmatrix} 1 \\ 0 \end{bmatrix} E_o \quad (5)$$

Now, since the irradiance of the exiting light is proportional to the square of its electric field, it is found that (see complete derivation in Appendix):

$$I = \frac{1}{2}(1 + \rho\rho^*) \left[1 + \left(\frac{\rho\rho^* - 1}{1 + \rho\rho^*} \right) \cos 2A + \left(\frac{\rho + \rho^*}{1 + \rho\rho^*} \right) \sin 2A \right] \quad (6)$$

$$I = I_o [1 + \alpha \cos 2A + \beta \sin 2A] \quad (7)$$

Where ρ^* is the complex conjugate of the reflectance ratio. α and β are the normalized second order Fourier coefficients that can be determined by Fourier analysis of the exiting light intensity as a function of the analyzer angle.

Upon reflection from a dielectric film on an absorbing substrate, linearly polarized light becomes elliptically polarized (Aspnes, 1974). This ellipse can be characterized by two parameters. The azimuth angle, Q, is the angle between the x axis of the reference
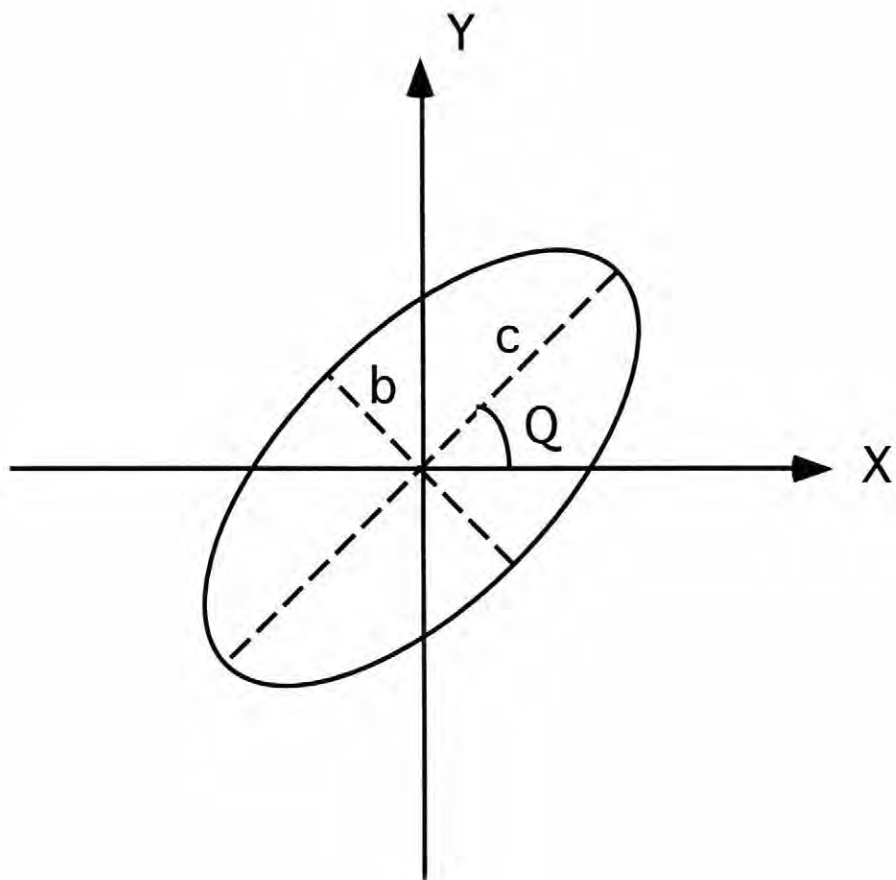
Figure 3.2 : Description of elliptically polarized light.

frame and the major axis of the ellipse. "a" is the ratio of the minor to major axis (see figure 3.2). Therefore, the exit light in the analyzer transmission-extinction axes can also be characterized by:

$$\begin{bmatrix} E_1 \\ E_2 \end{bmatrix}_{t,e} = \begin{bmatrix} 1 & 0 \\ 0 & 0 \end{bmatrix} \begin{bmatrix} \cos(A-Q) & \sin(A-Q) \\ -\sin(A-Q) & \cos(A-Q) \end{bmatrix} \begin{bmatrix} 1 \\ ia \end{bmatrix} \qquad (8)$$

It has been proven by Aspnes (1974) that the parameters of the elliptically polarized light can be calculated from the Fourier coefficients by:

$$Q = \frac{1}{2}\tan\left(\frac{\beta}{\alpha}\right) + \frac{\pi}{2}u(-\alpha)\text{sgn}(\beta) \qquad (9)$$

$$\text{where} \quad u(x) = \begin{cases} 0 & \text{if } x < 0 \\ 1 & \text{if } x \geq 0 \end{cases}$$

$$\text{sgn}(x) = \begin{cases} -1 & \text{if } x < 0 \\ +1 & \text{if } x \geq 0 \end{cases}$$

and:

$$a = \frac{\pm\sqrt{1-\zeta^2}}{1+\zeta} \qquad \zeta = \sqrt{\alpha^2 + \beta^2} \qquad (10,11)$$

By equating the two equations that result in the electric field of the exiting light in the analyzer transmission-extinction frame (equations #5 and #8), it is shown that:

$$\rho = \left(\frac{\cot Q - ia}{1 + ia \cot Q}\right)\tan P \qquad (12)$$

where P is the angle of the polarized light.

From this, Δ and Ψ are calculated via equation 4.

In summary, the measured light intensity is first transformed by Fourier methods in order to determine the second order Fourier coefficients, α and β. Next, these values are used to calculate the parameters of ellipticity of the exiting light, Q and a. Last, the complex ratio, ρ, is found and is used to determine the ellipsometric parameters, Δ and Ψ, from the above equations. It is important to note that the above description assumed a system with perfect components and ideal samples. There are several calibrations that will be discussed which must be included in order to account for non-idealities in the system.

3.2.1 Ellipsometer Alignment and Operation

The configuration of the ellipsometer used in this study is shown in figure 3.3. It is a rotating analyzer ellipsometer which operates as described above. The instrument is interfaced with an IBM PS/2 computer which maintains control over such operations as monitoring the photomultiplier tube signal, determining the timing signals for taking data, converting light intensity as a function of analyzer angle to the ellipsometric angles Δ and Ψ, as well as other functions (McMarr, 1985 and Chindaudom, 1991). An electronic feedback circuit is employed in the system in order to maintain a constant average signal level from the photomultiplier tube at all energies of incident light. Therefore, comparisons of the ellipsometric parameters at different wavelengths are more reliable (Collins, 1990).

There are four procedures used to align and calibrate the ellipsometer. They are: 1) the system alignment, 2) the system calibration, 3) the eta calibration, and 4) the dark current calibration.

The system alignment is done after large system disruptions, such as replacing the light source, are completed. This calibration consists of removing the photomultiplier detector and putting a HeNe laser in its place. This allows for the tracing and centering of the light beam path throughout the system. Once this is done, the detector is replaced and final adjustments can be made.

The system calibration accounts for the difference between the azimuth of the analyzer, A, when it reads zero and the x axis of the laboratory reference frame. There is a similar discrepancy with the polarizer which must also be accounted for. The procedure used was first developed by Aspnes (1974). The Jones matrix representation of the system given above can be generalized for this case. Including the difference in zero positions and the optical activity of the Rochon quartz polarizer and analyzer, the equation is:
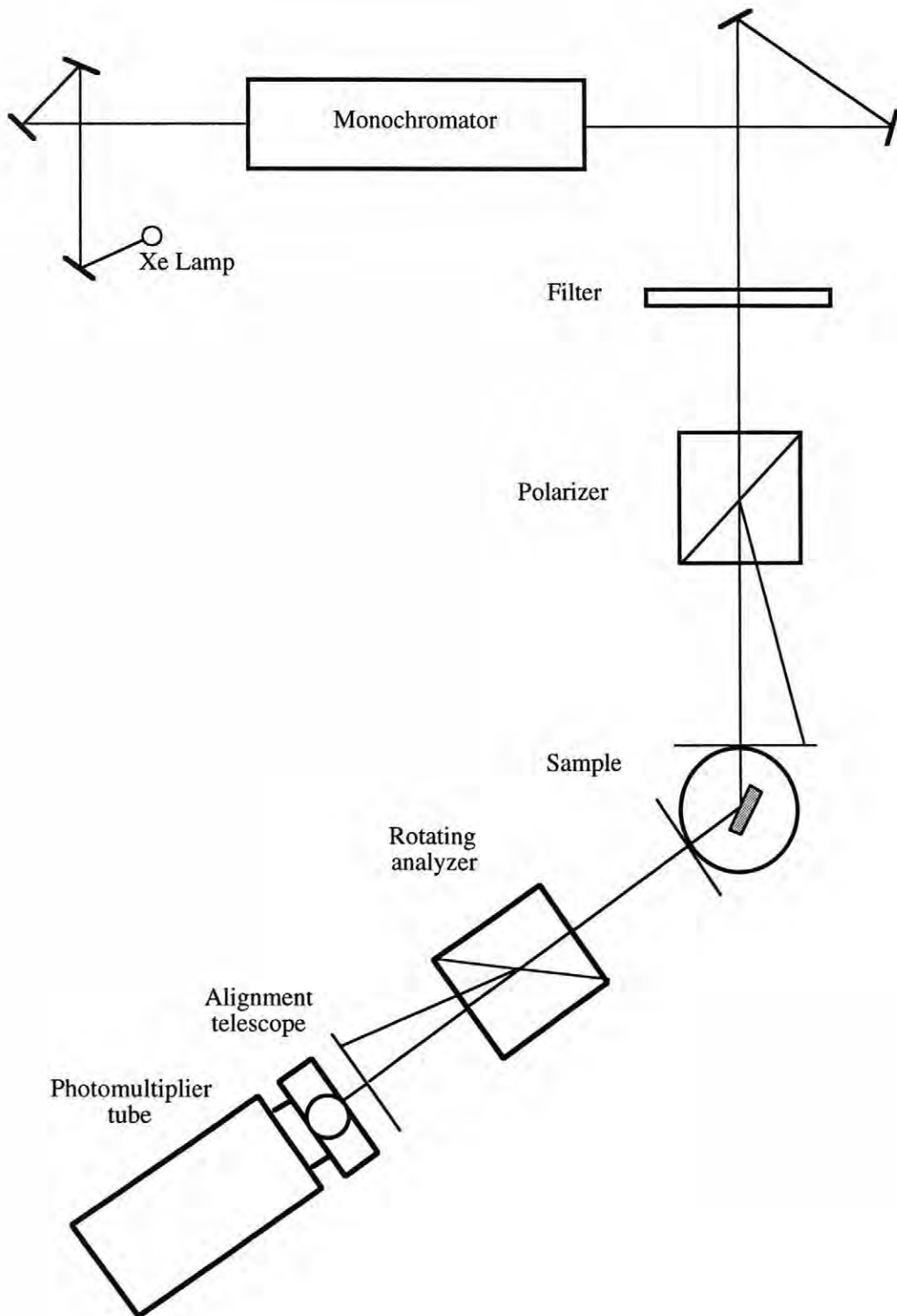
Figure 3.3 : Diagram of spectroscopic ellipsometer.

$$\begin{bmatrix} E_1 \\ E_2 \end{bmatrix}_{t,e} = \begin{bmatrix} 1 & -i\gamma_A \\ 0 & 0 \end{bmatrix} \begin{bmatrix} \cos(A-A_s) & \sin(A-A_s) \\ -\sin(A-A_s) & \cos(A-A_s) \end{bmatrix} \begin{bmatrix} \rho & 0 \\ 0 & 1 \end{bmatrix} \begin{bmatrix} \cos(P-P_s) & -\sin(P-P_s) \\ \sin(P-P_s) & \cos(P-P_s) \end{bmatrix} \begin{bmatrix} 1 \\ i\gamma_P \end{bmatrix}$$

(13)

Where P_s and A_s are the calibrations for the exact zero positions and γ_A and γ_P are the optical activity coefficients of the analyzer and polarizer, respectively. All of these values are characteristic of the system, and therefore once they are determined the calculation of the ellipsometric parameters can proceed as described above. A perfectly absorbing material with linearly polarized light incident upon it will reflect linearly polarized light if the incident light is parallel or perpendicular to the plane of incidence (polarized at 0° or 90°). In addition, the light that is reflected is 100% modulated, or the minimum of the ac component amplitude is equal to the dc background (Aspnes, 1974). However, if the incident light is not polarized precisely at 0° or 90° with respect to the sample, the reflected light will have slight elliptical polarization and the modulation will be somewhat less than 100%. The optical activity of the polarizer and analyzer must be considered as well. The rotation imparted by these components causes the angle of 100% modulation to shift away from the zero position (P_s) to a position P_1. P_1 can be determined by utilizing a residual function, $R(P) = 1 - \alpha^2 - \beta^2$. The data for this function is obtained by aligning a highly absorbing gold sample in the system at a 70° angle of incidence. The polarizer is then stepped from about 5° - 10° below zero to 5° - 10° above. A similar procedure is done at 90°. The values for the Fourier coefficients in these ranges are then fitted to a quadratic equation describing the residual function. The minimum of this function is the position of maximum modulation and therefore equal to P_1. P_s is then calculated from (Aspnes, 1974):

$$P_s = P_1 - \left(\frac{\gamma_A \tan\Psi + \gamma_P \cos\Delta}{\sin\Delta} \right)$$

(14)

Then, A_s is calculated from:

$$A_s = A_1 - \left(\frac{\gamma_P \cot\Psi + \gamma_A \cos\Delta}{\sin\Delta} \right)$$

(15)

where:

$$A_1 = \frac{1}{2}\tan^{-1}\left(\frac{\beta}{\alpha}\right)\Bigg|_{P=P_1} \qquad (16)$$

The values obtained from the two ranges are then averaged for accuracy.

The η calibration accounts for the change in the ratio of the ac to dc components of the incident light as the voltage on the photomultiplier tube is increased. Chindaudom (1991) was the first to use a different value for η at different voltages rather than one single value. This is necessary as the gain of the ac and dc components of the signal are different at different PMT voltages. The calibration is done by inserting a neutral density filter into the system when it is set at a 90° angle of incidence (straight through). The second order coefficients, α and β, are then calculated and used to find η by:

$$\eta = \frac{1}{\sqrt{\alpha^2 + \beta^2}} \qquad (17)$$

Then, by rotating the filter, η can be calculated for several different PMT voltages. η is then fit as a linear function to the PMT voltage. During measurements, calculated η values are used to correct the experimental Δ and Ψ values.

The dark current calibration gives the amount of current detected when the beam is blocked. It is measured for voltages from 550V - 1000V and fit to a fifth order polynomial in terms of the voltage. This calibration is especially important when taking data on samples with low reflectivity because the contribution from dark current can greatly affect the measured intensities and hence the measured ellipticities. To correct for this error, the calculated intensity due to the dark current is directly subtracted from the measured intensity after data collection.

3.2.2 Obtaining Ellipsometric Data

Once all of the calibrations were completed, the sample was placed on a vacuum mount in the path of the beam. The angle of incidence was then set, typically at 70°. The sample was then aligned by rotating it around the x and y directions and translating it in the

z direction. Alignment was completed by using a telescope which looked into a mirror that diverted the light beam from the detector to the operator's eye. By focusing the telescope to different locations on the light beam, different images could be viewed. These views were centered in the scope to align the sample. The spectrometer was then set to 300 nm and the computer was programmed to take data at 5 nm increments to 800 nm. For each rotation of the analyzer the reflected light intensity was measured at 90 points. To minimize scatter in the data, 50 mechanical cycles were averaged at each wavelength. The computer then converted the measured intensity data to the ellipsometric angles, Δ and Ψ, as a function of wavelength as described above. The entire measurement takes approximately 15 minutes.

3.2.3 Interpretation of Ellipsometric Data

Once the data for Δ and Ψ have been obtained, it can be converted to values for the depth profile of the dielectric function. This was done using a program developed by the spectroscopic ellipsometry group at the Intercollege Materials Research Laboratory. The basic premise of the program is to model the film as a number of discrete layers (including the substrate), each with a specific thickness, density, and refractive index. Then, values of the ellipsometric parameters are calculated and compared to the experimental data. The values are averaged over the entire area of the light beam. For this study, beam diameters of 1 mm and 2 mm were utilized.

First, reference optical data for the substrate was found. These values were obtained through direct inversion of ellipsometric data. Optical data for the PZT was modeled in the program as an oscillator function. Specifically, a damped Sellmeier oscillator was used. The relation is:

$$n^2 = A_1 + \frac{A_2 \lambda^2}{\left(-A_3 + \lambda^2 - 2iA_4\lambda\right)} \qquad (18)$$

Where A_1, A_2, A_3 and A_4 are constants determined from the program. Then, a sample geometry was postulated. This consisted of assigning starting values and step values to

each layer's thickness, the volume fraction of any second or third phase present, and the refractive index and its dispersion. This set up a grid that the program could search. Δ and Ψ versus wavelength at each point in the grid were calculated and compared to the experimental data. The calculated data was compared using an unbiased estimator of error, σ, where:

$$\sigma = \left(\frac{1}{N-P-1}\right)\left[\sum_{i=1}^{N}\left(\cos\Delta_{exp}^{i} - \cos\Delta_{cal}^{i}\right)^2 + \left(\tan\Psi_{exp}^{i} - \tan\Psi_{cal}^{i}\right)^2\right]^{\frac{1}{2}} \qquad (19)$$

Here, N is the number of data points taken and P is the number of unknown variables in the model. The grid search located the position in parameter space with the minimum error function. With that, the program moved on to an iteration around that point and a linear regression analysis to obtain a lower error function. The linear regression analysis also allows for the calculation of 90% confidence limits and an approximate Jacobian for the system. This shows any correlation between parameters.

For each sample, several different geometries were postulated. The best fit model was chosen by simultaneously satisfying the following conditions: 1) a good fit to the experimental Δ and Ψ values, 2) a low sigma value (<.07), 3) a physically realistic model, 4) low correlation between parameters, and 5) reasonable values for the 90% confidence limits.

3.3 Physical and Electrical Film Characterization

The PZT thin films were characterized using several standard techniques including X-ray diffraction, scanning electron microscopy, and others. These measurements, in addition to the spectroscopic ellipsometry data, permit a good description of the microstructure and electrical properties of the films prior to the fatigue studies.

The PZT films deposited ranged in thickness from 150 nm to 650 nm. The base electrode was the platinum surface of the substrate and the top electrode was gold sputtered on the film for 40 seconds. For *in situ* fatigue measurements the top electrode area was

0.09 cm^2. For dielectric permittivity and loss measurements, the area was 7.065 x 10^{-4} cm^2. To measure the capacitance and loss of the films, a Hewlett Packard multi frequency LCR meter (model 4275A) was used at 10 kHz with a bias of 1 mV. Thicknesses used to calculate the dielectric constant, ε, from the capacitance were obtained from spectroscopic ellipsometry measurements prior to fatiguing the film.

Microstructural characterization of the films was carried out using a scanning electron microscope from ISI (model ISI-DSI30). Compositional and structural analysis was done on a Scintag thin film diffractometer (model XDS2000) using Cu K$_\alpha$ radiation. Initial x-ray studies were completed using normal diffraction. To obtain better data, the final X-ray studies were done using a grazing angle method in order to eliminate the high intensity peak caused by the substrate which tended to dominate some peaks from the perovskite PZT phase. The grazing angle was set to between 6° and 9° depending on the thickness of the sample.

Hysteresis and *ex situ* fatigue measurements were completed on an RT66A Standardized Ferroelectric Tester. The conditions for fatigue were 10 kHz and 5 - 12 Volts. *In situ* fatigue measurements were carried out at 1 kHz using a triangle type wave supplied from a Goldstar FG - 2002C function generator. The polarization was measured using a custom built Sawyer-Tower circuit and the data was plotted on a Fluke digital oscilloscope (model 800).

Chapter 4

RESULTS and DISCUSSION

The microstructure of a ferroelectric thin film is determined by the deposition method and conditions as well as the annealing process chosen to crystallize and densify the film. The two most common post-deposition processes, conventional furnace annealing and rapid thermal processing, were utilized in this study. This allowed for a wide range of microstructure - processing - property relationships to be investigated.

The most widely used annealing process for ceramics is the conventional furnace process. This technique is frequently used for sintering of bulk ceramics and has also been used extensively for thin film processing. The low cost of this method compared to others is its most attractive feature. If variables such as temperature, atmosphere, and heating rate are controlled correctly thin films can be prepared with properties comparable to bulk ceramics (Xu and Mackenzie, 1992).

This chapter will focus on the processing parameters' influence on the final microstructure of the films and subsequent influence on the electrical properties. Initially, the microstructural characterization will be described, focusing on the surface characteristics of the films obtained from spectroscopic ellipsometry and scanning electron microscopy as well as the crystallographic information from x-ray diffraction. The dispersion behavior of the films will then be discussed along with theoretical models utilized to interpret the data. Finally, the electrical properties of the films, including the relative dielectric constant, hysteresis and fatigue behavior will be discussed in relation to the microstructural data.

4.1 Microstructural Study

In this study, sol-gel derived ferroelectric thin films of the composition PZT (52/48) were prepared with varying thicknesses and were subsequently conventionally annealed at

650° C for 60 minutes and 700° C for 30, 45 and 60 minutes. It has been shown that sol-gel derived PZT films can begin to crystallize at temperatures as low as 500° C due to the inherent compositional homogeneity of the sol (Yi and Sayer, 1991). The processing conditions used here were chosen in order to avoid the formation of a pyrochlore phase that is centrosymmetric and thus not ferroelectric. This type of structure is highly detrimental to the properties of the ferroelectric (Kwok and Desu, 1991).

Figure 4.1(a, b) shows the microstructures of two films annealed conventionally. For the film processed at 700° C for 30 minutes, the average grain size determined by linear averaging is 0.68 µm. As the time is increased to 45 minutes, the average grain size increases to 1.05 µm. Figure 4.2 shows another film that was annealed at 650° C for 60 minutes. Here there is a dense, much more fine-grained microstructure present with a grain size of 0.05 - 0.08 µm. These results indicate that the temperature at which a thin film is crystallized is more significant in determining the final grain size than the time that the film is held at a specific temperature.

Grain size is not the only parameter that needs to be controlled when annealing a thin film sample. The extent of crystallinity of the desired phase is of obvious importance to the properties of the sample. If a lead based ferroelectric, such as PZT, is held for a long enough time at high temperature, lead loss from the surface becomes a concern (Tani and Payne, 1994). Also, the formation of a pyrochlore phase can occur and a marked effect can be seen in the properties of the sample (Kwok and Desu, 1991). Figure 4.3 (a, b) show x-ray diffraction data taken on two samples that were conventionally annealed. The characteristic pyrochlore peak at $2\vartheta = 29°$ is present in the first diagram while the second shows a fully developed perovskite phase. Visually on the surface, films that were annealed for longer times and higher temperatures appeared cloudy, indicating a significant amount of surface roughness . This observation was often coupled with the appearance of the pyrochlore peak in the x-ray patterns of the samples.
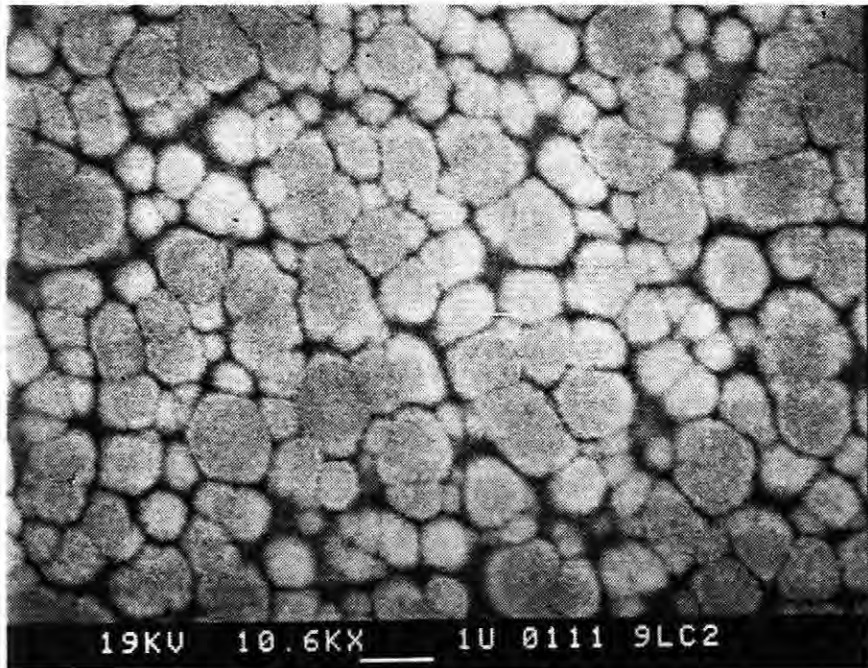
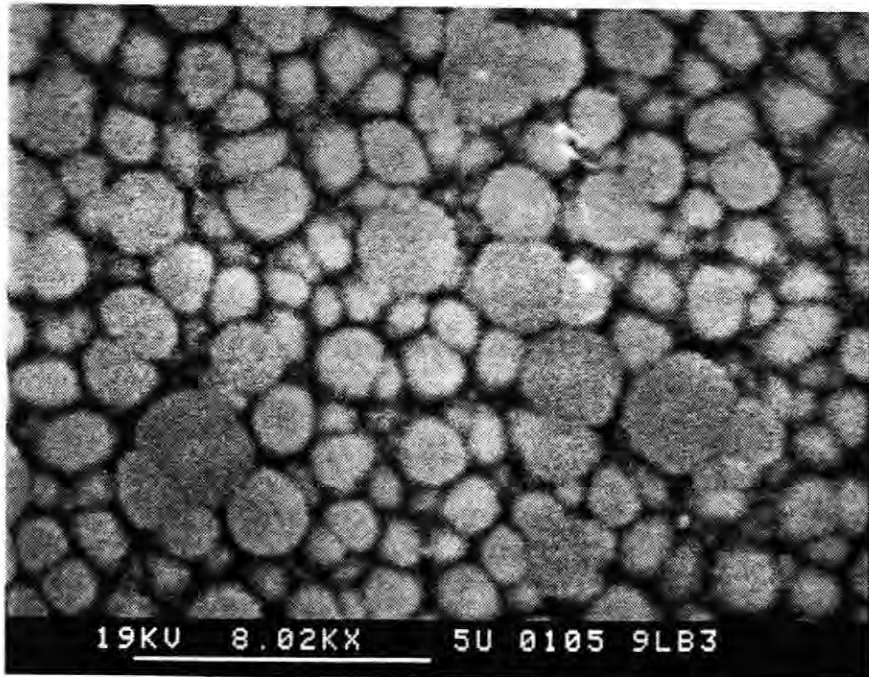Figure 4.1(a) : 9 layer film annealed at 700°C for 30 minutes.

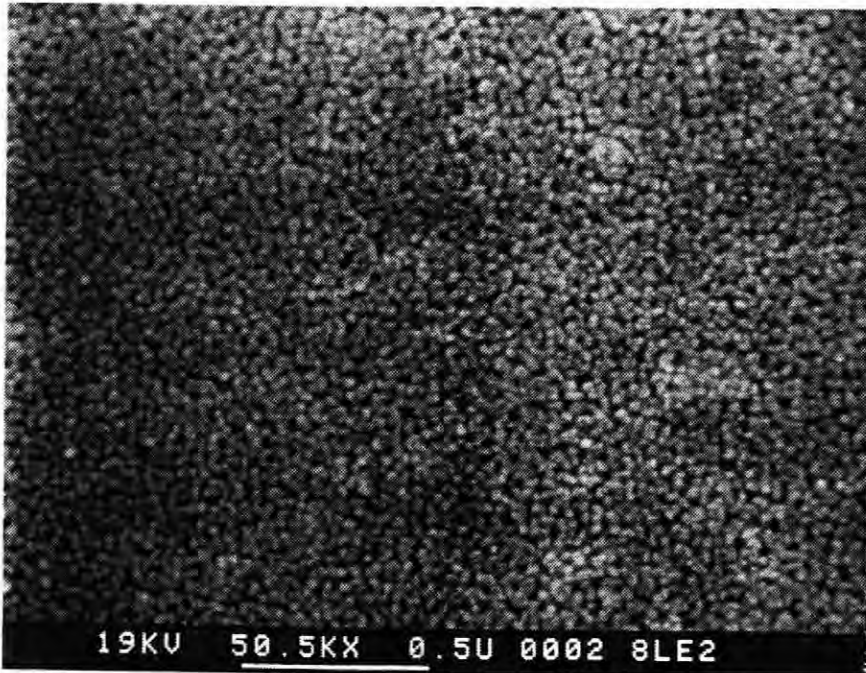Figure 4.1(b) : 9 layer film annealed at 700° C for 45 minutes.

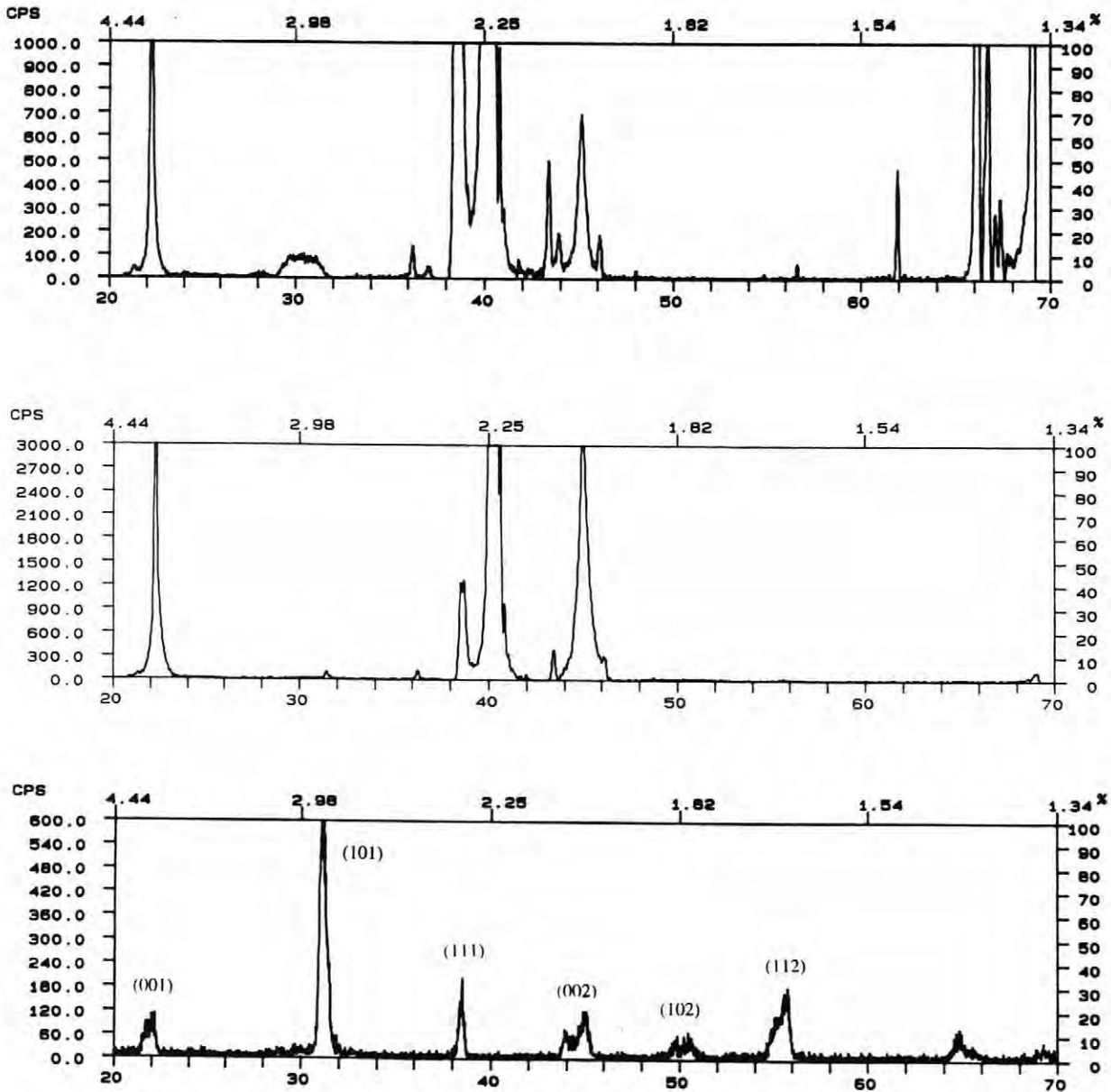Figure 4.2 : 8 layer film annealed at 650° C for 60 minutes.

Figure 4.3 : a) X-ray pattern showing pyrochlore peak at 29°. b) X-ray pattern showing no pyrochlore content. c) Reference x-ray pattern.

Other problems that can develop while annealing a thin film at high temperatures are the formation of an interfacial reaction layer between the substrate and the film or a roughening of the substrate surface. McKinstry and Fox (1992) showed that when heating a platinum coated silicon substrate to 650° C and holding, a considerable growth of the platinum grains occurs and hillocking on the surface results. Also, through ellipsometric measurements and Auger analysis, they showed migration of the titanium atoms from the bonding layer through the platinum to the surface then oxidizing to form a transparent layer. The roughening of the substrate surface can be corroborated, as will be discussed later. These types of problems can create serious difficulties in utilizing these materials for electronic applications.

In order to avoid many of the difficulties associated with conventional furnace processing, especially surface and interface effects, the rapid thermal process (RTP) was investigated. For electronic applications, it is essential to minimize any reactions or interdiffusion that may occur which would be detrimental to the properties of the film. By reducing the time that the sample is held at high temperature and increasing the heating rate up to 100° C/minute the possibilities of substrate roughening, interfacial reactions, or lead volatilization are greatly limited. In this study, films of PZT (52/48) were annealed at temperatures between 700° C and 750° C for 10 - 30 seconds.

Figure 4.4(a, b, c) shows x-ray diffraction patterns for films annealed at various time/temperature combinations. At 700° C for 10 seconds, there is a peak at 29° corresponding to a pyrochlore phase. However, there is evidence of the perovskite phase beginning to form. As the time is increased to 15 seconds, the perovskite phase peaks are becoming more intense while the pyrochlore peak is diminishing. At 30 seconds, the x-ray pattern shows a complete transformation to the perovskite phase. Visually, the films have a much higher reflectivity than the conventionally annealed samples, indicating smoother surfaces. This is reasonable since the films are not exposed to the high temperature for
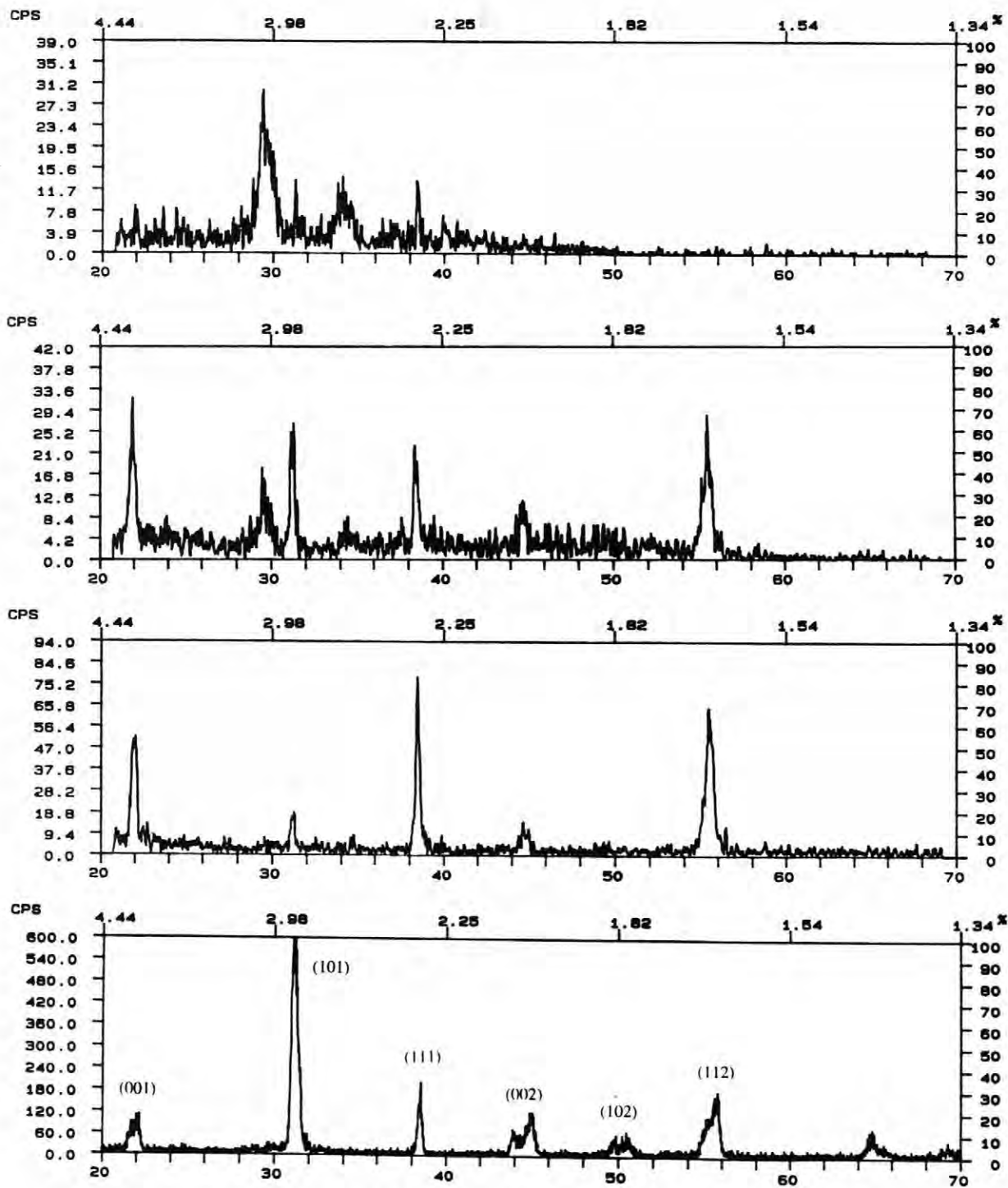
Figure 4.4 : Rapid thermally annealed films showing
decreasing pyrochlore content annealed at a) 700° C
for 10 seconds, b) 700° C for 15 seconds, c) 700° C
for 30 seconds and d) Reference data.

very long and the grains do not have time to grow. This will be corroborated in the ellipsometric study section.

4.1.1 Effect of Hydrolysis on Microstructure

In preparing these samples for analysis, it became clear that the most important pre-deposition variable of the solution was the amount of water added for the controlled hydrolysis reactions. The final microstructures of films with varying amounts of water added showed considerable differences even when the processing parameters remained constant. Figure 4.5(a, b) shows two films both conventionally annealed at 700° C for 30 minutes. The difference in the microstructures is striking and the only change in sample preparation was the amount of water added to the sol prior to spin coating. The film in figure 4.5(a) has a ratio of 1.5 moles of water to 1 mole of PZT. The microstructure is dense with a grain size from 0.2 - 0.5 μm. The film in figure 4.5(b) has a 4:1 molar ratio of water to PZT and it is diphasic with 1 - 2 μm perovskite rosettes in a fine grained pyrochlore matrix compositionally confirmed by energy dispersive spectroscopy. This indicates that the controlled hydrolysis of the sol prior to spin coating is pivotal in determining the final microstructure of the film. The amount of water added can influence the pH of the sol and in turn change the structure of the polymeric network of the gel (Chen, 1993; Lakeman and Payne, 1992). This would then affect how the gel densifies and crystallizes. In addition, due to the high surface area to volume ratio of these films, the amount of water absorbed from the atmosphere must also be taken into account. Lakeman and Payne (1992) determined an optimal water to PZT molar ratio to be 2:1. For this study, molar ratios of 4:1, 3:1, and 1.5:1 were used. It was found that samples of the 3:1 and 4:1 ratios generally resulted in the diphasic microstructure described above. A ratio of 1.5:1 was chosen for the remainder of this study because the films were deposited in an open air environment where the relative humidity was consistently 50% - 75% and the samples were sure to absorb some of this water. The discrepancy with Payne's group can
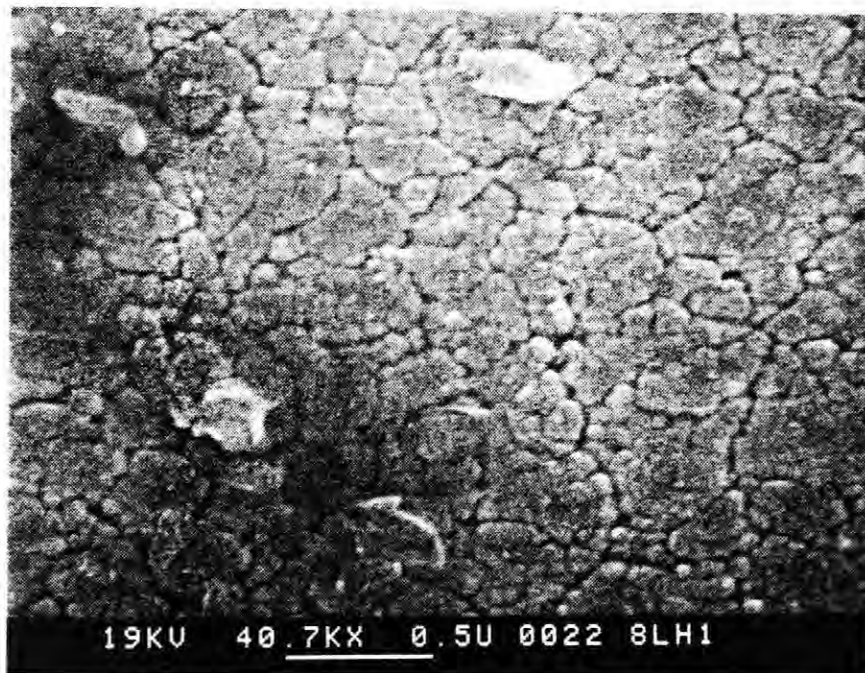
4 2

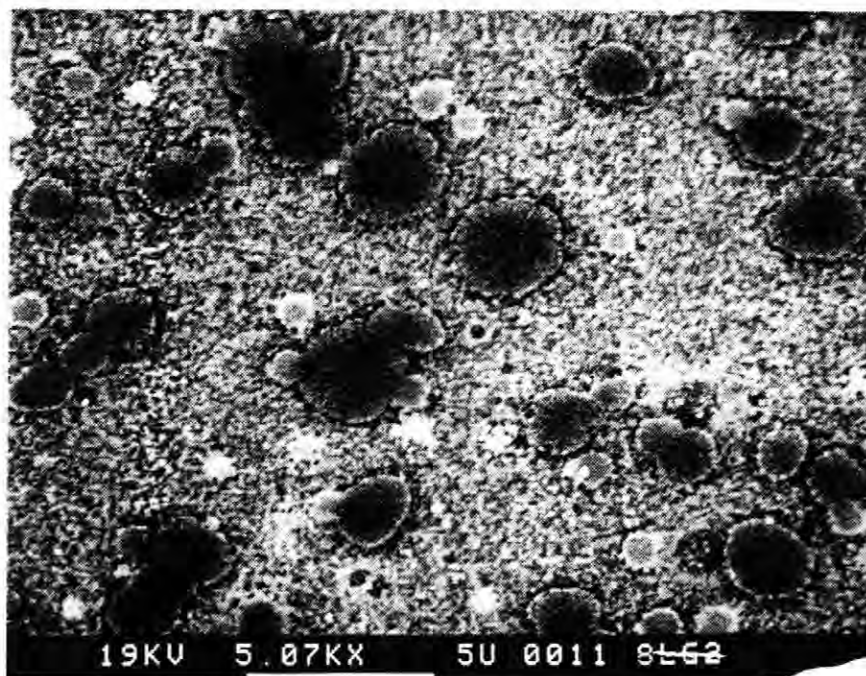Figure 4.5(a) : Microstructure of film with 1.5:1 molar ratio of water to PZT.

Figure 4.5(b) : Microstructure of film with 4:1 molar ratio of water to PZT.

be attributed to variations in precursor stock and the lack of a vacuum distillation of the solution in our method.

4.2 Ellipsometric Study

Spectroscopic ellipsometry (SE) is a unique tool which can be used to non-destructively depth profile a thin film. Since the film is modeled as a collection of homogeneous layers, values for the thickness of a dense layer and a surface roughness layer, comprised of PZT and a volume fraction of air, can be determined. Thus, for films annealed at various times and temperatures, the microstructure can be obtained and the same film can then be tested for its properties.

4.2.1 Conventionally Annealed Films

The first step in characterizing these samples is to obtain the ellipsometric parameters as a function of wavelength (300 nm - 800 nm). Subsequently, according to the method outlined in chapter three, the data is reduced to acquire a depth profile of the film. Figure 4.6(a - d) shows representative schematic microstructures for samples annealed conventionally. The output consists of the A_2 - A_4 coefficients describing the oscillator (A_1 is fixed), the unbiased estimator of the error (σ), the thickness of each layer and the volume fraction of any guest in each layer. In order to be most confident in a model of the data, the conditions given in chapter three must be satisfied, especially the restriction on σ ($\sigma \leq 0.07$). In this study, σ typically varied between 0.025 and 0.07 for the final models. The inclusion of PZT in the substrate in parts (c) and (d) is representative of the substrate roughening phenomenon and will be discussed later. It has been shown that some ferroelectric films fabricated by a wide variety of methods have a low density layer at the film/substrate interface (Trolier-McKinstry and Fox, 1994). This type of geometry was tried in several of these models, however it did not improve the fit. Figure 4.7 shows a characteristic model of the measured ellipsometric parameters, Δ and Ψ, for a

369 Å ± 37 Å   Vol. frac. of air = 18% ± 2%

a)   3884 Å ± 158 Å   Dense PZT

$\sigma = 0.055$
$A_1 = 1.0$
$A_2 = 4.9 \pm 0.3$
$A_3 = 226.5 \pm 1.0$
$A_4 = 5.4 \pm 0.3$

Substrate

328 Å ± 18 Å   Vol. frac. of air = 33% ± 2%

b)   2600 Å ± 58 Å   Dense PZT

$\sigma = 0.053$
$A_1 = 1.0$
$A_2 = 4.9 \pm 0.2$
$A_3 = 221.2 \pm 1.3$
$A_4 = 3.2 \pm 0.3$

Substrate

273 Å ± 32 Å   Vol. frac. of air = 46% ± 1%

c)   4593 Å ± 117 Å   Dense PZT

$\sigma = 0.052$
$A_1 = 1.0$
$A_2 = 4.7 \pm 0.3$
$A_3 = 218.8 \pm 1.0$
$A_4 = 1.1 \pm 0.3$

Substrate   Vol. frac. of PZT = 19% ± 2%

553 Å ± 19 Å   Vol. frac. of air = 32% ± 2%

d)   5223 Å ± 169 Å   Dense PZT

$\sigma = 0.067$
$A_1 = 1.0$
$A_2 = 4.7 \pm 0.3$
$A_3 = 226.5 \pm 1.8$
$A_4 = 8.9 \pm 0.3$
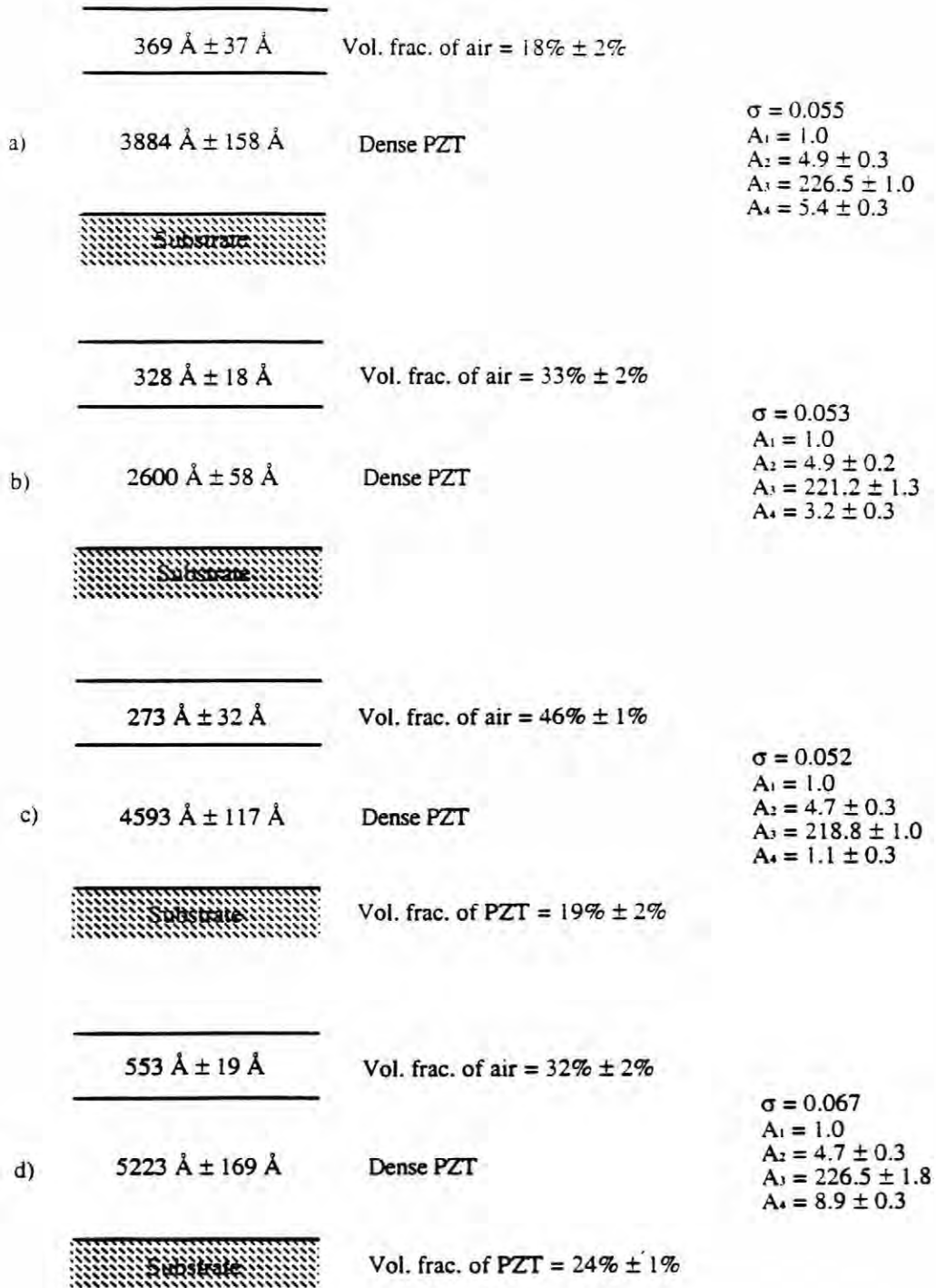
Substrate   Vol. frac. of PZT = 24% ± 1%

Figure 4.6(a - d) : a) 9 layer sample annealed at 650° C for 60 minutes, b) 6 layer sample annealed at 700° C for 30 minutes, c) 6 layer sample annealed at 700° C for 45 minutes, d) 7 layer sample annealed at 700° C for 60 minutes.
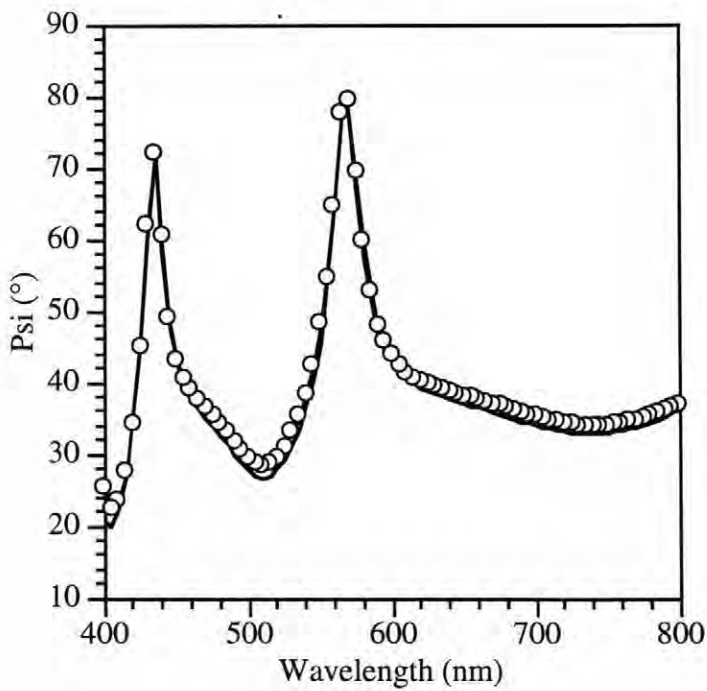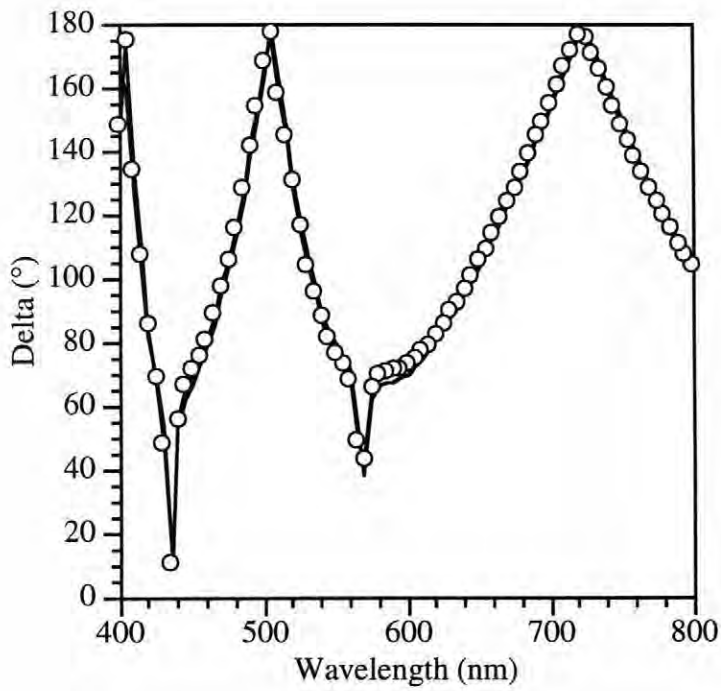
Figure 4.7 : Experimental and calculated values for Δ and Ψ for a 6 layer film annealed at 650° C for 60 minutes.

film. This is for a 6 layer sample annealed at 650° C for 60 minutes. The value of σ for this model was 0.025 and it is clear that the fitting is quite good.

The values of most interest that are obtained from the modeling of the ellipsometric parameters are the total thickness of the surface roughness and the volume fraction of air contained within that layer. Figure 4.8 shows those values as a function of thickness for films annealed at 650° C for 60 minutes. The majority of the samples have a surface roughness layer between 300Å and 500Å thick with a volume fraction of 20% - 35% air. The low scatter in the data indicates there is no strong correlation between these values and the total film thickness. Thus the processing conditions have a more dominant influence on the surface roughness. For samples annealed at 700° C for 30 minutes, figure 4.9 shows a surface roughness of 300Å - 500Å and a volume fraction of air between 30% and 40%. Again, there is no evident correlation of these values to the total film thickness. The amount of surface roughness for these samples is comparable to those annealed at 650° C for 60 minutes, and the volume fraction of air is as well. In figure 4.10 films annealed at 700° C for 45 minutes show a surface roughness of 300Å to 500Å and a volume fraction of air between 35% and 45%. Compared to films fired at 700° C for 30 minutes, this is not a significant change. Thus it can be deduced that the extent of grain growth is more responsive to increases in temperature rather than to increases in annealing time. Also, a relation between these values and the total film thickness is not apparent. Figure 4.11 shows the same values for samples annealed at 700° C for 60 minutes. Here, the surface roughness has increased to 500Å - 600Å and the volume fraction of air is between 15% and 35%. Again, there is no correlation to the thickness of the film.

Based on these measurements, a model of the grain structure for the samples annealed at 700° C can be developed. For the samples processed for 30 and 45 minutes, there is little change in surface roughness thickness or volume fraction of air incorporated. The basis for these models is as follows: The primary difference between the two
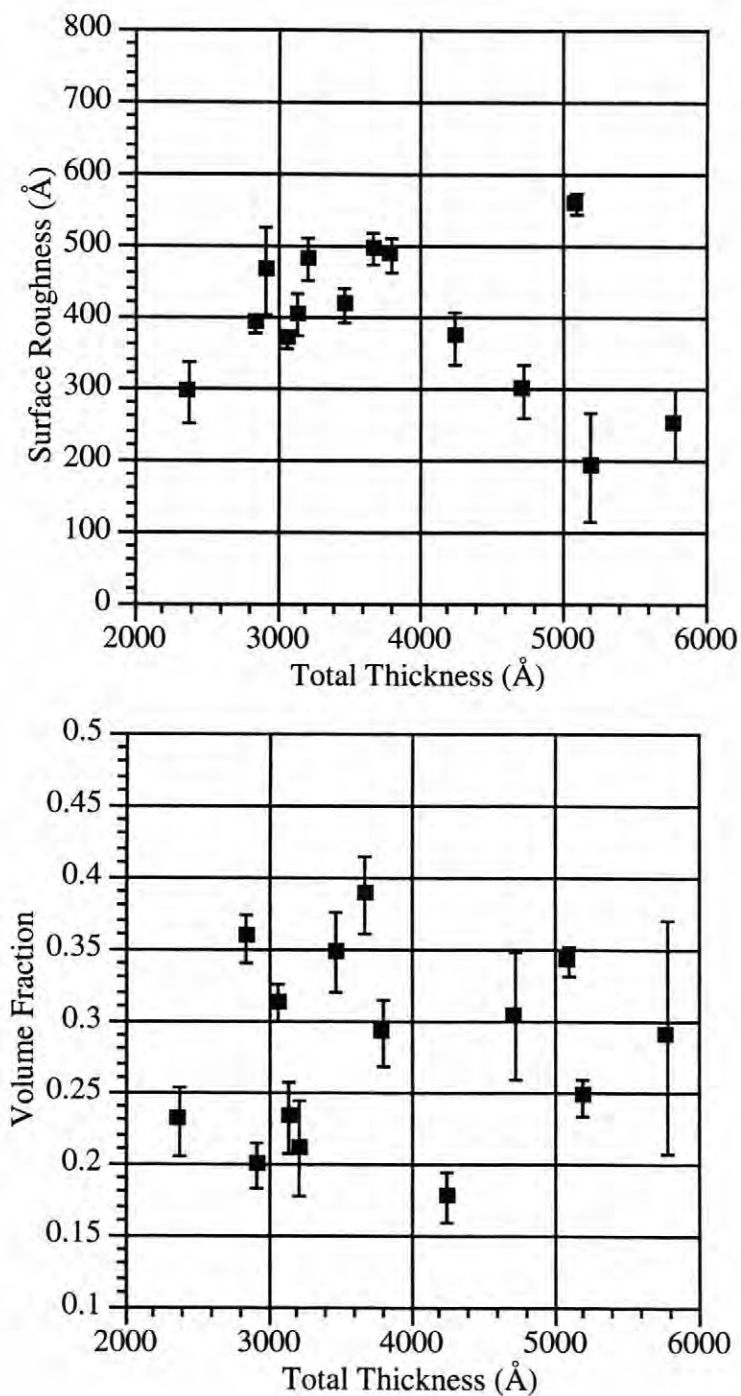
Figure 4.8 : Surface roughness and volume fraction of
air as a function of thickness for films annealed at
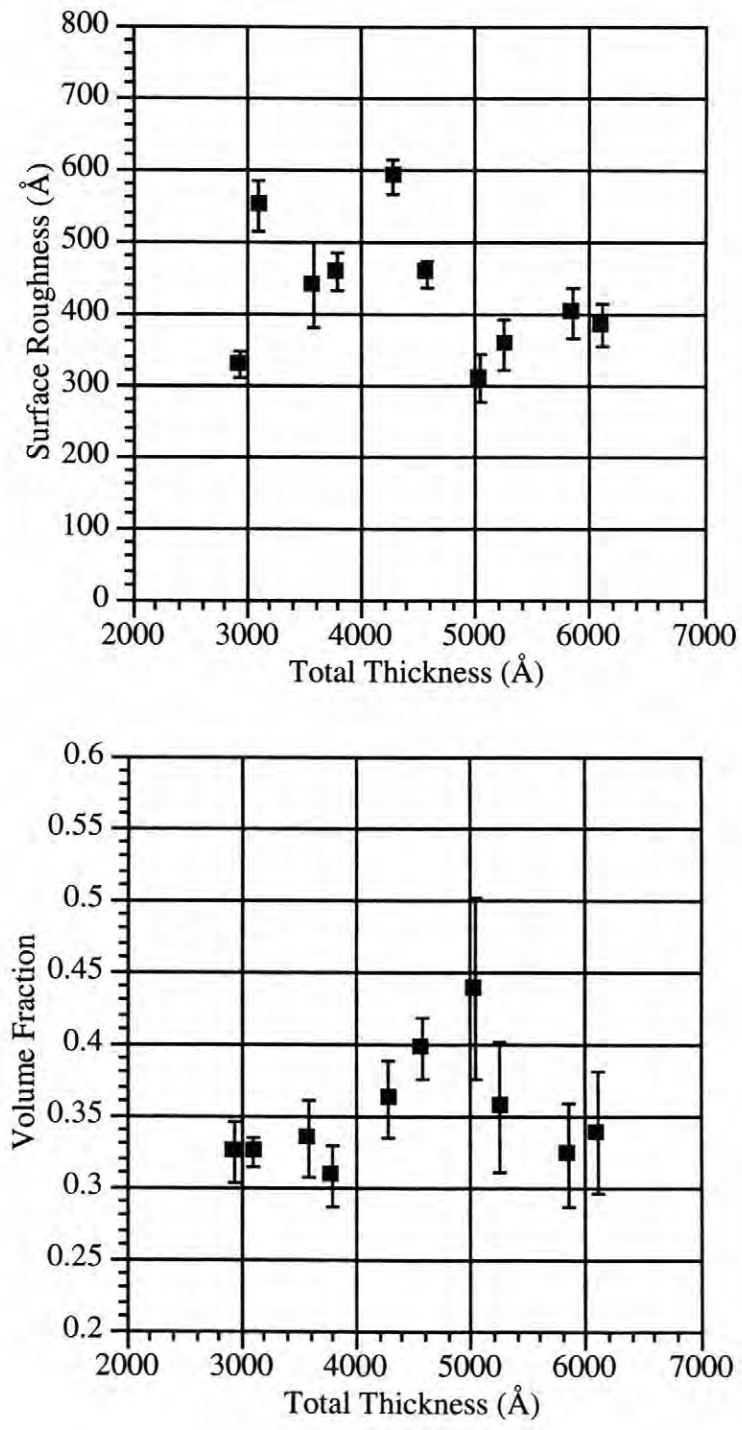650° C for 60 minutes.

Figure 4.9 : Surface roughness and volume fraction of air as a function of thickness for films annealed at 700° C for 30 minutes.
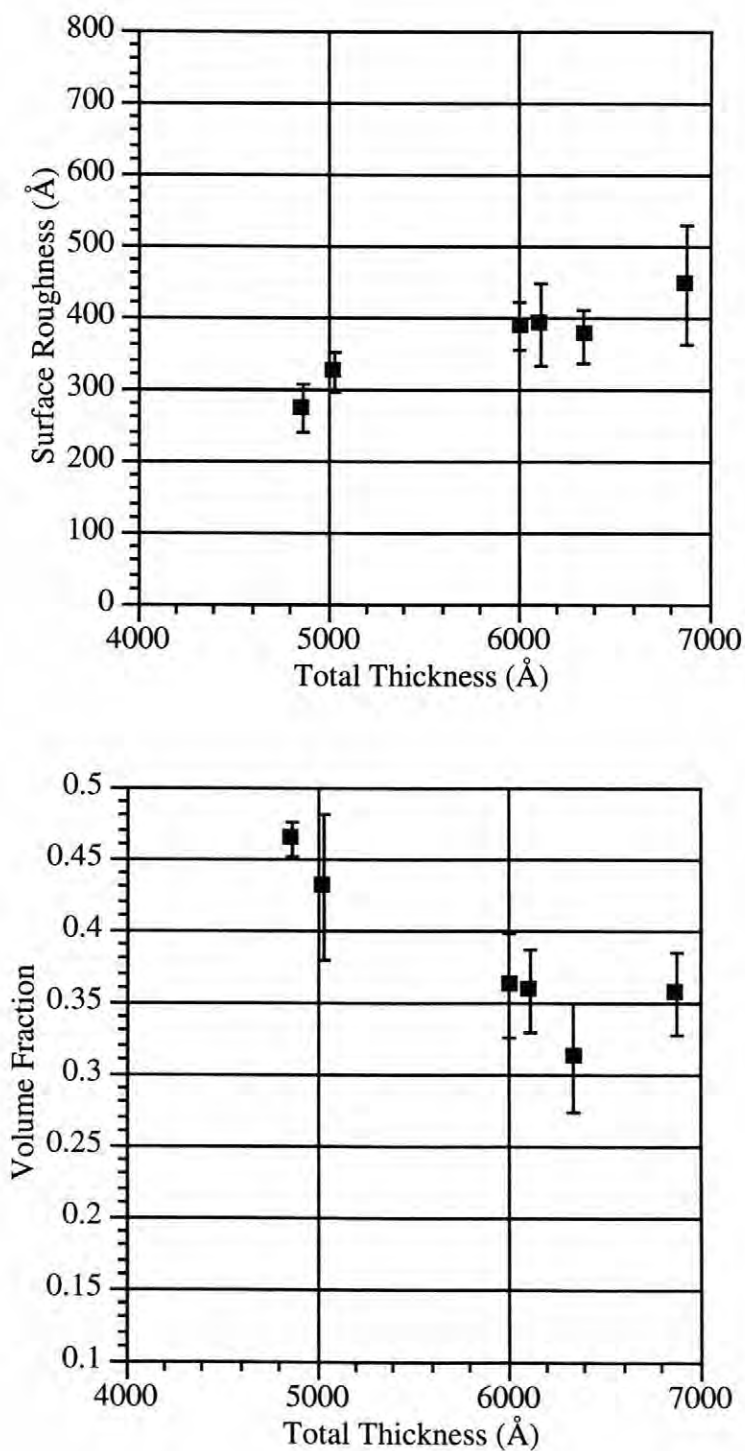
Figure 4.10 : Surface roughness and volume fraction of air as a function of thickness for films annealed at 700° C for 45 minutes.
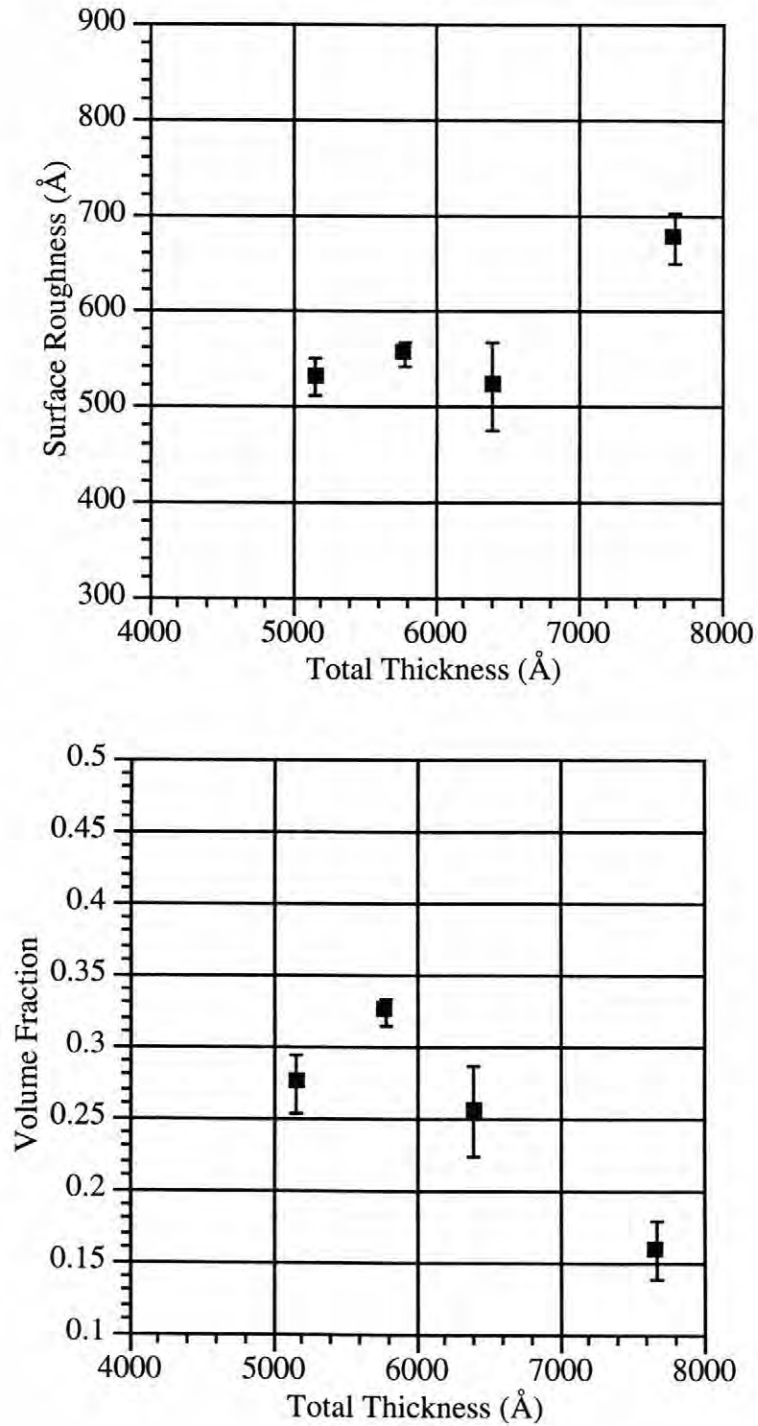
Figure 4.11 : Surface roughness and volume fraction
of air as a function of thickness for films annealed at
700° C for 60 minutes.

microstructures is the grain size, 0.68 μm for 30 minute samples versus 1.05 μm for 45 minutes. The optically-determined roughnesses, are however, quite comparable. One geometry which satisfies these restrictions for both conditions is shown in figure 4.12(a, b). Here, there are approximately twice as many grains per unit area in the 30 minute samples. If it is assumed that the morphology of the individual grains does not depend on the grain size, (i.e., grains are hemispherical for both large and small grain sizes) then as the grains grow, the volume fraction of air within the roughness layer does not change (see figure 4.12 for clarification). This is consistent with the observation of nearly constant surface roughness parameters for the two conditions. Thus it appears that the morphology of the grains for these two conditions are similar, but on different scales. The 700° C for 60 minute samples have higher surface roughness and less air in the layer. This implies a more plateau-like morphology as shown in figure 4.12(c).

The surface roughness as a function of time for samples annealed at 700° C is shown in figure 4.13(a). Here it is also apparent that the amount of time a film is annealed has less of an influence on the amount of roughness than the temperature does. This can be seen in figure 4.13(b) where the roughness shows a definite increase with annealing temperature due to the grain growth described earlier.

4.2.2 Rapid Thermal Processed Films

As mentioned above, rapid thermal processing of thin films entails a smaller thermal budget (i.e., time spent at temperature). The very rapid heating and cooling rates, along with the short soak time, reduce the possibilities of interfacial reactions, pyrochlore formation and lead volatilization. Also, the shorter time at high temperature drastically reduces the amount of surface roughness of the films. This can be seen in figure 4.14 where the SE determined surface roughness varies between 175Å and 250Å and the volume fraction of air between 25% and 45%. The scatter in the data is low again so it can
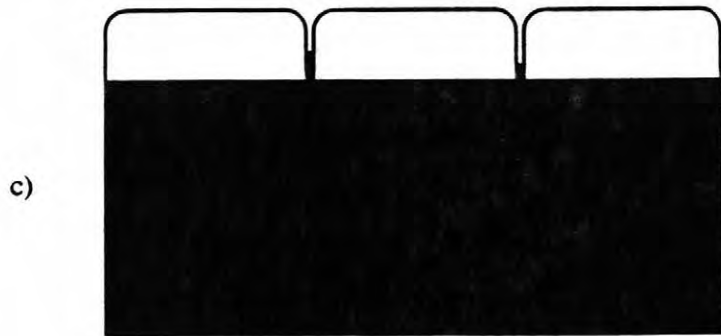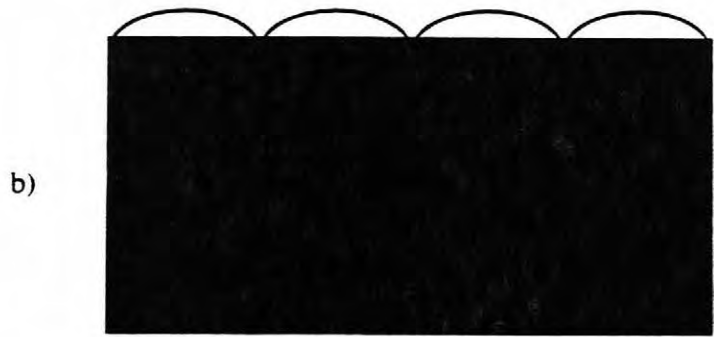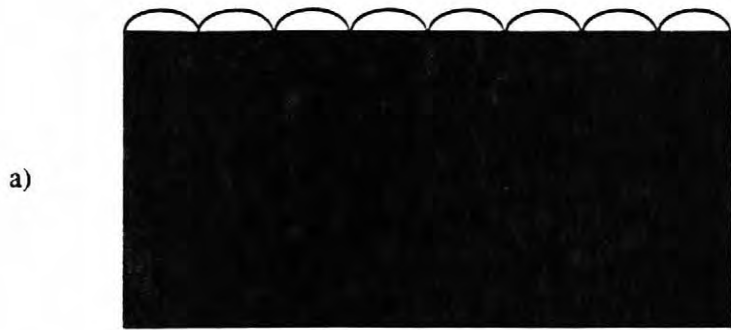
Figure 4.12(a, b, c) : Schematic grain morphologies for samples annealed at a) 700° C for 30 minutes, b) 700° C for 45 minutes and c) 700° C for 60 minutes.
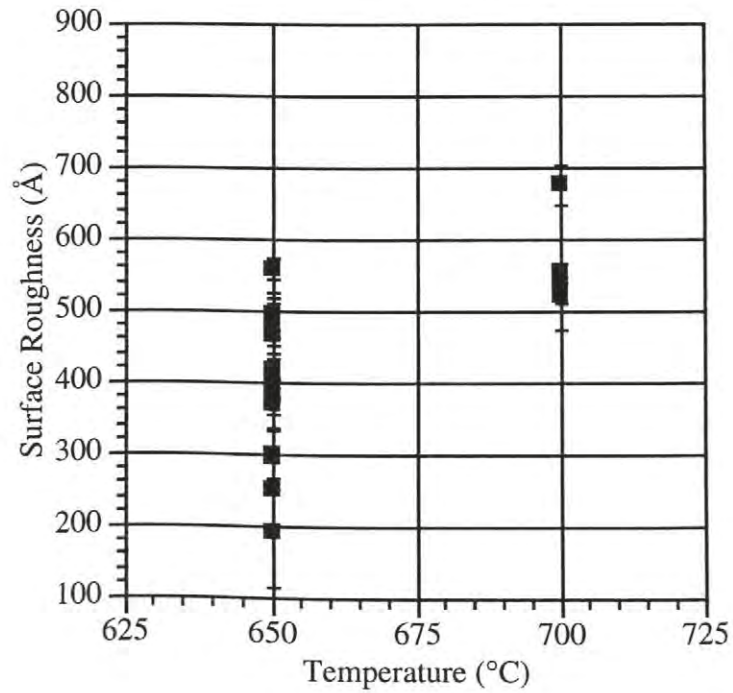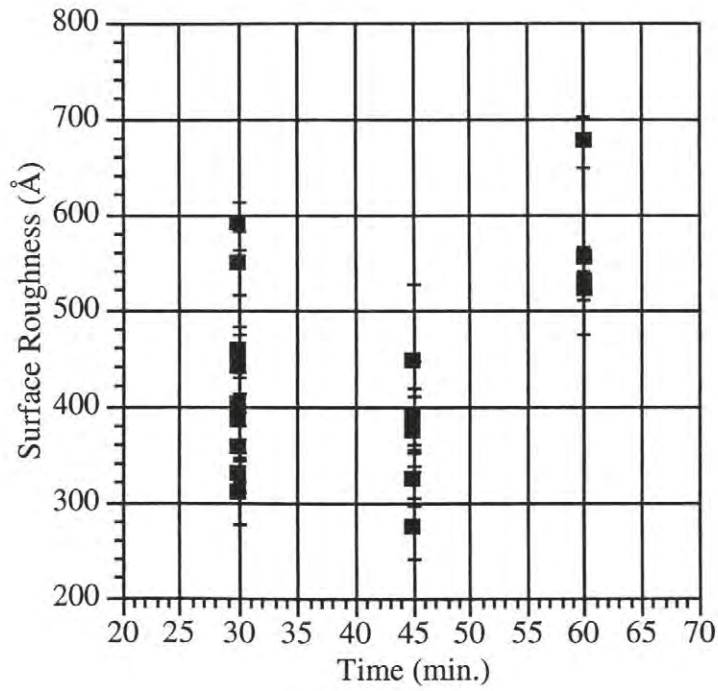
Figure 4.13(a, b) : Surface roughness as a function of
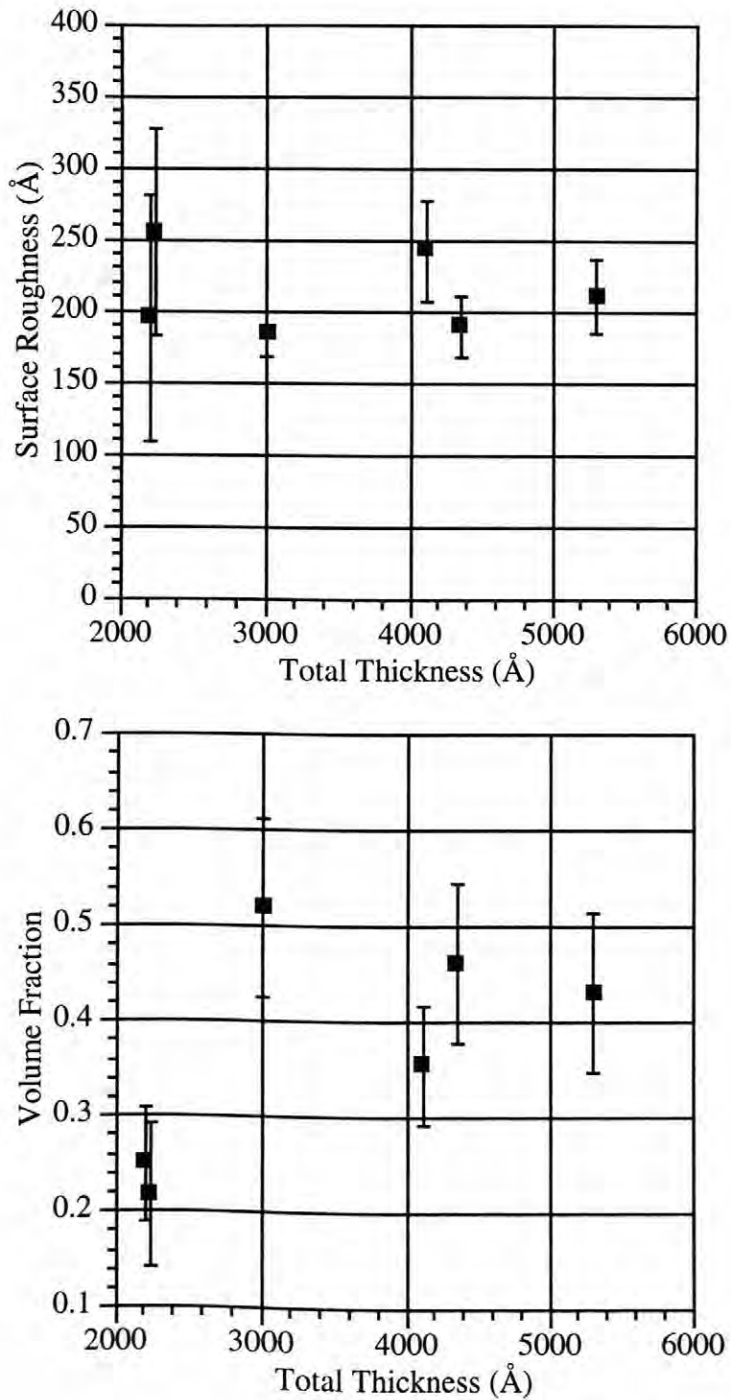a) time and b) temperature.

Figure 4.14 : Surface roughness and volume fraction
of air as a function of thickness for rapid thermally
annealed films.

be concluded that there is no strong correlation between surface roughness and total film thickness. These films were annealed at 700° C and 750° C for 10, 20, and 30 seconds. There was no apparent relation between annealing temperature and/or time with surface roughness.

4.2.3 Refractive Index Calculations

As shown, spectroscopic ellipsometry is a very useful tool to determine the thickness and surface characteristics of thin film samples. Other information that can be obtained from SE measurements includes the refractive index and the dispersion behavior of the film via the Sellmeier Oscillator. Comparisons between values for the films annealed under different conditions and reference values can be useful to determine the quality of the samples.

Reference data for the dispersion behavior of PZT was obtained from work done by Trolier-McKinstry, et al. (1993) and is given in figure 4.15(a). The refractive index at 550 nm is 2.556; in this thesis all refractive index values for comparison between processing conditions will be quoted for that wavelength. For comparison, the values for the films annealed at 650° C for 60 minutes are shown in figure 4.15(b). There is considerable scatter in the calculated refractive index data, but on average the curves for these samples are higher than expected. The average refractive index is 2.620. Figures 4.16(a and b) show the dispersion behavior for films processed at 700° C for 60 and 45 minutes. Again the values appear to be high with average refractive indices of 2.570 and 2.736, respectively. For films annealed at 700° C for 30 minutes, the dispersion is given in figure 4.17(a). The average n here is 2.667. In contrast, the rapid thermally processed samples showed more normal refractive indices (see figure 4.17(b)). The average refractive index is 2.500.

The perovskite crystal structure is a densely packed one, the density of PZT is 7.9 g/cm^3. Thus it is difficult to visualize a mechanism whereby the refractive index could be
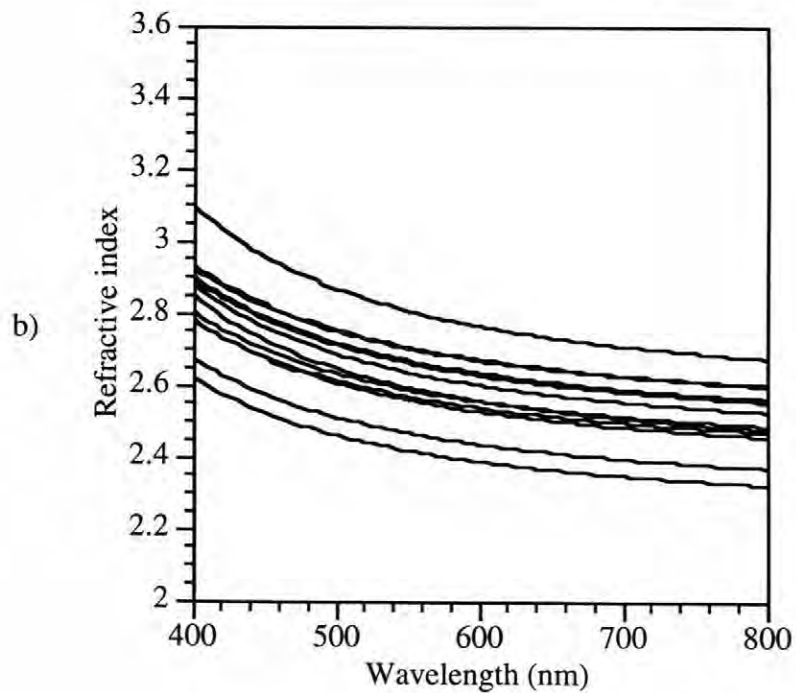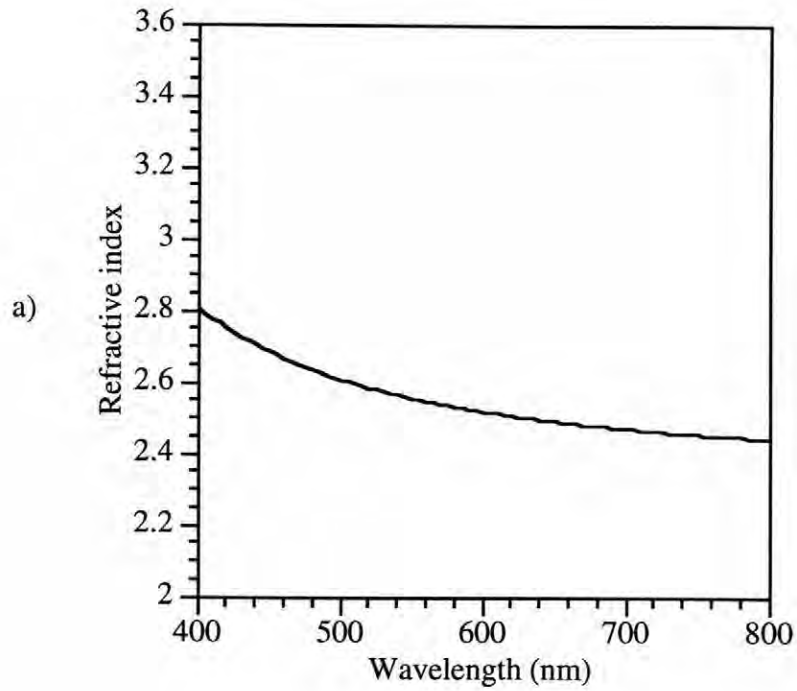
Figure 4.15(a, b) : Dispersion data for a) reference
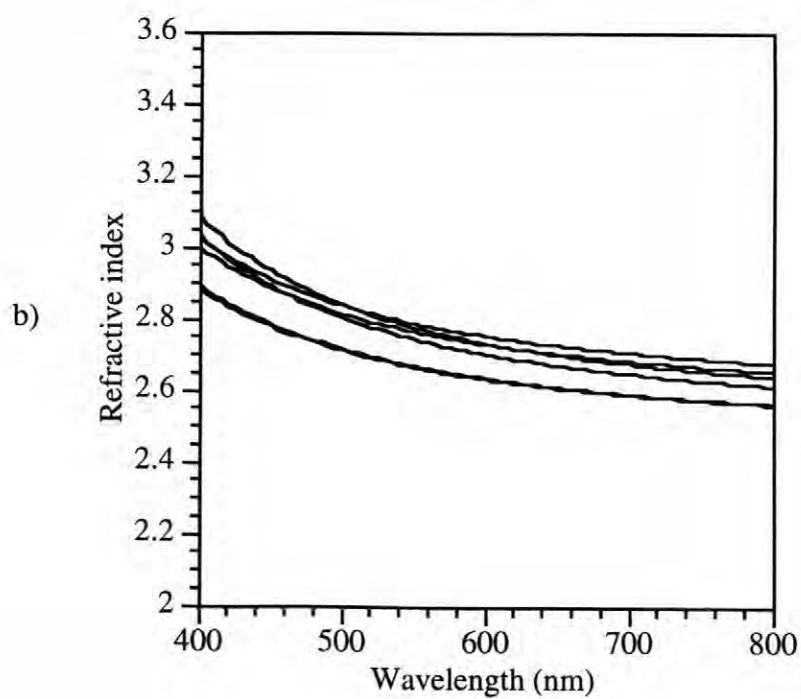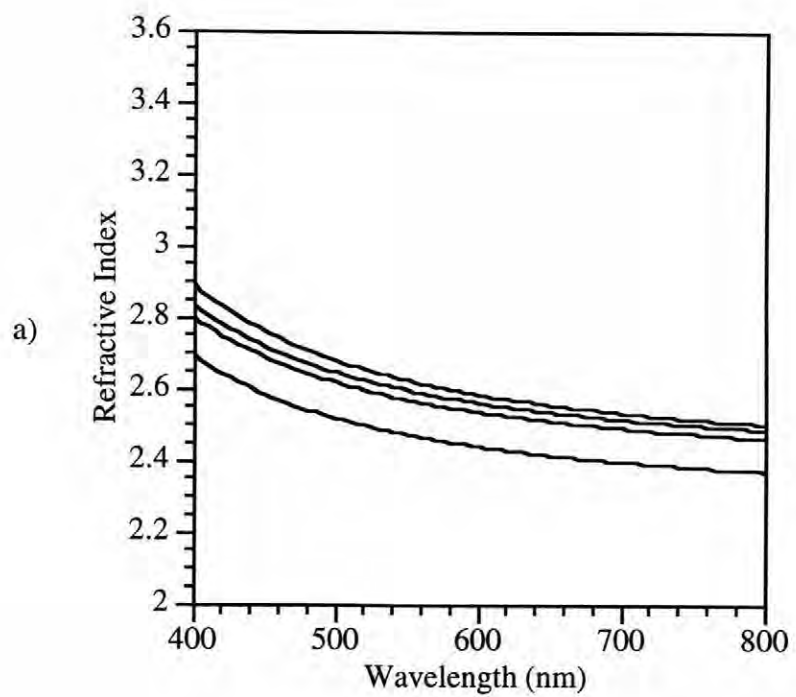PZT, b) samples annealed at 650° C for 60 minutes.

a)

b)

Figure 4.16(a, b) : Dispersion data for a) samples
annealed at 700° C for 60 minutes, b) samples
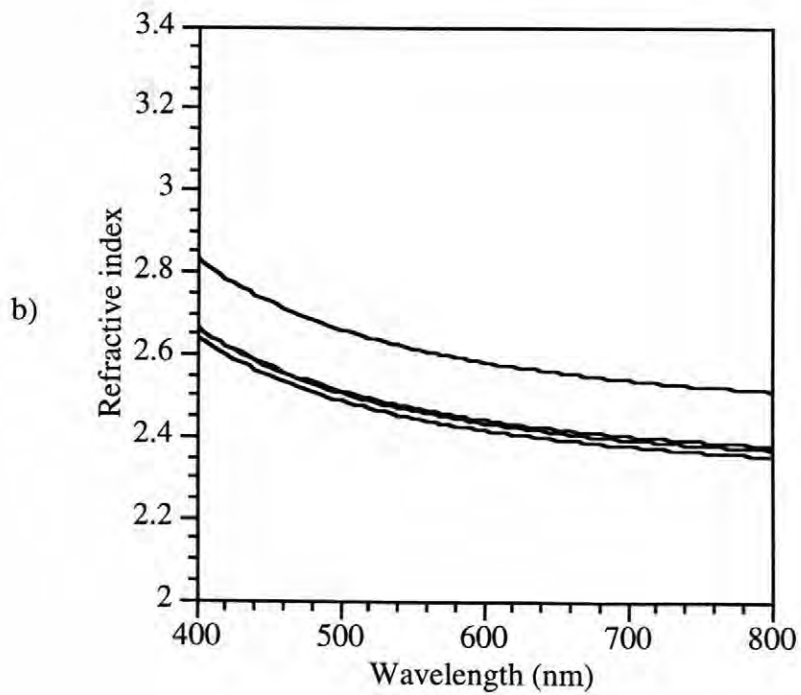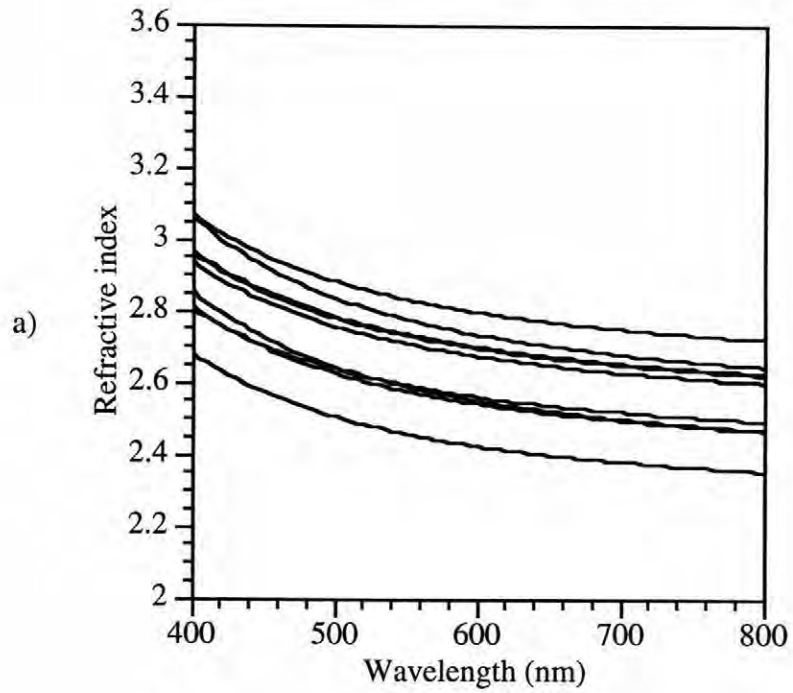annealed at 700° C for 45 minutes.

Figure 4.17(a, b) : Dispersion data for a) samples annealed at 700° C for 30 minutes, b) samples rapid thermally annealed.

significantly increased. Therefore, it was proposed that the high apparent index of the films was due to the assumption that the $Si/SiO_2/Ti/Pt$ substrate is not affected by the annealing process, when in fact it is. Support for this theory is based on observations that anomalously high refractive index values were never obtained for PZT films on sapphire substrates (Trolier-McKinstry et al., 1993). In previous work, $Si/SiO_2/Ti/Pt$ substrates annealed at 650°C were shown to roughen. Figures 4.18 and 4.19 show a platinum substrate as grown and after exposure to 650° C (Trolier-McKinstry and Fox, 1994). Grain growth is clearly visible, and the roughness increased on annealing. In addition, SE measurements taken on a substrate *in situ* during a heating cycle show the appearance of an interference fringe in the data at 550° C. This indicates that a transparent layer is forming on the surface of the substrate. This was also confirmed through Auger analysis and energy dispersive spectroscopy where titanium was shown to have migrated to the surface and partially oxidized (Trolier-McKinstry and Fox, 1994).

To account for this effect, roughening of the substrate was tried in the ellipsometric modeling of the films. Some films in this study, especially those annealed for longer times, showed better models when platinum roughening was included. Figure 4.20 shows one example of this where the unbiased error estimator is decreased when roughness is included at the Pt/PZT interface. The resulting fit had a significantly lower average refractive index of 2.525 compared to 2.807 without the roughness. In addition, the A_4 parameter, which describes the extinction coefficient of the film, dropped considerably (ideally $A_4 \approx 0$ for a transparent film). Another geometry that was proposed was one in which a discrete layer of platinum + PZT was added at the film/substrate interface. However, this resulted in models which contained too many variables to fit with confidence. As a result, the model was simplified so that the discrete layer of platinum roughening was replaced by a substrate composed of a mixture of Pt and PZT. This is not unrealistic given the fact that the high absorption coefficient of Pt limits the penetration depth to the near surface region of the roughness layer. To investigate further whether
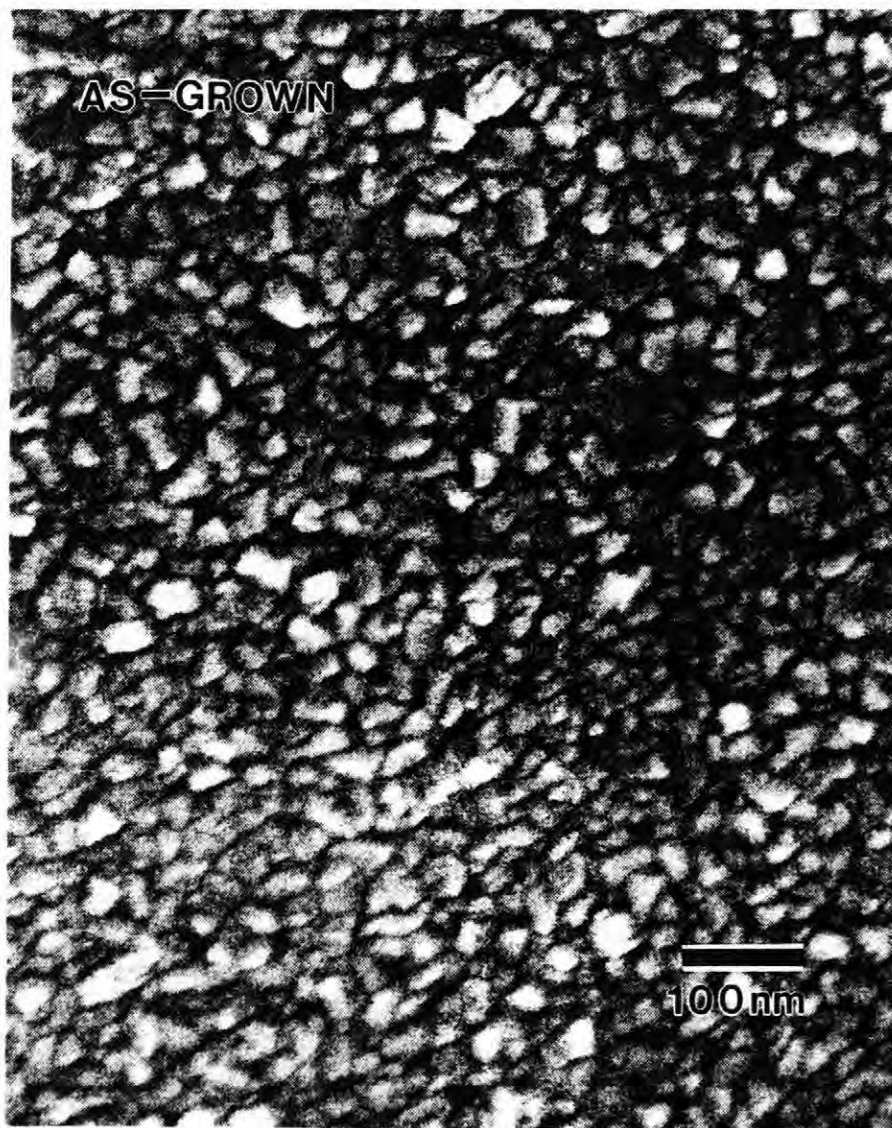
Figure 4.18 : Microstructure of as grown platinum
substrate (Trolier-McKinstry and Fox, 1994).
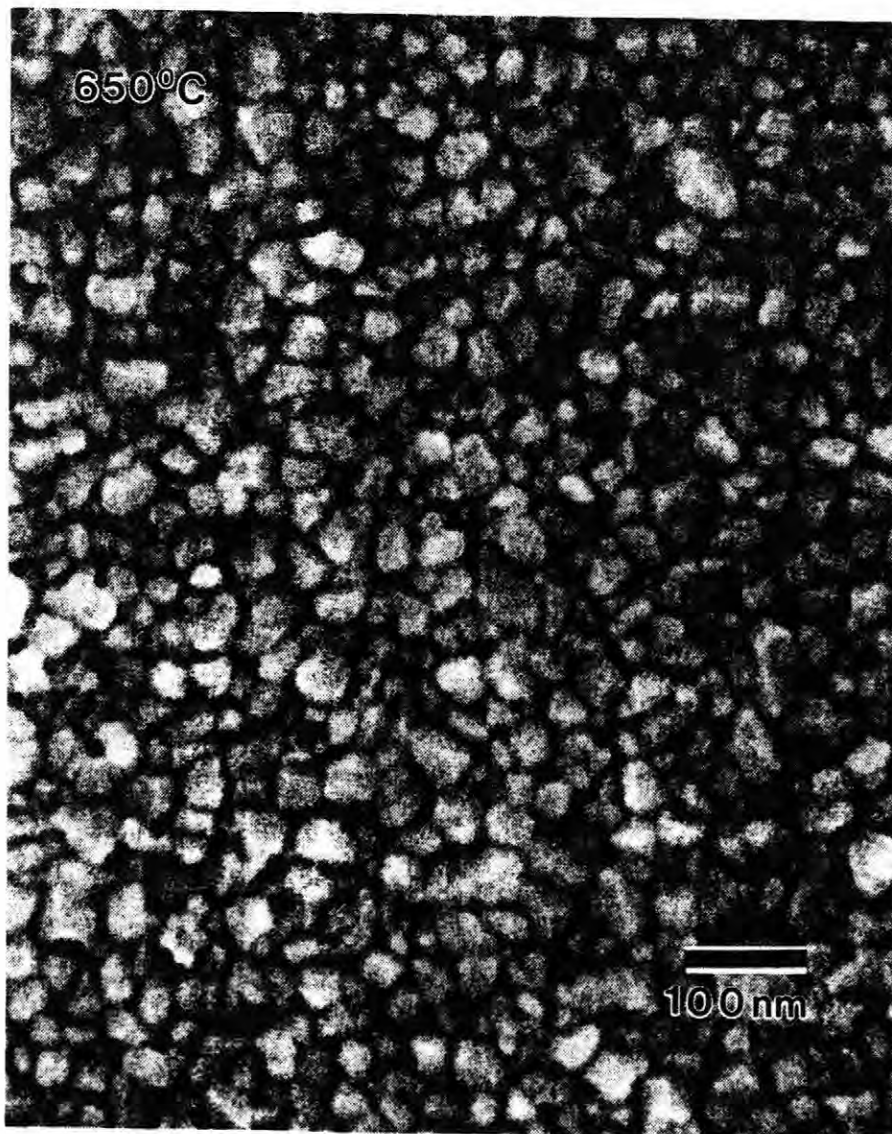
Figure 4.19 : Microstructure of platinum substrate after exposure to 650° C (Trolier-McKinstry and Fox, 1994).

PZT + air 480 Å ± 29 Å Vol. frac. air = 21% ± 3%

Dense PZT 2734 Å ± 175 Å

$\sigma = 0.094$
$A_1 = 1.0$
$A_2 = 5.6 \pm 0.7$
$A_3 = 236.8 \pm 2.4$
$A_4 = 13.2 \pm 0.7$

Substrate

PZT + air 443 Å ± 42 Å Vol. frac. air = 17% ± 3%

Dense PZT 2922 Å ± 209 Å

$\sigma = 0.071$
$A_1 = 1.0$
$A_2 = 4.3 \pm 0.5$
$A_3 = 244.0 \pm 2.1$
$A_4 = 6.6 \pm 1.1$

Substrate + PZT Vol. frac. PZT = 30% ± 4%

Figure 4.20 : Ellipsometric models with and without platinum roughness.

unaccounted-for changes in the substrate microstructure were responsible for the anomalously high refractive indices, several models were completed to observe how the microstructure of the samples influences the modeled optical properties.

To do this, a hypothetical film geometry including platinum roughening was created. To obtain the data file for the film, the fixed geometry was entered into the modeling program previously described and Δ and Ψ were calculated from reference data for the substrate, PZT and air. This data was then modeled as the substrate (without roughening), a dense layer of PZT and a roughness layer of air + PZT. This model provided the apparent A_2 - A_4 coefficients for the film when modeled incorrectly. This would also show how the modeled film geometry would change when the Pt roughening is omitted from the model. Figure 4.21(a, b, c) shows the results for a film that was created with a 10% volume fraction of PZT mixed with the su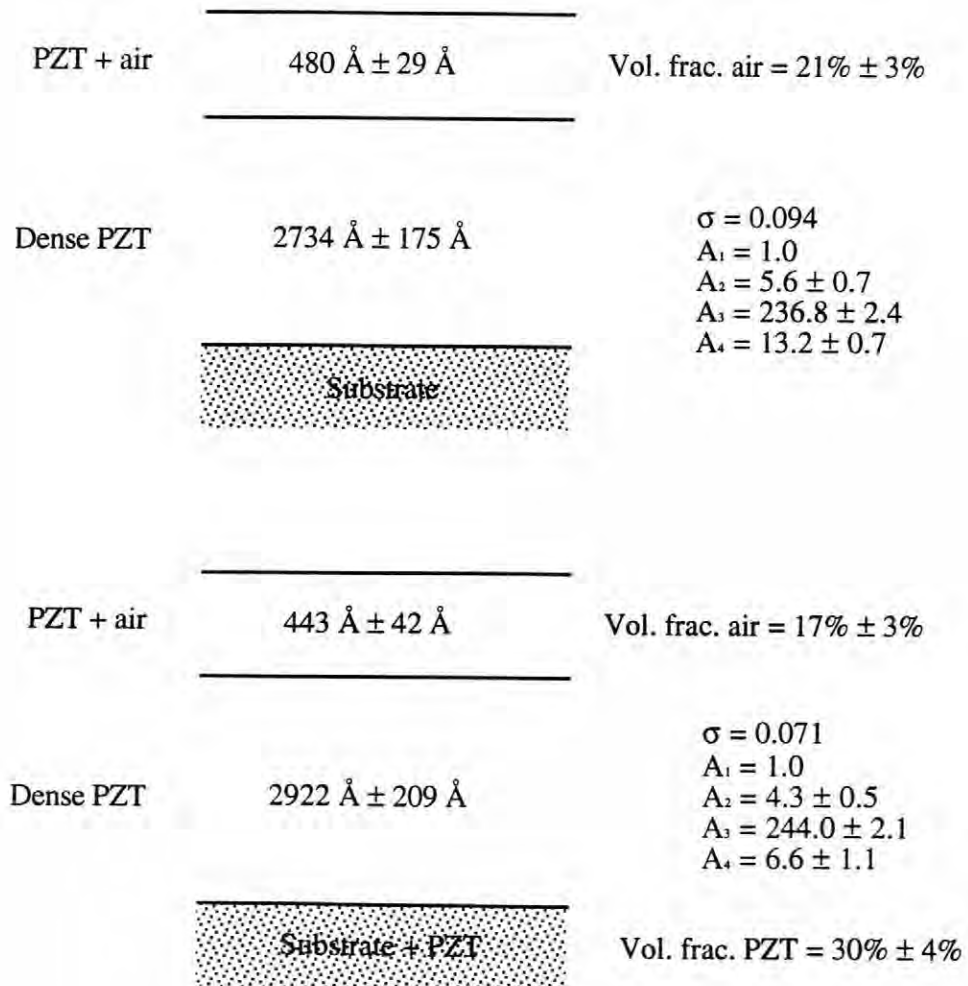bstrate. It is clear that when a simple model is used to fit the data a reasonable depth profile is achieved, but the A_2 value is 5.17 corresponding to n = 2.651. When it was modeled to converge to the true microstructure (i.e., including substrate changes), the A_2 value dropped to 4.85 corresponding to n = 2.587. The corresponding dispersion curves are given in figure 4.23(a). For the simple model fit the curve is higher, as expected. It is also important to note that the final microstructure of the simple model is not very different from the true microstructure. Thus the majority of the effect of adding the guest in the substrate is shown by the change in A_2. Next, a film was created with a 15% volume fraction of TiO_2 mixed with the substrate. This would correspond to Ti migration through the platinum and partially oxidizing. Figure 4.22(a, b, c) show the various models. Again, the simple model produces reasonable results except for a high n of 2.725. Also the microstructure is not far from the true values. When modeled with the change in the substrate, A_2 drops to 2.587. This gives a similar result for the dispersion behavior as shown in figure 4.23(b). From these data, in addition to McKinstry and Fox's, it can be shown that the platinum roughening is

on a much smaller scale than the roughness on the film surface. Figure 4.24 shows a model of this.

It seems clear then that the conventionally annealed samples could exhibit this substrate/film interface phenomenon due to the extended time at higher temperatures during processing. This would also imply that samples which were rapidly processed should not show this effect and have more normal dispersion behavior. This agrees with our observation where the RTP'd films had the smallest deviation from the reference data. The theoretical models utilized here showed that the anomalous dispersion behavior is due to the changes in the substrate, possibly via a combination of Pt roughening and Ti migration at the substrate/film interface. It cannot be determined which effect is dominating from the SE measurements.

Created Data File

a)

300 Å	PZT + 20% Air

1500 Å   dense PZT

Substrate + 10% PZT

Simple Model

b)

307 Å ± 9 Å   vol. frac. air = 22% ± 1%

1465 Å ± 14 Å   dense PZT

Substrate

$\sigma = 0.017$
$A_1 = 1.0$
$A_2 = 5.2 \pm 0.04$
$A_3 = 207.8 \pm 0.84$
$A_4 = 2.4 \pm 0.08$

Model as Created

c)

300 Å ± 0.13 Å   vol. frac. air = 20% ± 0.01%

1500 Å ± 0.24 Å   dense PZT

Substrate + PZT   vol. frac. PZT = 10% ± 0.01%

$\sigma = 0.00023$
$A_1 = 1.0$
$A_2 = 4.85 \pm 0.001$
$A_3 = 211.5 \pm 0.001$
$A_4 = 0.00$

Figure 4.21(a, b, c) : Hypothetical film containing 10% PZT mixed with substrate. (b, c) are incorrectly and correctly modeled outputs.

Created Data File

a)

300 Å	PZT + 20% Air
1500 Å	dense PZT

Substrate + 15% TiO_2

Simple Model

b)

328 Å ± 14 Å	vol. frac. air = 22% ± 1%
1400 Å ± 26 Å	dense PZT
Substrate	

$\sigma = 0.027$
$A_1 = 1.0$
$A_2 = 5.6 \pm 0.1$
$A_3 = 201.2 \pm 1.7$
$A_4 = 4.7 \pm 0.2$

Model as Created

c)

300 Å ± 0.09 Å	vol. frac. air = 20% ± 0.01%
1500 Å ± 0.19 Å	dense PZT
Substrate + TiO_2	vol. frac. TiO_2 = 15% ± 0.01%

$\sigma = 0.00024$
$A_1 = 1.0$
$A_2 = 4.85 \pm 0.001$
$A_3 = 211.5 \pm 0.001$
$A_4 = 0.00$

Figure 4.22(a, b, c) : Hypothetical film containing 15% TiO_2 mixed with substrate. (b, c) are incorrectly and correctly modeled outputs.
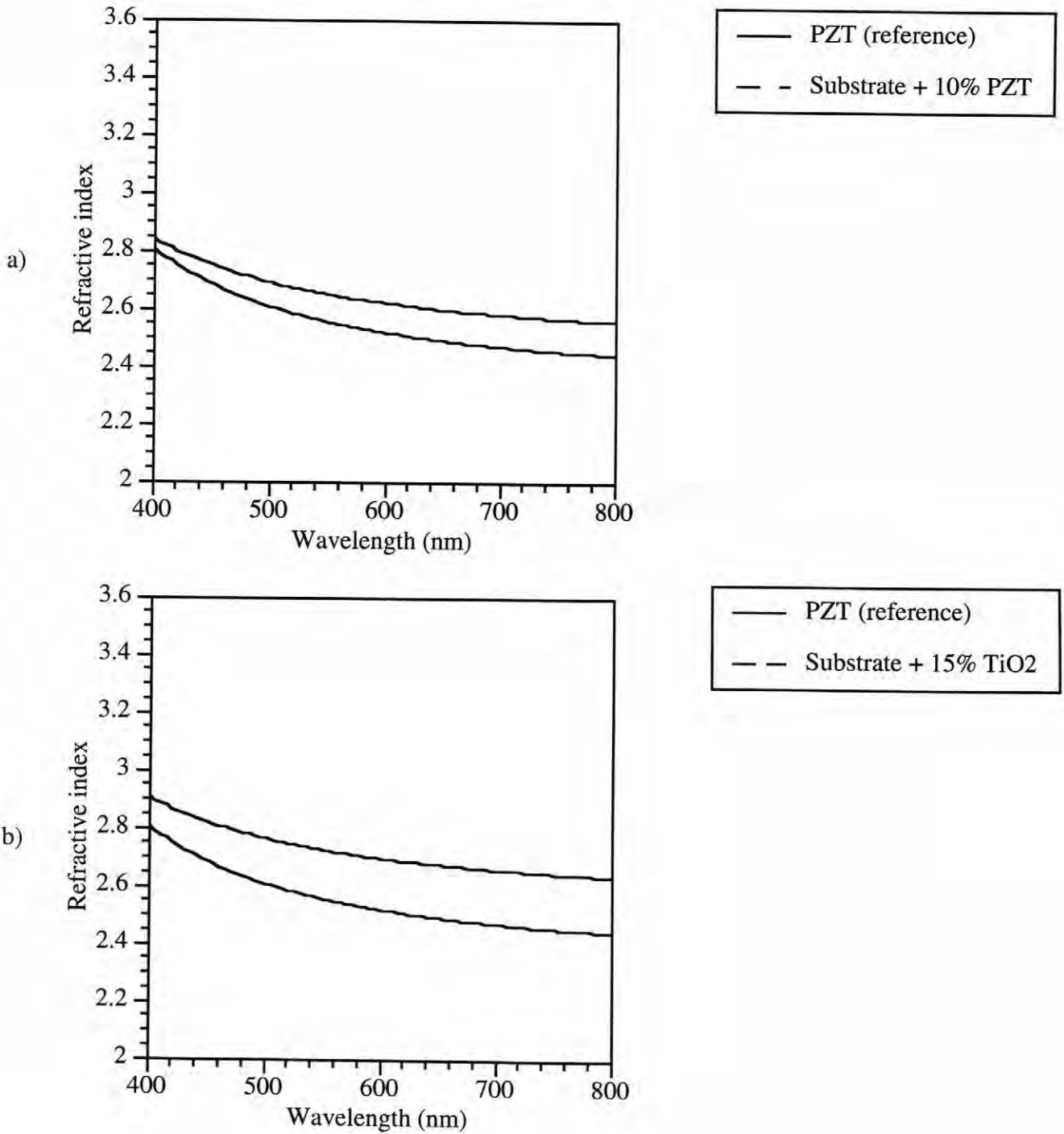
a)

b)

Figure 4.23(a, b) : Dispersion data for
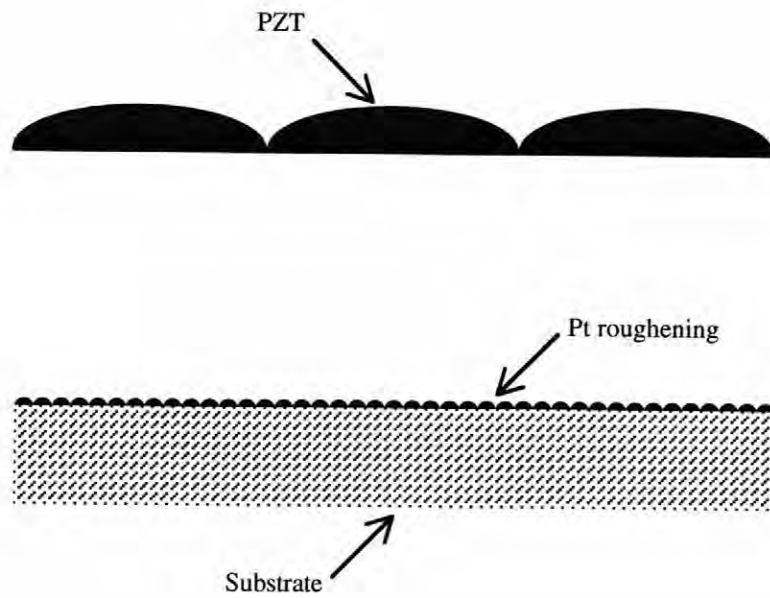incorrectly modeled films and reference data.

Figure 4.24 : Schematic microstructure
displaying scale of platinum roughening.

4.3   Electrical Measurements

Just as the processing parameters of these ferroelectric thin films can affect the final microstructures, the electrical properties will be very different depending on how the films are prepared. Testing of the dielectric and ferroelectric properties of these films is necessary to determine how these materials will perform under device operating conditions. Along with the previous measurements, these will provide a qualitative and quantitative analysis of the microstructure - processing - property relationships.

4.3.1 Relative Dielectric Constant

A good measure of the homogeneity of a ferroelectric is the value of the relative dielectric constant, ε_r. PZT (52/48) in bulk ceramic form has a dielectric constant of about 1600. Much of the work done on thin films of this material has shown dielectric constants between 800 and 1300 depending on deposition method, orientation and annealing conditions. Inhomogeneous films, or films with undesired second phases, may have lower dielectric constants (i.e., a pyrochlore phase mixed with perovskite greatly degrades the dielectric properties (Kwok and Desu, 1991)).

Figure 4.25(a) shows the dielectric constant for films of varying thickness which were annealed conventionally at 650° C for 60 minutes. There is little scatter in the data with a value for these films largely between 770 and 800. Figure 4.25(b) shows the values for samples annealed at 700° C for 30 minutes. Here, the dielectric constant is higher, ranging from 800 to 850. As the time at 700° C is increased, however, the properties degrade. This can be seen in figures 4.26(a, b) where films annealed at 700° C for 45 and 60 minutes are shown. The samples fired 45 minutes show an average dielectric constant of 610, and those fired for 60 minutes are similar with an average of 634. Figures 4.27(a, b) illustrate the effects of time and temperature on the thin films. Both of these effects can be attributed to the formation of a pyrochlore phase as well as lead volatilization from the

surface of the sample during annealing, the latter being more important for longer times. In addition to these problems, the platinum roughening effect described earlier was seen most generally for these conditions. The dielectric losses in the films annealed at 650° C for 60 minutes and 700° C for 30 minutes were generally low, ranging from 0.02 to 0.05. Those of the two other conventional processes had higher losses, ranging from 0.05 to 0.07. Finally, figure 4.28 shows the results from the rapid thermal processed films. The dielectric constants for these samples varied from 700 to 840 and were centered around 820. These values were not as high as was expected, but this is most likely due to the much finer grain sizes of these samples. The losses in these films were comparable to the conventionally processed ones, ranging from 0.03 to 0.06. Several studies have been completed on the effects of rapid thermal processing on the electrical properties of thin films. In general, the literature suggests this technique can improve the properties by lowering the coercive field and increasing the breakdown strength (Chen, et al., 1992; Reaney, et al., 1994).

4.3.2 Hysteresis and Fatigue Measurements

In addition to the relative dielectric constant, the hysteresis and fatigue behavior of the PZT films were measured for each processing method. These measurements can give a qualitative assessment of how these samples perform under device operating conditions. In recent years there have been numerous studies on the use of PZT in non-volatile memory devices. For this purpose, the sample must be able to endure up to 10^{15} polarization reversal cycles (Swartz and Wood, 1992). It has been exhibited that films deposited on platinum electrodes fatigue too rapidly for reliable operation (Vijay and Desu, 1993) and these measurements in conjunction with the previous data may be able to explain some observed related effects.

Hysteresis data before and after a fatigue cycle for two samples are shown in figure 4.29(a, b). They are representative of films annealed conventionally and rapidly,

Figure 4.25(a, b) : Relative dielectric constant versus thickness for samples annealed at a) 650° C for 60 minutes b) 700° C for 30 minutes.
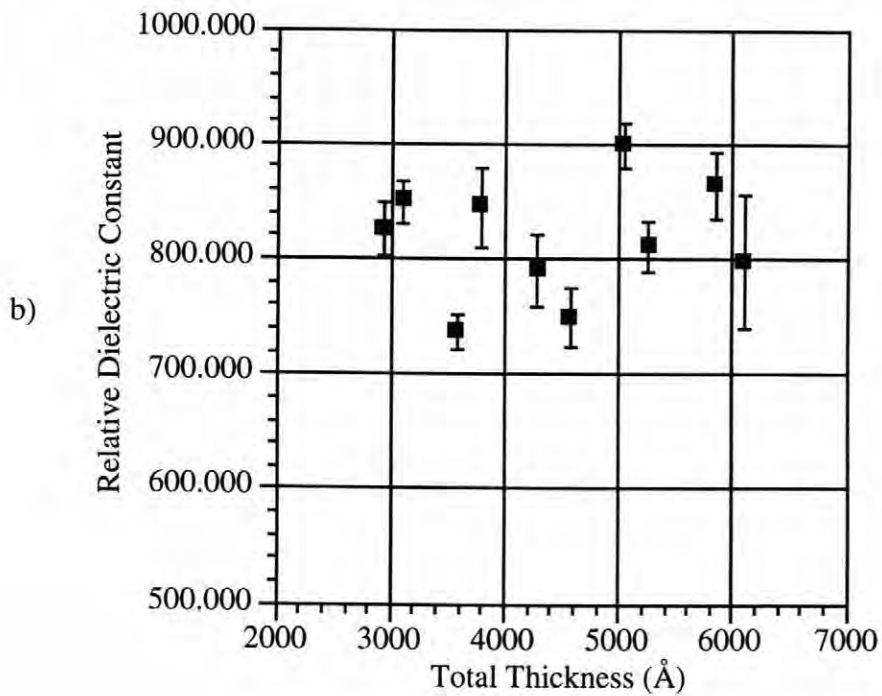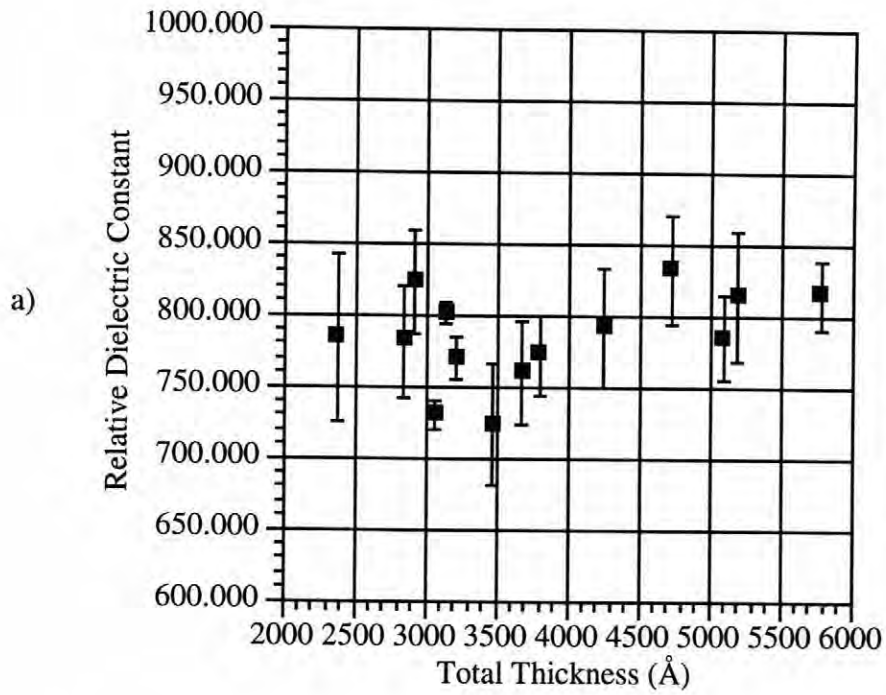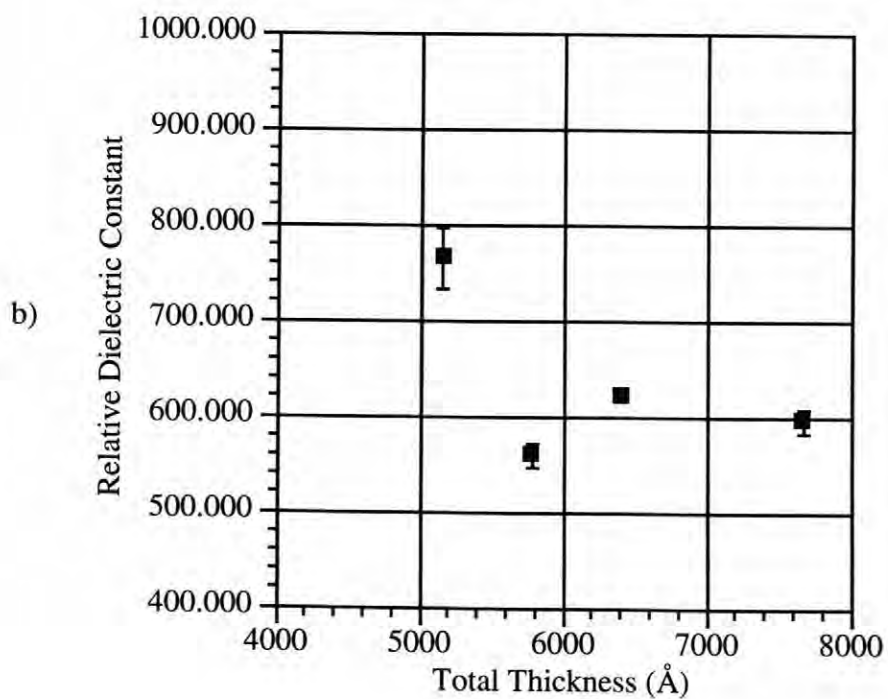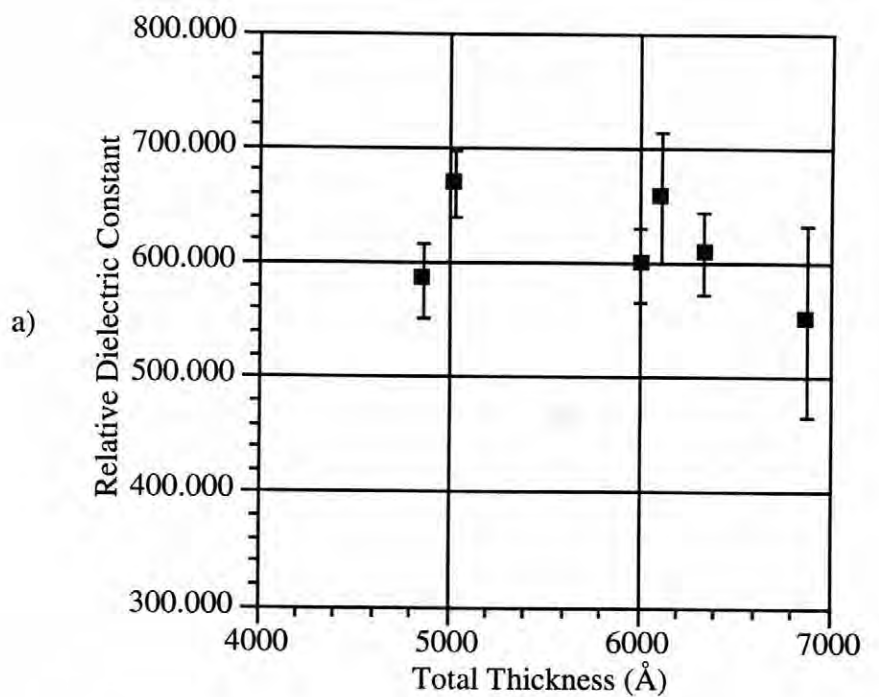
Figure 4.26(a, b) : Relative dielectric constant versus
thickness for samples annealed at a) 700° C for 45
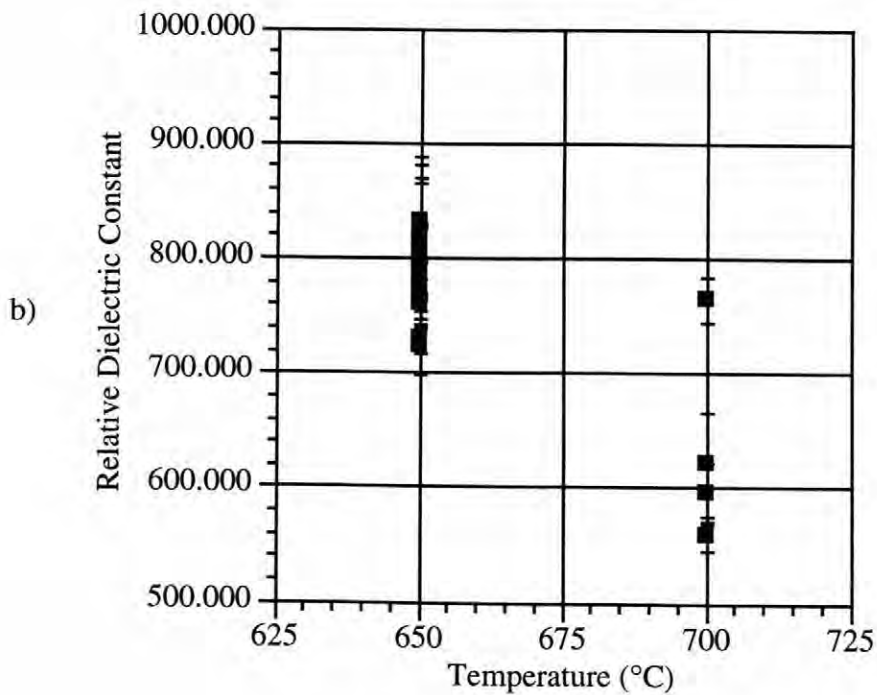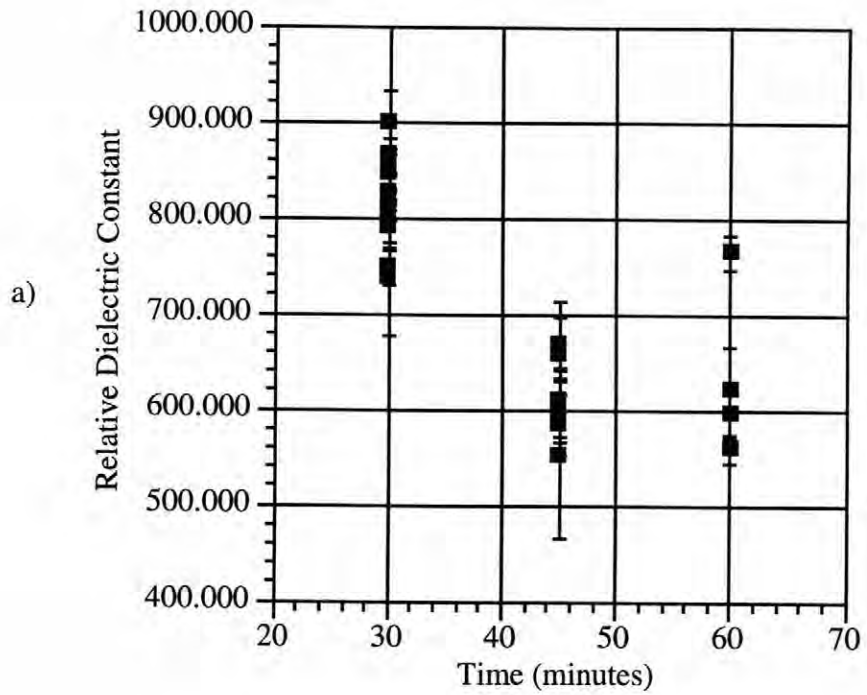minutes b) 700° C for 60 minutes.

Figure 4.27(a, b) : Relative dielectric constant as a
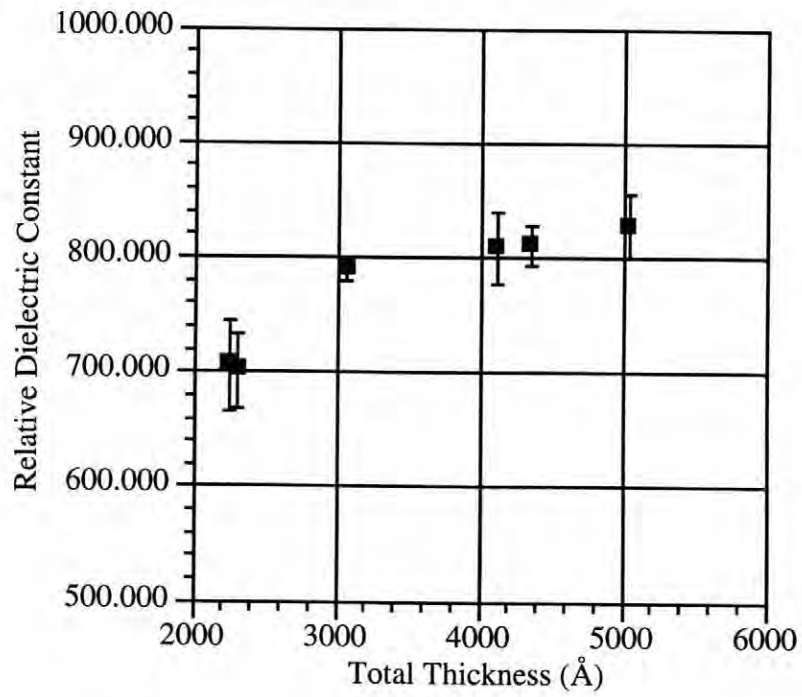function of a) time, b) temperature.

Figure 4.28 : Relative dielectric constant versus
thickness for rapid thermally annealed samples.

respectively. In part a, the data is for a film annealed at 700° C for 30 minutes. The coercive field increases after 10^8 cycles from an average of 8.3 MV/m to 10.1 MV/m while the remanent polarization decreases from 21.8 $\mu C/cm^2$ to 10.7 $\mu C/cm^2$. The measurements for the rapidly thermal processed film are shown in part b. Here the coercive field grows from 7.8 MV/m to 11.0 MV/m and the remanent polarization drops from 23.2 $\mu C/cm^2$ to 20.3 $\mu C/cm^2$, also after 10^8 cycles. Thus a significant difference can be seen since in P_r where the conventionally annealed film decreases to 49% of its initial value while the RTP'd film only drops to 87% of its starting value. In both cases the coercive field increases; 1.2 times and 1.4 times, respectively. This increase is typically found in the literature and is related to the increased difficulty of switching domains during fatigue. This difficulty could be due to the pinning of domain walls at various defects over time (Kwok and Desu, 1992). This necessitates a higher field to promote switching of the domains. The values of E_c and P_r for the RTP'd films are comparable to the conventional samples.

The fatigue behavior of these samples was measured at 10 kHz for 10^8 to 10^9 polarization reversal cycles. Typical values found in the literature show the largest drop in remanent polarization to occur between 10^5 and 10^7 cycles. It is important to note here that the purpose of this study was not to create fatigue-free films, but to study the mechanism(s) of fatigue, hence the selection of our measuring conditions. Figures 4.30 - 4.32 show data for several samples annealed conventionally and rapidly. The data is summarized in table 4.1.
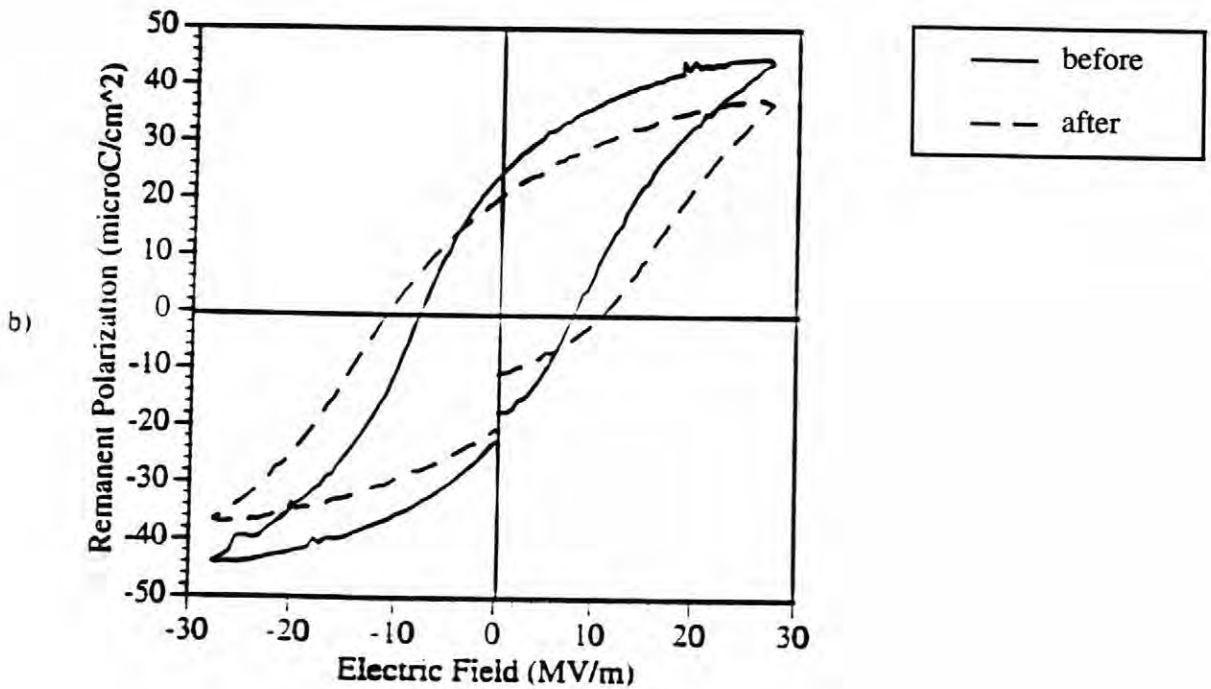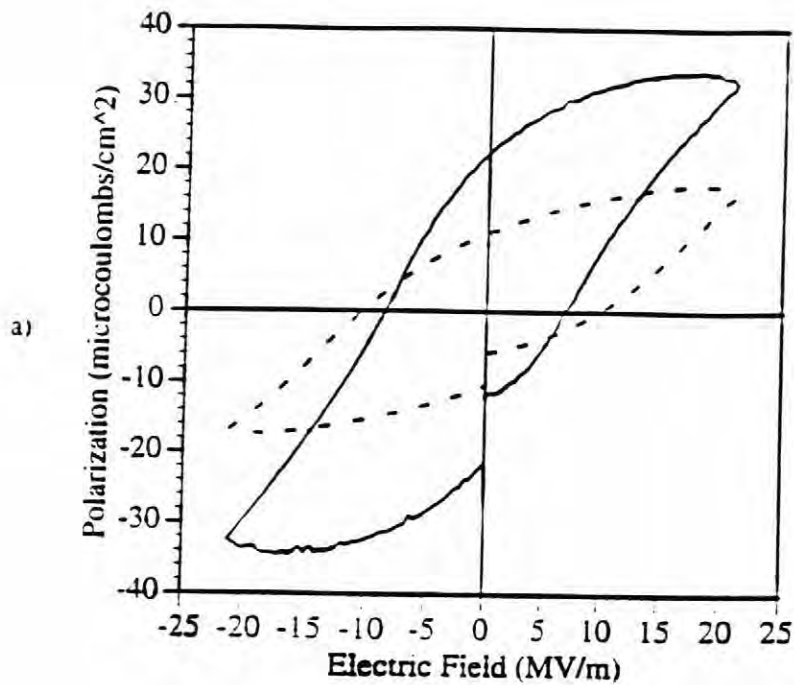
Figure 4.29(a, b) : Hysteresis loops before and after
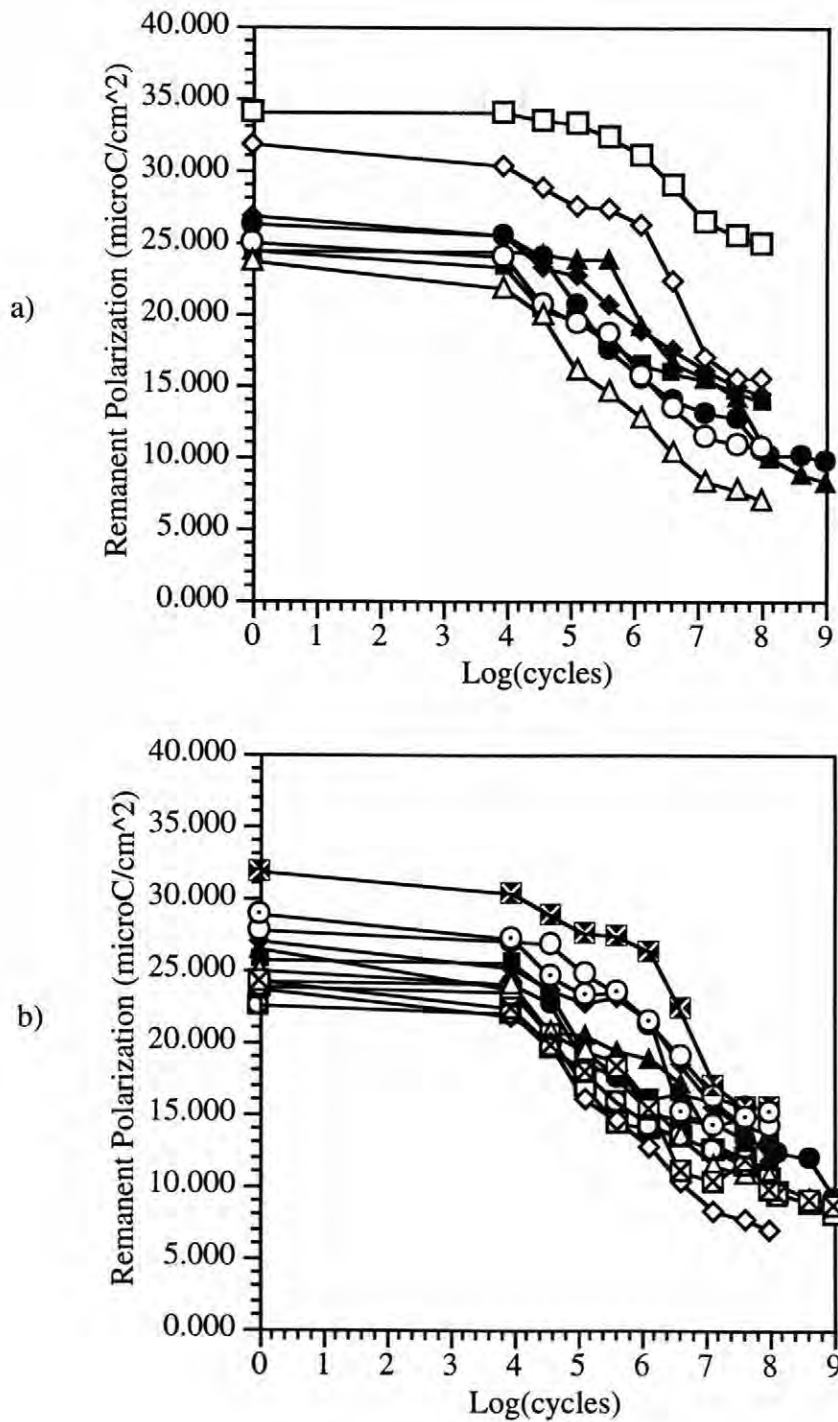fatigue for a) conventional sample, b) RTP'd sample.

Figure 4.30(a, b) : Fatigue data for samples annealed at a) 650° C for 60 minutes, b) 700° C for 30 minutes.
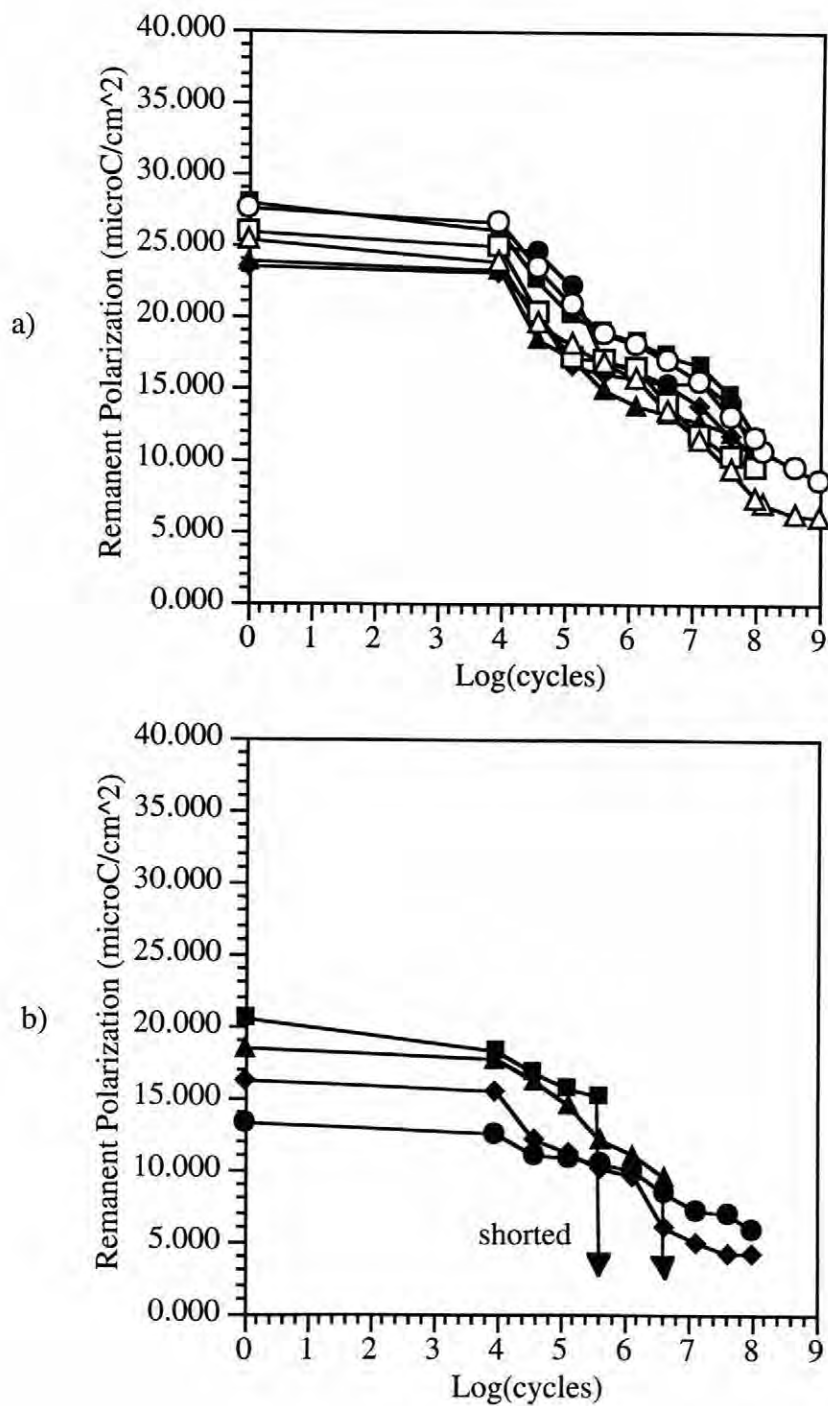
Figure 4.31(a, b) : Fatigue data for samples annealed at a) 700° C for 45 minutes, b) 700° C for 60 minutes.
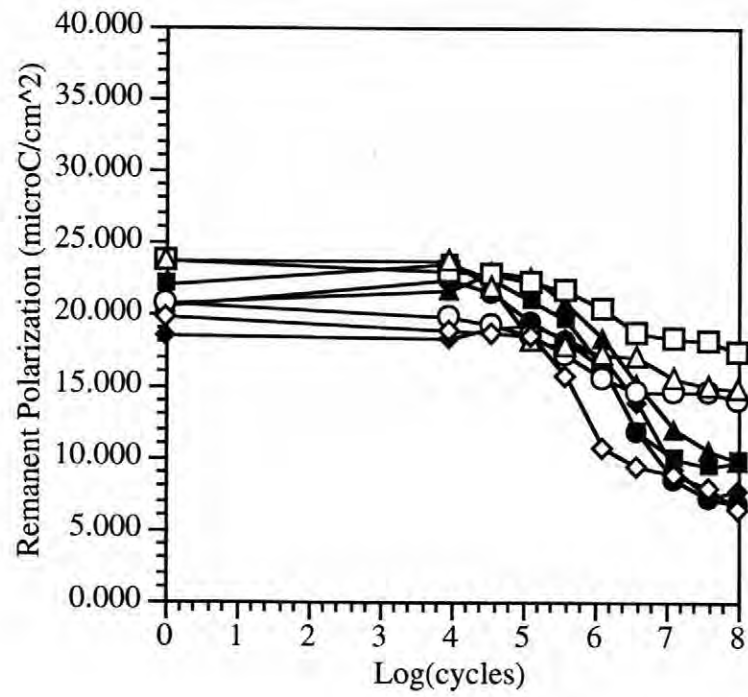
Figure 4.32 : Fatigue data for samples rapid thermally annealed.

Table 4.1: Summary of fatigue data.

Annealing Conditions	Initial P_r ($\mu C/cm^2$)	Final P_r ($\mu C/cm^2$)	Drop Off at
650° C 60 minutes	22 - 29	7 - 15	$10^5 - 10^6$
700° C 30 minutes	23 - 30	7 - 15	10^5
700° C 45 minutes	22 - 27	6 - 10	10^4
700° C 60 minutes	15 - 20	shorted - 7	$10^4 - 10^5$
RTP	20 - 25	8 - 15	$10^5 - 10^6$

On analyzing this data, it is clear that the values for samples annealed at 650° C for 60 minutes and those at 700° C for 30 minutes are comparable. This is analogous to the relative dielectric constant data and the surface characteristics as well. The knee of the fatigue curve corresponds well with typical values but the decrease in P_r to 25% - 50% is significant enough to cause memory retention degradation. For the samples processed at 700° C for 45 and 60 minutes the performance is considerably worse. The knee of the curve occurs at 10^4 to 10^5 cycles, well below the values typically quoted. The drop-off of P_r for the 45 minute samples is similar to that of the previous conditions. The 60 minute samples start with much lower remanent polarizations. Those films that did not electrically short during the fatigue cycle dropped to 30% - 45% of the initial values. Again, the performance of these samples correlates to the previous results discussed. The rapidly thermal processed films showed slightly different fatigue behavior than the conventional samples. The knee of the curves are found at the expected location, $10^5 - 10^6$ cycles, but the remanent polarization fatigues less, on average. The post-fatigue values range from 45% to 75% of the initial values. The lesser fatigue of P_r for these samples could be attributed to the absence of Ti migration or the Pt roughening. These values correspond with the somewhat lower relative dielectric constant data reported earlier. It is important to note that electrical shorts were observed in samples annealed by all methods. However, shorts were more common in samples annealed at 700° C for 45 and 60 minutes. The shorting happened at various times throughout the fatigue cycles.

The greater frequency with which the electrical shorting occurred in the conventionally annealed samples can be attributed to the substrate roughening phenomena described above. Figure 4.33 shows a schematic illustration of conventionally and rapidly processed films; the roughening exhibited here is exaggerated to clarify the explanation. The platinum roughening causes electric field concentrations across the thinnest regions of the sample. This can lead to accelerated breakdown in the film. If the film does not break down, then the higher field would cause accelerated fatigue (Yoo and Desu, 1992). The RTP'd samples, which did not exhibit roughening, instead experience a more uniform electric field.

In order to observe electrical fatigue and obtain spectroscopic ellipsometric measurements *in situ* during the cycle, there were special sample requirements. Most importantly, the area of the film which was being cycled had to be large enough for the light beam to fit on. An electrode size of 2 mm x 2.5 mm would be ideal for these measurements. Unfortunately, we were unable to obtain films homogeneous enough to satisfy this need. That is, an area that large consistently encompassed one or more pinholes through the film which caused instant electrical shorting. Alternatively, in the conventionally annealed samples, the roughening across an area this size would lead to several electric field concentrations and thus accelerate breakdown. In this case the shorting occurred in the first few seconds, generally. For the samples which did last longer (to 10^4 - 10^6 cycles), it was possible to obtain data before, during and after the cycle. Figures 4.34(a) and 4.35(a) show an example of this. This sample experienced approximately 2 x 10^7 polarization reversals and did show fatigue. The changes in Δ and Ψ are expected to be much smaller than the magnitude of the interference fringes. Thus, figures 4.33(b, c) and 4.34(b) show smaller scale regions of the spectra where the effects can be viewed. It is not entirely clear what these differences are due to because of the limited number of samples available to analyze. Improving the ability to produce pinhole

free thin films and possibly switching to a different top electrode material may allow for more precise measurements using this technique.

PZT

E_1 E_2

← Roughening

Substrate

$E_2 > E_1$

PZT E_1 E_2
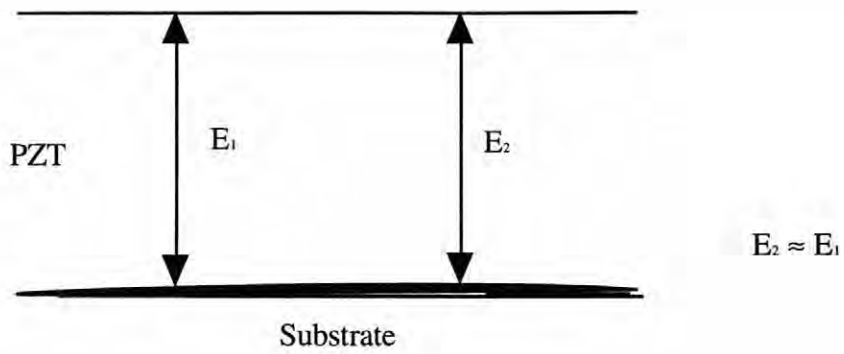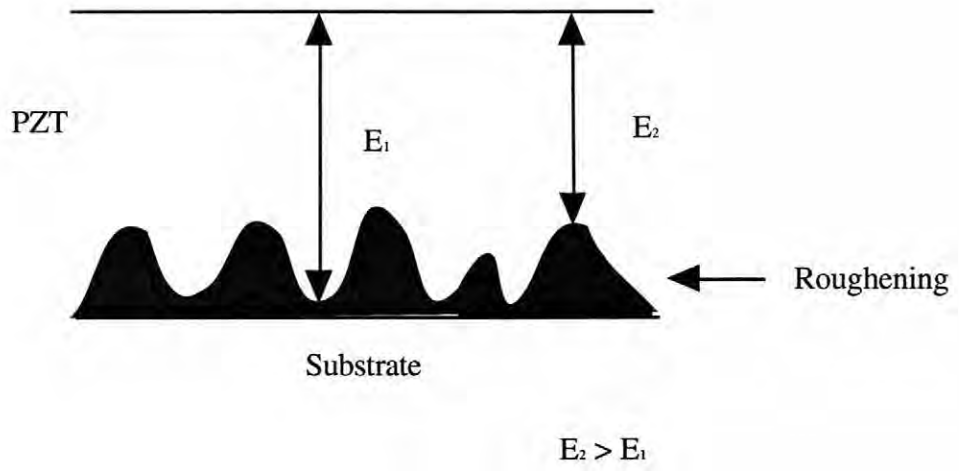
$E_2 \approx E_1$

Substrate

Figure 4.33 : Schematic of Pt roughening and its influence on electrical shorting.
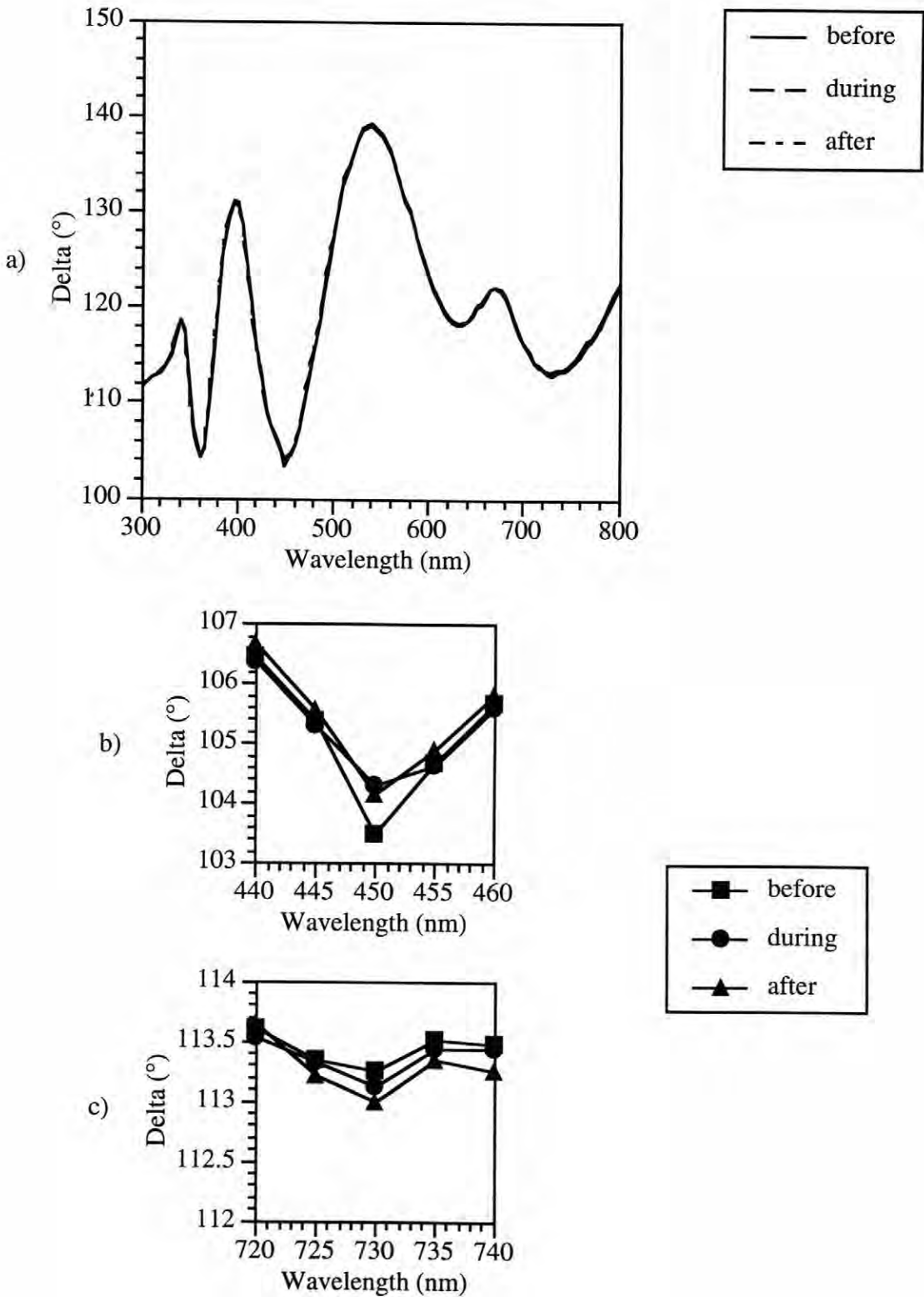
Figure 4.34(a, b, c) : a) Δ values as a function of
wavelength before, during, and after fatiguing. (b, c)
Expanded views to show changes.
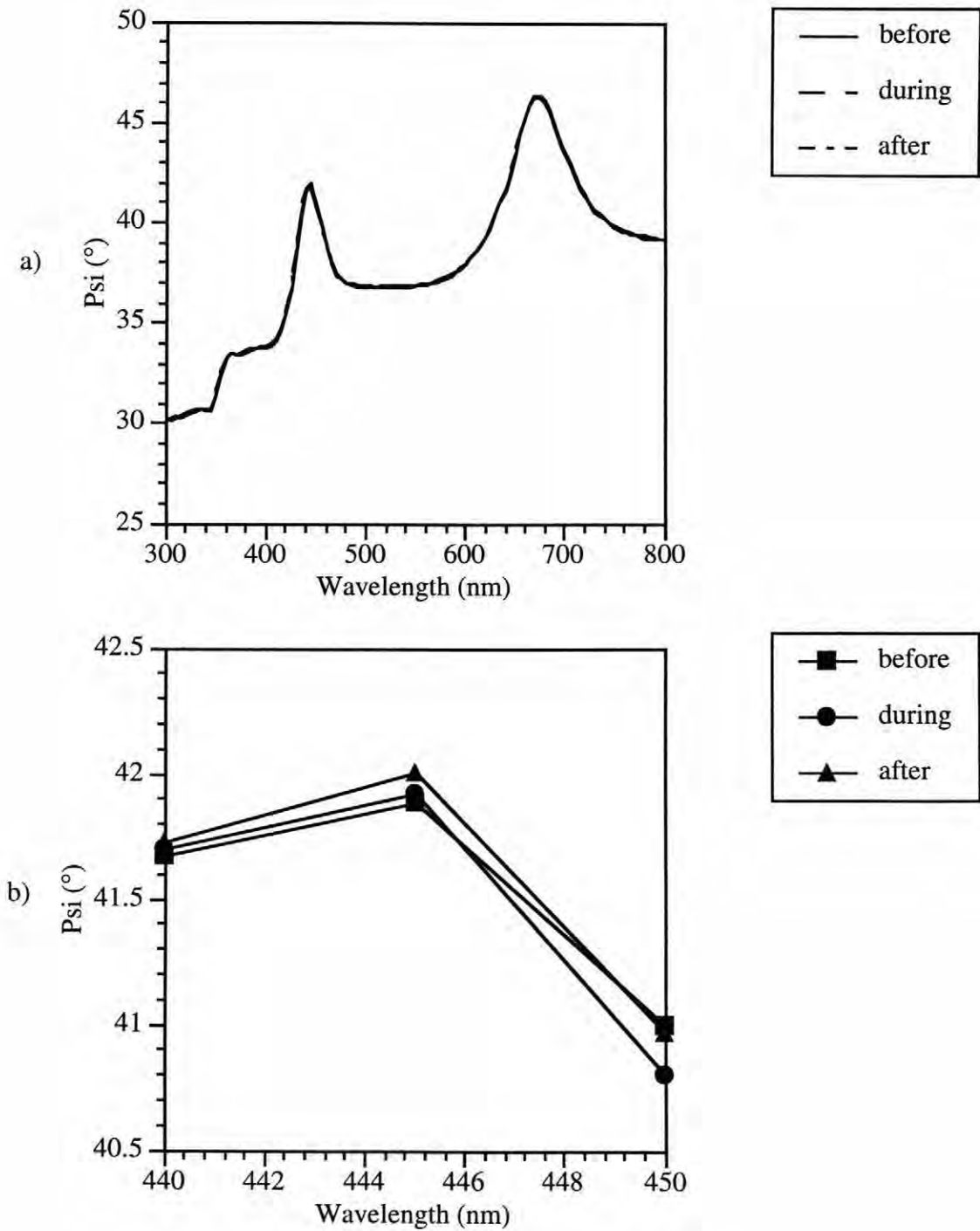
Figure 4.35(a, b) : a) Ψ values as a function of wavelength before, during, and after fatiguing. (b) Expanded view to show changes.

Chapter 5

SUMMARY and FUTURE WORK

5.1   Summary

Lead Zirconate Titanate (PZT) thin films were fabricated successfully using the sol-gel process. The microstructural, optical, dielectric and ferroelectric properties were measured along with the fatigue behavior of the films. This combination allowed for the microstructure-processing-property relationships to be investigated. The significant results are summarized as follows:

The thin films were annealed using two methods. Conventional furnace processing was used at 650° C for 60 minutes and 700° C for 30, 45 and 60 minutes. Also a rapid thermal processing (RTP) method was used. Here, the samples were annealed at 700° C and 750° C for 10, 15 and 30 seconds. The microstructure of the thin films was investigated using scanning electron microscopy (SEM) and x-ray diffraction. The SEM study indicated the final grain size of the 650° C for 60 minute samples was 0.05 - 0.08 μm while the sizes for the 700° C for 30 and 45 minutes samples were 0.68 μm and 1.05 μm, respectively. Lead loss from the surface and the formation of a pyrochlore phase were concerns for conventional processing at higher temperatures and longer times. X-ray diffraction studies showed characteristic pyrochlore peaks in several of these samples. Rapid thermal processing was used to avoid some of the problems associated with conventional annealing. Lead loss especially can be avoided due to the smaller thermal budget of the RTP method. X-ray diffraction showed films with decreasing pyrochlore content at conditions of 700° C for 10 and 15 seconds. At 30 seconds, there was no pyrochlore peak visible in the diffraction pattern.

Prior to deposition of the sol, a fixed amount of water is added to the solution to promote condensation and gelation reactions. This controlled hydrolysis step is important

because it influences the pH of the sol and in turn the polymeric network of the gel (Chen, 1992; Lakeman and Payne, 1992). It was found that the final microstructure is a function of how much water is added. Films with 3:1 and 4:1 molar ratios of water to PZT resulted in diphasic microstructures with 1 - 2 μm perovskite rosettes in a fine-grained pyrochlore matrix. The microstructures of films with a 1.5:1 molar ratio were much more homogeneous with a grain size of 0.2 - 0.5 μm. These results are in relatively good agreement with Lakeman and Payne (1992), who showed an optimal molar ratio to be 2:1.

Spectroscopic ellipsometry (SE) was shown to be a useful tool to non-destructively characterize the thickness and optical properties of ferroelectric thin films. The total surface roughness and volume fraction of air were determined for each processing method. Table 5.1 summarizes the results:

Table 5.1 : SE determined microstructural parameters for films annealed differently.

Processing Condition	Total Surface Roughness	Volume Fraction Air in Roughness Layer
650° C 60 minutes	300Å - 500Å	20% - 35%
700° C 30 minutes	300Å - 500Å	30% - 40%
700° C 45 minutes	300Å - 500Å	35% - 45%
700° C 60 minutes	500Å - 600Å	15% - 35%
RTP	175Å - 250Å	25% - 45%

There was no evident correlation between the total surface roughness and the total thickness of the films. This indicates the processing conditions are primarily responsible for the surface roughness. Based on the SE measurements, schematics of the grain structure were developed for samples annealed at 700° C for 30, 45 and 60 minutes. The films annealed for shorter times had similar structures with the primary difference being grain size, while the 60 minute samples showed a more plateau-like structure. Also based on the SE measurements, it was shown that temperature had a greater influence on the total

surface roughness than the time. Finally, the rapid thermally processed films exhibited lower surface roughness than the conventionally processed ones, as expected due to the smaller thermal budget.

Other information obtained from SE data includes the optical properties of the thin films. The refractive index versus wavelength data for the conventionally processed samples consistently showed values that were higher than expected when modeled assuming that the substrate was unchanged by annealing. The RTP'd samples exhibited more normal dispersion behavior. Table 5.2 summarizes the data for each processing condition.

Table 5.2 : Summary of refractive index data.

Processing Condition	Average Refractive Index (@ 550 nm)
Reference	2.556
650° C 60 minutes	2.620
700° C 30 minutes	2.667
700° C 45 minutes	2.736
700° C 60 minutes	2.570
RTP	2.500

Due to observations that the optical properties of PZT thin films on sapphire never showing an anomalously high refractive index, and the fact that the perovskite structure is a dense one, the high apparent n was assumed to result from changes in the substrate, not the film. It had been shown (McKinstry and Fox, 1994) that the $Si/SiO_2/Ti/Pt$ substrates became roughened when exposed to temperatures of 650°C and above. They also determined through SE measurements that the Ti from the bonding layer was migrates through the Pt and oxidizes to form a transparent layer on the surface. Using this

information, the SE data on our samples was modeled including Pt roughening. Some of the films, especially those annealed at longer times and higher temperatures, showed better models using this geometry. Models were developed to confirm that reasonable changes in the substrate microstructure during annealing could result in the observed behavior. It was clear, then, that the conventionally annealed samples could exhibit this substrate roughening effect. It was also expected that the RTP'd films should not due to the less time at high temperature. This was the case, as these samples showed less deviation from the reference data.

The electrical data measured consisted of the relative dielectric constant and the hysteresis and fatigue behavior of the samples. Hysteresis data was obtained before and after fatiguing the films. The conventional samples showed an increase in the coercive field, E_c, after 10^8 cycles from 8.3 MV/m to 10.1 MV/m and a decrease in the remanent polarization, P_r, from 21.8 $\mu C/cm^2$ to 10.7 $\mu C/cm^2$. RTP'd samples showed an increase in E_c from 7.8 MV/m to 11.0 MV/m and a decrease in P_r from 23.2 $\mu C/cm^2$ to 20.3 $\mu C/cm^2$. The increase seen in E_c is typical of data found in the literature and is attributed to the pinning of domain walls at defect sites. As more domain walls become pinned, it takes a higher field to switch them. The decrease in P_r is also attributed to this. Some of the domains may not be able to be switched, thus fewer will be aligned and the net polarization will be lower. The fatigue behavior was measured at 10 kHz for 10^8 or 10^9 polarization reversal cycles. A summary of the fatigue results and the dielectric constant data is given in Table 5.3:

Table 5.3 : Summary of fatigue and dielectric constant data.

Annealing Conditions	Initial P_r ($\mu C/cm^2$)	Final P_r ($\mu C/cm^2$)	Drop Off at	Dielectric Constant
650° C 60 minutes	22 - 29	7 - 15	$10^5 - 10^6$	770 - 800
700° C 30 minutes	23 - 30	7 - 15	10^5	800 - 850
700° C 45 minutes	22 - 27	6 - 10	10^4	600 - 625
700° C 60 minutes	15 - 20	shorted - 7	$10^4 - 10^5$	600 - 630
RTP	20 - 25	8 - 15	$10^5 - 10^6$	800 - 840

It is clear that the samples annealed for longer times and higher temperatures show a strong decrease in the relative dielectric constant. This can be related to lead loss from the surface during annealing or to the formation of a pyrochlore phase. The fatigue behavior exhibited is analogous to the dielectric constant data in that the films with lower ε_r show worse fatigue behavior. This can partly be attributed to the Pt roughening effect. That is, the areas of the film with more roughening will experience a higher electric field and fatigue will be accelerated or breakdown will occur sooner.

Finally, *in situ* ellipsometric studies of fatigue were attempted. The primary difficulty in performing this experiment was obtaining samples which were pinhole and crack free over an area large enough to encompass the light beam of the ellipsometer (1 mm in diameter). For samples that we were able to observe, the data in Δ and Ψ was obtained before, during and after fatigue. Small changes in the data were observed. Additional work to clarify the causes of these changes is necessary.

5.2 Proposed Future Work

This study was intended to examine the influence of the processing conditions of ferroelectric thin films on the microstructure and electrical properties. The fatigue behavior

was of most interest, however, the lack of a large number of samples appropriate for an *in situ* ellipsometric study did not allow for a complete investigation. The primary obstacle that must be overcome to continue this study is the ability to prepare sol-gel PZT thin films that are pinhole free over a large enough area for the ellipsometer beam. Significant progress toward this was made by utilizing the rapid thermal processing method described above. Further data obtained from fatigued films could determine whether the dominating fatigue mechanism is a space charge effect, electrode or substrate effect, etc.

Since this was the first study to quantitatively compare surface roughnesses as a function of processing conditions, it would be appropriate to further investigate this effect. Atomic force microscopy (AFM) would be an ideal technique to confirm the SE measurements of roughness. It also gives roughness information over a smaller area, which would be interesting to compare to the large area average obtained from the optical measurements. The dimensions of a memory element can be as small as 4 μm^2, thus since the roughness can affect the electrical properties, small scale surface information is necessary. In addition, a compositional analysis as a function of depth (perhaps by Auger electron spectroscopy) for the rapidly and conventionally annealed samples would show any differences at the surface caused by processing. Lead loss from the surface would be expected for the conventional samples, but not for the RTP'd films.

The platinum roughening effect was shown to be detrimental to the performance of the films. This should be explored further by first confirming the effect using SEM or cross-sectional transmission electron microscopy (XTEM). AFM would also be a useful technique to examine this. It could be interesting to see if a similar effect is observed for thin films of other potential ferroelectric memory materials deposited on platinum substrates.

There are more electrical studies which could be performed, as well. If large area electroded samples were fabricated, fatigue testing of samples with different electrode materials would be interesting. Previous studies have shown differences in fatigue

behavior when the electrode is changed (Vijay and Desu, 1993). Thus the changes in the ellipsometric parameters could be increased or diminished. Ideally, a transparent electrode such as Indium Tin Oxide (ITO) would be used as it transmits light much better than an opaque material, i.e., gold.

Finally, it would be interesting to investigate space charge migration during time dependent dielectric breakdown optically. Space charge migration has been proposed as a fatigue mechanism in memory devices. In this set of experiments, rather than fatiguing a film, a d.c. voltage would be applied to the sample and Δ and Ψ would be measured as a function of time. It may be possible to see a change in the optical properties as the space charge moves through the film. And this would facilitate interpretation of fatigue data.

REFERENCES

Abt, N., *"Electrical Measurement of Ferroelectric Capacitors for Non-volatile Memory Applications,"* Mat. Res. Soc. Symp. Proc, Vol. 200, pp303-12 (1990)

Araujo, C.A., McMillan, L.D., Melnick, B.M., Cuchiaro, J.D., Scott, J.F., *"Ferroelectric Memories,"* Ferroelectrics **104** pp241-56 (1990)

Aspnes, D.E., *"Effects of Component Optical Activity in Data Reduction and Calibration of Rotating Analyzer Ellipsometers,"* J. Opt. Soc. Am. **64** pp812-19 (1974)

Blum, J.B., *"Sol-Gel Technology for Thin Films, Fibers, Performance Electronics and Speciality Shapes,"* ed. Klein, L.C., Chp 14, Noyes Publications, Park Ridge, pp296-302 (1988)

Budd, K.D., Dey, S.K., Payne, D.A., *"Sol-Gel Processing of $PbTiO_3$, $PbZrO_3$, and PLZT Thin Films,"* Br. Cer. Proc. **36** pp109-21 (1985)

Carl, K., Hardtle, K.H., Ferroelectrics **22** p473 (1978)

Chen, J., *"Electrical and Electromechanical Properties of Ferroelectric Thin Films for Microelectromechanical Applications,"* PhD Thesis, Penn State University (1993)

Chen, J., Udayakumar, K.R., Brooks, K.G., Cross, L.E., *"Rapid Thermal Annealing of Sol-Gel Derived Lead Zirconate Titanate Thin Films,"* J.Appl. Phys. **71** [9] pp4465-69 May (1992)

Chindaudom, P., *"Characterization of Inhomogeneous Transparent Thin Films on Transparent Substrates by Spectroscopic Ellipsometry,"* PhD Thesis, Penn State University (1991)

Collins, R.W., *"Automatic Rotating Element Ellipsometers: Calibration, Operation and Real-Time Applications,"* Rev. Sci. Instrum **61** [8] pp2029-62 August (1990)

Cross, L.E., Hardtl, K.H, *"Ferroelectrics,"* Encyclopedia of Chemical Technology, Vol 10, Edited by K. Othmer, Third Edition, John Wiley & Sons (1980)

Duiker, H.M., Beale, P.D., Scott, J.F., *"Properties of KNO_3 Thin Film Memories,"* Bull. Am. Phys. Soc. **33** p539 (1988)

Eom, C.B., Van Dover, R.B., Phillips, Fork, D.K., "*Fabrication and Properties of Epitaxial Ferroelectric Heterostructures with (SrRuO₃) Isotropic Metallic Oxide Electrodes*," Appl. Phys. Lett **63** [18] pp2570-72 November (1993)

Fatuzzo, E., Merz, W., Ferroelectricity, North-Holland Publishing Co., Amsterdam (1967)

Fukushima, J., Kodaira, K., Tsunashima, A., Matsushita, T., Yogyo Kyoaishi, **83** p204 (1975)

Fukushima, J., Kodaira, K., Matsushita, T., J. Mater. Sci., **19** p595 (1984)

Huang, Y., Reaney, I.M., Bell, A.J., "*Rapid Thermal Processing of PZT Thin Films*," Ferroelectrics **134** pp285-90 (1992)

Jaffe, B., Cook, W.R., Jaffe, H., Piezoelectric Ceramics, Academic Press, London, p136 (1971)

Jiang, Q., Cao, W., Cross, L.E., "*Electric Fatigue in Lead Zirconate Titanate Ceramics*," J. Am. Ceram. Soc. **77** [1] pp211-15 (1994)

Johnson, D.J., Amm, D.T., Griswold, E., Sreenivas, K., Yi, G., Sayer, M., "*Measuring Fatigue in PZT Thin Films*," Mat. Res. Soc. Symp. Proc. Vol 200, pp289-95 (1990)

Kingery, W.D., Bowen, H.K., Uhlmann, D.R., Introduction to Ceramics, John Wiley & Sons, New York, p964 (1960)

Kinney, W.I., Gealy, F.D., "*Applications of Integrated Ferroelectric Technology*," Presented at International Solid State Circuits Conference, San Francisco, February 18, (1994)

Kudzin, A.Y., Panchenko, T.V., Yudin, S.P.,"*Behavior of 180° Domain Walls of Barium Titanate Single Crystals During the "Fatigue" and Recovery of Switching Properties*," Fiz. tverd. Tela **16** p1589 (1975)

Kwok, C.K., Desu, S.B., "*Pyrochlore-Perovskite Phase Transformation of Lead Zirconate Titanate (PZT) Thin Fllms*," App. Phys. Lett. **60** [12] p1430, March (1992)

Kwok, C.K., Desu, S.B., Kammerdiner,L., "*Effect of Thermal Processing Conditions on Ferroelectric PZT Thin Films*," Mat. Res. Soc. Symp. Proc, Vol. 200, pp83-89 (1990)

Kwok, C.K., Desu, S.B., "*Role of Oxygen Vacancies on the Ferroelectric Properties of PZT Thin Films*," Mat. Res. Soc. Symp. Proc, Vol. 200, pp393-98 (1990)

Lakeman, C.D., Payne, D.A., "*Processing Effects in the Sol-Gel Preparation of PZT Dried Gels, Powders, and Ferroelectric Thin Layers*," J. Am. Ceram. Soc. **75** [11] pp3091-96 (1992)

Lambeck, P.V., Jonker, G.H., "*Nature of Domain Stabilization in Ferroelectric Perovskites*," J. Phys. Chem. Solids **47** pp451-61 (1986)

Lampe, D.R., Adams, D.A,. Austin, M., Polinsky, M., Dzimianski, J., Sinharoy, S., Buhay, H., Brabant, P., Liu, Y., "*Process Integration of the FerroElectric Memory FETs (FEMFETs) for NDRO Ferram*," Ferroelectrics **133** pp61-72 (1992)

Lee, J., Johnson, L., Safari, A., Ramash, R., Sands, T., Gilchrist, H., Keramidas, V., "*Effects of Crystalline Quality and Electrode Material on Fatigue in Pb(Zr,Ti)O3 Thin Film Capacitors*," Appl. Phys. Lett. **63** [1] pp27-29 July 5 (1993)

Mansour, S.A., Vest, R.W., "*The Dependance of Ferroelectric and Fatigue Behaviors of PZT Films on Microstructure and Orientation*," Integrated Ferroelectrics **1** pp57-69 (1992)

McMarr, P., "*Characterization of Surfaces, Thin Films, and Ion-implanted Silicon by Spectroscopic Ellipsometry,* " PhD Thesis, Penn State University (1985)

Pan, W., Sun, S., Fuierer, P., "*Effects of Ferroelectric Switching on the Dielectic and Ferooelectric Properties in Lead Zirconate Titanate Ceramics and their Modeling*," J. Appl. Phys. **74** [2] pp1256-64 July 15 (1993)

Peng, J.L., Bursill, L.A., "*Electron Microscopic Studies of Ferroelectric Crystals*," Ferroelectrics **70** pp191-203 (1986)

Reaney, I.M., Brooks, K., Klissurska, R., Pawlaczyk, C., Setter, N., "*Use of Transmission Electron Microscopy for the Characterization of Rapid Thermal Annealed, Solution-Gel, Lead Zirconate Titanate Films*," J. Am. Ceram. Soc. **77** [5] pp1209-16 (1994)

Saleneck, W., "*Some Fatiguing Effects in 8/65/35 PLZT Fine Grained Ferroelectric Ceramic*," Ferroelectrics **4** pp97-101 (1972)

Sanchez, L.E., Dion, D.T., Wu, S.Y., Naik, I.K., *"Processing and Characterization of Sol-Gel Derived Very Thin Film Ferroelectric Capacitors,"* Ferroelectrics **116** pp1-17 (1991)

Scott, J.F., Araujo, C.A., Melnik, B.M., McMillan, L.D., Zuleeg, R., *"Quantitative Measurement of Space-Charge Effects in PZT Memories,"* J. Appl. Phys. **70** pp382-88 (1991)

Sumi, T., Moriwaki, N., Nakane, G., Nakakuma, T., Judai, Y., Uemoto, Nagano, S., Hayashi, I., Azuma, M., Otsuki, T., Kano, G., McMillan, L., Paz de Araujo, C., *"256Kb Feroelectric Nonvolatile Memory Technology for 1T/1C Cell with 100ns Read/Write Time at 3V,"* Presented at International Solid State Circuits Conference, San Francisco, February 18 (1994)

Swartz, S.L., Wood, V.E., *"Ferroelectric Thin Films,"* Condensed Matter News, **1** [5] pp4-13 (1992)

Takahashi, M., *"Space Charge Effect in PZT Ceramics Caused by the Addition of Impurities,"* Jap. J. Appl. Phys. **9** [10] pp1236-46 (1970)

Tani, T., Payne, D.A., *"Lead Oxide Coatings on Sol-Gel-Derived Lead Lanthanum Zirconium Titanate Thin Layers for Enhanced Crystallization into the Perovskite Structure,"* J. Am. Ceram. Soc. **77** [5] pp1242-48 (1994)

Taylor, G.W., *"Properties of Niobium Doped Ferroelectric Pb(Zr, Sn, Ti)O$_3$ Ceramics, "* J. Appl. Phys. **38** p4697 (1967)

Thakoor, S., Maserjian, J., *"Photoresponse Probe of the Space Charge Disribution in Ferroelectric Lead Zirconate Titanate Thin Film Memory Capacitors,"* J. Vac. Sci. Technol. A **12** [2] pp295-99, Mar/Apr (1994)

Trolier-McKinstry, S. *"Characterization of Ferroelectric Surfaces and Thin Films by Spectroscopic Ellipsometry,"* PhD Thesis, Penn State University (1992)

Trolier-McKinstry, S., Hu, H., Krupanidhi, S.B., Chindaudom, P., Vedam, K., Newnham, R.E., *"Spectroscopic Ellipsometry Studies on Ion Beam Sputter Deposited Pb(Zr, Ti)O$_3$ Films on Sapphire and Pt-coated Silicon Substrates, "* Thin Solid Films **230** pp15-27 (1993)

Trolier-McKinstry, S., Fox, G.R., Casas, L.M., Krupanidhi, S.B., *"Pt/Ti/SiO$_2$/Si Substrates,"* Unpublished Work (1994)

Tuttle, B., Voigt, J., Goodnow, D.C., Lamppa, D.L., Headley, T.J., Eatough, M.O., Zender, G., Nasby, R.D., Rodgers, S.M., *"Highly Oriented, Chemically Prepared Pb(Zr,Ti)O$_3$ Thin Films,"* J. Am. Ceram. Soc. **76** [6] pp1537-44 (1993)

Udayakumar, K.R., Krupanidhi, S.B., Cross, L.E., Kushida, K., *"Origin of Orientation in Sol-Gel Derived Lead Titanate Films,"* J. Am. Cer. Soc. **76** [5] pp1345-48 (1993)

Valasek, J., *"Piezoelectric and Allied Phenomena in Rochelle Salt,"* Phys. Rev. 2nd Ser. **17** pp475-81 (1921)

Vijay, D.P., Desu, S.B., *"Electrodes for PbZr$_x$Ti$_{1-x}$O$_3$ Ferroelectric Films,"* J. Electrochem. Soc., **140** [9] pp2640-5 September (1993)

Wu, S.Y., *"A New Ferroelectric Memory Device: Metal-Ferroelectric-Semiconductor Transistor,"* IEEE Trans. on Electron. Devices, **ED-21**, p499 (1974)

Wu, E., Chen, K.C., MacKenzie, J.D., *" Ferroelectric Ceramics - The Sol-Gel Method versus Conventional Processing, "* Mater. Res. Soc. Symp. Proceed., vol. 32, pp162-74 (1984)

Xu, Y., MacKenzie, J.D., *"Ferroelectric Thin Films Prepared by Sol-Gel Processing,"* Integrated Ferroelectrics, **1** pp17-42 (1992)

Yi,G., Sayer, M., *"Sol-Gel Processing of Complex Oxide Films,"* Am. Ceram. Soc. Bull. **70** [7] pp1173-79 (1991)

Yoo, I.K., Desu, S.B., *"Mechanism of Fatigue in Ferroelectric Thin Films,"* Journ. of Intell. Mat. Sys. and Struc. **4** [4] pp490-5 (1993)

Zuleeg, R., Wieder, H.W., *"Effect of Ferroelectric Polarization on Insulated-Gate Thin Film Transistor Parameters, "* Sol. St. Electronics, **9** p657-61 (1966)

APPENDIX

THE FOURIER ANALYSIS of INTENSITY

The derivation of the intensity of light as a function of analyzer angle is as follows:

Starting from equation 5 in chapter 3:

$$\begin{bmatrix} E_1 \\ E_2 \end{bmatrix}_{t,e} = \begin{bmatrix} 1 & 0 \\ 0 & 0 \end{bmatrix}\begin{bmatrix} \cos A & \sin A \\ -\sin A & \cos A \end{bmatrix}\begin{bmatrix} \rho & 0 \\ 0 & 1 \end{bmatrix}\begin{bmatrix} \cos P & -\sin P \\ \sin P & \cos P \end{bmatrix}\begin{bmatrix} 1 \\ 0 \end{bmatrix} E_o$$

For a given polarizer angle of 45°:

$$\begin{bmatrix} E_1 \\ E_2 \end{bmatrix}_{t,e} = \begin{bmatrix} 1 & 0 \\ 0 & 0 \end{bmatrix}\begin{bmatrix} \cos A & \sin A \\ -\sin A & \cos A \end{bmatrix}\begin{bmatrix} \rho & 0 \\ 0 & 1 \end{bmatrix}\begin{bmatrix} 1/\sqrt{2} & -1/\sqrt{2} \\ 1/\sqrt{2} & 1/\sqrt{2} \end{bmatrix}\begin{bmatrix} 1 \\ 0 \end{bmatrix} E_o$$

Multiplying out gives:

$$\begin{bmatrix} E_1 \\ E_2 \end{bmatrix}_{t,e} = \frac{1}{\sqrt{2}}\begin{bmatrix} \rho\cos A + \sin A \\ 0 \end{bmatrix}$$

The intensity is the square of the resultant electric field, so:

$$I = E \times E^* = (\rho\cos A + \sin A)\times(\rho^*\cos A + \sin A)$$

Thus:

$$I = \rho\rho^*\cos^2 A + \rho\cos A\sin A + \rho^*\cos A\sin A + \sin^2 A$$

$$I = \rho\rho^*\left(\frac{1+\cos 2A}{2}\right) + \frac{1}{2}\rho\sin 2A + \frac{1}{2}\rho^*\sin 2A + \left(\frac{1-\cos 2A}{2}\right)$$

$$I = \left(\frac{\rho\rho^* + \rho\rho^*\cos 2A}{2}\right) + \frac{1}{2}\sin 2A(\rho+\rho^*) + \left(\frac{1-\cos 2A}{2}\right)$$

$$I = \frac{1}{2}\cos 2A(\rho\rho^* - 1) + \frac{1}{2}\rho\rho^* + \frac{1}{2} + \frac{1}{2}\sin 2A(\rho+\rho^*)$$

$$I = \frac{1}{2}(\rho\rho^* + 1) + \frac{1}{2}(\rho\rho^* - 1)\cos 2A + \frac{1}{2}(\rho+\rho^*)\sin 2A$$

So finally:

$$I = \frac{1}{2}(1+\rho\rho^*)\left[1+\left(\frac{\rho\rho^* - 1}{1+\rho\rho^*}\right)\cos 2A + \left(\frac{\rho+\rho^*}{1+\rho\rho^*}\right)\sin 2A\right]$$

Or more conveniently:

$$I = I_o[1 + \alpha \cos 2A + \beta \sin 2A]$$

where:

$$I_o = \frac{1}{2}(1 + \rho\rho^*)$$

$$\alpha = \left(\frac{\rho\rho^* - 1}{1 + \rho\rho^*}\right)$$

$$\beta = \left(\frac{\rho + \rho^*}{1 + \rho\rho^*}\right)$$